ADDIS ABABA UNIVERSITY

SCHOOL OF GRADUATE STUDIES

FACULTY OF NATURAL AND COMPUTATIONAL SCIENCES

SCHOOL OF EARTH SCIENCES

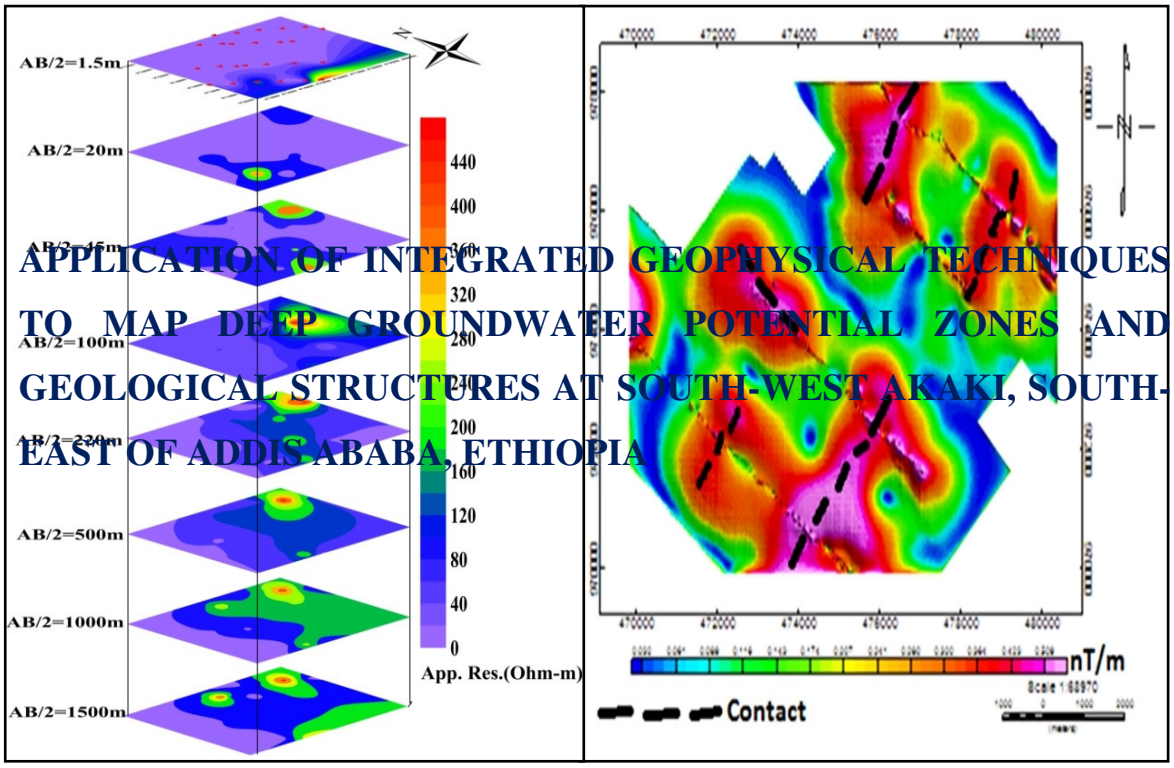

APPLICATION OF INTEGRATED GEOPHYSICAL TECHNIQUES TO MAP DEEP GROUNDWATER POTENTIAL ZONES AND GEOLOGICAL STRUCTURES AT SOUTH-WEST AKAKI, SOUTH-EAST OF ADDIS ABABA, ETHIOPIA

By

EYASU LETA ALEMU

A Thesis Submitted to the School of Earth Sciences of Addis Ababa University in Partial Fulfillment of the Requirements for the Degree of Master of Science in Exploration Geophysics

Addis Ababa
May 2014

Addis Ababa University

School of Graduate Studies

Faculty of Natural and Computational Sciences

APPLICATION OF INTEGRATED GEOPHYSICAL TECHNIQUES TO MAP DEEP GROUNDWATER POTENTIAL ZONES AND GEOLOGICAL STRUCTURES AT SOUTH-WEST AKAKI, SOUTH-EAST OF ADDIS ABABA, ETHIOPIA

By: **EYASU LETA ALEMU**

School of Earth Sciences

Approved by board of examiners:

Dr. Seifu Kebede	_____	_____
Chairman, School of Earth Sciences	Signature	Date
Dr. Tigistu Haile	_____	_____
Advisor	Signature	Date
Dr. Tilahun Mammo	_____	_____
Co-advisor	Signature	Date
Dr. Abera Alemu	_____	_____
Internal Examiner	Signature	Date
Dr. Bekele Abebe	_____	_____
External Examiner	Signature	Date

Abstract

This study entitled 'Application of Integrated Geophysical Techniques to Map Deep Groundwater Potential Zones and Geological Structures, South-West Akaki, South-East of Addis Ababa, Ethiopia' was done using Vertical Electrical Sounding and Magnetic geophysical methods. The aims of the study are to investigate the deeper high potential groundwater saturated zones and linear geologic structural elements which dissect the study area and could possibly act as a hydraulic barrier that impedes or enhance the movement of the groundwater. Further, the work is aimed at determining the depth to water table and identification of drilling point through interpretation of the geophysical, geological and borehole data. Geophysical data have been measured, processed and interpreted in one and two dimensions using special software. The results of interpretation indicate that the study area composed of two aquifers, the first is the Upper Basalt aquifer which is slightly confined between alluvial deposits (upper) and Massive Basalt and Trachytes (lower) and the second is Lower Basalt aquifer which is confined by the Tarmaber Basalt. The depth of the upper aquifer is ranging from 40 to 70m while the depth of the lower aquifer is greater than 250m. The area is dissected by fault elements of NW–SE and NE–SW trend.

Key words: Magnetic anomalies and Pseudo and Geo-electric section; Magnetic and electrical properties of Earth materials.

Acknowledgements

First and foremost, I would like to have great thanks to the Almighty God that strengthens me throughout my life.

A lot of people have contributed in many ways to the success of this thesis and as part of my appreciation to the contribution of these people I would want to express my profound gratitude to each of them:

Firstly, I would like to thanks Dr. Tigistu Haile and Dr. Tilahun Mammo for their help and patience through the difficult periods I encountered during this research. I always remember and cherish your valuable contributions and constructive comment and suggestions during the problem that I faced. Their experience enabled this research work to be carried out successfully.

Secondly, I count myself very lucky to have met Ato Yohannes Engida who has been like a brother and contributor (like material and inspirational) during this research as well as class time. Old boy, I really appreciate your contribution to my professional and academic success. You have been the beginning and the end and I would always cherish everything that you have done in my professional carrier. Like the proverbial teacher, your reward is in heaven; God bless you.

Thirdly, I am grateful and appreciate the efforts of Ato Engida Zemedagegnehu, chief hydrogeologist in Water Works Design and Supervision Enterprise for his support during field and provided equipment's for data collection and that is greatly appreciated.

Furthermore, my mother, Mihret Hailu supported me throughout this study, especially during the frustrating periods when my research progressed slowly due to collection of data and field work. I will always be thankful to you, my lovely mom.

Last, but not the least, I would like to thank all my friends who supported me during my stay in the campus.

Table of Contents

List of Figures

List of Tables

List of Appendices

Acronyms

CSA----------Central Statistical Agency

WWDSE----------Water Works Design and Supervision Enterprise

VES----------Vertical Electrical Sounding

AA----------Addis Ababa

MER----------Main Ethiopian Rift

m^3----------cubic meter

Km----------Kilometer

WF-03----------Well Field-03

WF03-PW1----------Well Field-03-Potentail well1

SWAWF2----------South West Akaki Well Field2

SWAWF-4B----------South West Akaki Well Field-4B

WF01PW8----------Well Field01-Potentail well8

UTM----------Universal Transverse Mercator

masl----------meter above sea level

m----------meter

NW----------North-West

SE----------South-East

mm----------millimeter

$^{\circ}C$----------degree Celsius

My----------Million years

NE-SW----------Northeast-Southwest

K/Ar----------Potassium over Argon

SW-NE----------Southwest-northeast

NW-SE----------Northwest-Southeast

SWAWF----------South-West Akaki Well Field

a.m. ----------anti-meridian

GPS----------Global Position System

J_r----------intensity of remanent magnetization

IGRF----------International Geomagnetic Reference Field

nT----------nanotesla

Am^{-1}----------Ampere per meter

N-S----------North-South

Mg/l----------milligram per liter

cm----------centimeter

Ω-m----------ohm-meter

DC----------Direct Current

micros/cm----------micros per centimeter

CHAPTER ONE

1. INTRODUCTION

1.1. Background

Water is one of the prime necessities of life next to air in the order of importance for the survival of man and a host of other living things. Water is available in oceans, ice caps and glaciers, seas, lakes and in the subsurface. Water stored in the subsurface-groundwater- is widely used in national economy of many countries for different purposes: potable water supply of the population and livestock, industrial water supply, irrigation, biological use (mineral water), as a raw material for extracting valuable components, such as iodine and bromine (industrial water) and for central heating (thermal power water). Fresh groundwater is of particular importance, as in many countries it is the main source of public water supply and its role in domestic and drinking water supply balance is growing every year because of continuing contamination of surface water resources (Igor et. al, 2004).

People's lives and livelihoods depend on water. Demand for clean water increases continually in line with a country's population growth. In the Ethiopian setting, people in many areas of the country lack fresh, drinkable water essential to their survival. Access to the fresh water resources development is beyond the reach of the overwhelming majority of the Ethiopian population. The fast growing population and the recurrent drought in many parts of the country has demanded such an effort more than ever. If the population is to prosper, because clean supply of water is related to health issues as well as to production of food for livelihood, more secure and low cost water supplies are needed. Maintaining secure water supplies for drinking, industry and agriculture would be impossible without groundwater-the largest and most reliable of all freshwater resources.

Groundwater plays an important role in Ethiopia as a major source of water for domestic, industries and livestock uses. At present, Ethiopia has a population of over 84 million; growing at a rate of over 2.9% per annum (CSA Ethiopia, 2012).The population of Addis Ababa, the country's capital, was over 3,041,002 as CSA forecasted on July 2012;out of this 201,216 people lived in the sub city(Akaki-Kaliti) where the study area is located.

Moreover, near the study area, there are a number of industries that account for the population increase and, due to the construction of many condominium houses and industries over and around the study area; there is a need for an increased volume of water resources for its usage. The region around the study area is also widely used for agricultural purpose and thus putting further demand on water supply. Regarding the industries that have come into existence, the industries have yet to be connected to a municipal water source and could possibly rely on groundwater resources of the area. All these demands, combined with further growth in population have imposed significant stress on the existing inadequate water scheme, which is based solely on groundwater abstraction from boreholes around the area. Consequently, it became very expedient to expand the existing water scheme with a focus to delineate the area into hydrogeologic zones in order to increase the number of effective or productive boreholes in the area.

Groundwater occurrence in the area can be variable due to abrupt discontinuity in lithology, thickness, and the properties of the overburden and the weathered bedrock. Consequently, groundwater exploration within such geologic setting requires integration of geophysical data types to effectively characterize the hydrogeologic zones and to enhance successful identification of well locations. In this project work proposed for the thesis, different geophysical methods are employed to map lithologic units suitable for groundwater accumulation, assess the potential zones of groundwater saturation and delineating fracture and faults in the study area that govern the flow and movement of groundwater.

In the final analysis, the thesis is expected to create awareness on the productive aquifer of the area so as to guide both the government and individuals involved in groundwater development on the possible areas and depth that more boreholes could be drilled for potable and sustainable water supply. This will be achieved by obtaining information on the subsurface aquifer distribution, formation and type, and controlling structures using Vertical Electrical Sounding (VES) and magnetic methods of prospecting.

1.2. Statement of the Problem

The largest amount of water on Earth (97.2 %) is contained in the oceans and seas as saline or salty water but only a small amount (2.8 %) exists as fresh water on land. This fresh water found on land is distributed as ice caps and glaciers (76.43 %), groundwater and soil moisture (21.96 %), freshwater lakes (0.32%), saline lakes (0.29 %) and a very small portion of it as streams in channels (0.004%) (Fetter, 2001 as cited in Mulugeta Chanie, 2011). The amount of fresh water which is available for domestic, industrial and agriculture purposes is very limited as compared to the total volume of water on planet Earth. However, it is found relatively in large amount next to that available in ice caps and glaciers. This fresh water requires less expense for purification and transport, occurs in places where there is scarce amount of surface water supply making it to be vital source for drinking, domestic and livestock use for rural populations including in countries like Ethiopia. Due to the above reasons, the search for deep ground water is vital as an immediate and sustainable solution to alleviate the scarcity of water for drinking and other domestic uses in heavily populated areas like Addis Ababa, the country's capital.

The daily consumption of water in Addis Ababa is 370,000m^3 but the available water from surface and groundwater presently is 350,000m^3 showing coverage of water supply at around 93 percent (Ethiopian Reporter Newspaper, 2013). Therefore, currently there is shortage of supply of water for drinking and any agricultural or economical activity in the city as well as in the sub city where the study area is found.

Moreover, Addis Ababa being the capital city of Ethiopia as well as Africa, there is a huge water demand for the population. It is as well apparent that the city has limitation in the coverage percentage of water to its need. Currently, the city gets its water from the water reservoirs located close to the city at Legedadi, Gefersa and from the Akaki groundwater scheme where the study area is found.

When one considers the Akaki groundwater resource, the geological situation and the structural setting of the area being in central Ethiopian highlands at the western edge of the Main Ethiopian Rift (MER) and the low lying and flat nature of the area favor the

accumulation of a considerable groundwater resource within it. Moreover because the study area is located in the lowest plain in Addis Ababa, the flow of groundwater is towards it due to the watershed of the rest of Addis Ababa. Some developmental activity has been done so far for the extraction and development of this resource.

To supplement these developments and increase the utilization of the groundwater resource in the study area, a more detailed assessment of the groundwater potential zones and delineating faults and fracture systems that could influence its storage and movement using different geophysical methods has become necessary. To this end, geophysical techniques like Vertical Electrical Sounding (VES) - to verify the inferred groundwater barrier and its possible connection to the linear geologic structures (WWDSE, 2009) and the magnetic methods- to delineate faults and fractures have been employed on the area.

Moreover, simulations made under different pumping rate conditions in the study area indicate that an increase in pumping rate results in a substantial regional groundwater level decline, which will lead to the drying of springs and shallow hand dug wells in addition to the depletion of the resource from the wells as well (Tenalem Ayenew et. al., 2008). In addition to this, heavy metal and nitrate pollution have been detected in samples collected from rivers, springs and shallow hand dug wells (Tamiru Alemayehu, 2000) and there is a need to understand the whole groundwater system with a view to designing mitigation measures for the movement of these potential pollutants.

Furthermore, due to population growth and the expansion of industrial and infrastructural activities, the groundwater reserve is decreasing and water demand is increasing at an alarming rate. There will thus continue to be increasing demands for groundwater especially in the developing cities like Addis Ababa and it is logical to expect that there will be a corresponding need to locate deep groundwater aquifers of regional extent.

1.3. Research Motivation

The cost of drilling for water supply boreholes almost demands that the risk of drilling a poorly yielding borehole should be lessened through the proper use of geophysics. Geophysics can be used to screen potential drilling locations and remarkably decrease the

risk of drilling in unproductive areas. In this respect, geophysics is cost effective and its proper application always increases the success of drilling.

In any groundwater project, simply drilling for groundwater is costly so that it affects the benefit of the project found from the result. In addition, there is the question to what depth should a borehole be sunk to get the potential zone of groundwater. Such project which has the probability of failure and incur a huge cost needs proper investigation for the accurate identification of potential groundwater zones and their depth in order to reduce the expected risks and cost of the project. Using the appropriate geophysical methods of prospecting does greatly reduce the risks involved.

Furthermore, in areas that depend heavily on groundwater (like in the area under study), groundwater models are often used to simulate subsurface flow for a more quantitative hydrogeological analysis of the effect of proposed water supply boreholes and for planning purposes. These groundwater models are usually limited in accuracy by the hydrogeological data available. Geophysics can provide additional data to improve the accuracy of groundwater models for hydrogeologists. Since very little is known about the volcanic layers below the depth of 250 meters, following the geophysical investigations and results, it is essential to study this system by drilling test wells and using proper geophysical methods (Tenalem Ayenew et. al, 2008).

What makes geophysical techniques even more attractive is that, the techniques have proved to be efficient tools in groundwater exploration and the steep technological growth of the last 15 years in geophysics, due mainly to advances in microprocessors and associated numerical modeling solutions, have greatly affected this field of geophysics. Not only has geophysics been used in the direct detection of the presence of water but also in the estimation of aquifer size and properties, groundwater quality and movement, mapping saline water intrusions and buried valleys even in areas of complex geology (UNESCO, 1998).

In the Ethiopian context and especially in the study area, the revealing complex nature of the geology and the groundwater system makes a detailed and a systematic geophysical study, the appropriate alternative, as the conventional hydrological approach so far has

proved its inability to exhaustively deal with the problem alone. In this research, therefore, ground based geophysical methods including the existing borehole data will be used to study the potential zone of groundwater and to identify linear geologic features of the study area. The archives of ground based VES report in the area were collected for the interpretation with the view to studying the identification of the layers of the study area. The actual work involved a dedicated geophysical fieldwork to collect VES and Magnetic data on the subsurface electrical properties and magnetic anomaly of the area.

1.4. Objectives of the Study

1.4.1. General Objectives

The general objective of this project is to characterize the Akaki well field, in the southeast of Addis Ababa, and investigate the potential of the area for deep groundwater resource, through the mapping of the subsurface lithologies and identification of geologic structures that could play a role in the storage and movement of groundwater.

1.4.2. Specific Objectives

The specific objectives of this project are:

- To establish the distribution of the electrical properties of the aquifer materials in the area,
- To map the location of faults or fractures,
- Mapping the saturated zone and trace the regional configuration of the water table of the site.
- To identify subsurface weak zones that could serve as a conduit or barriers for groundwater movement.
- To determine the depth to water table and to locate potential drilling sites for the extraction of groundwater.

1.5. Methodology

In order to achieve these objectives, a number of steps have been followed. These included reviewing different previous works, not only geophysical works (on groundwater exploration and identification of geological structures) but also geological and hydro-geological literatures on the study area. Finally, two different geophysical

methods were employed in the study area: VES and magnetic methods of prospecting. Data from both methods were collected along four selected traverses well distributed to cover all the study area. These VES data are analyzed using appropriate software like RESIST, Ip2win, SURFER, AutoCAD 2007 and Microsoft Excel while the magnetic data are analyzed using Oasis Montaj and SURFER, Paint and Microsoft Excel software. Consequently curves, maps and models are produced and interpreted to achieve at the objectives of the work. The detailed methodological approach of the thesis is indicated in the flow chart of Figure 1-1.

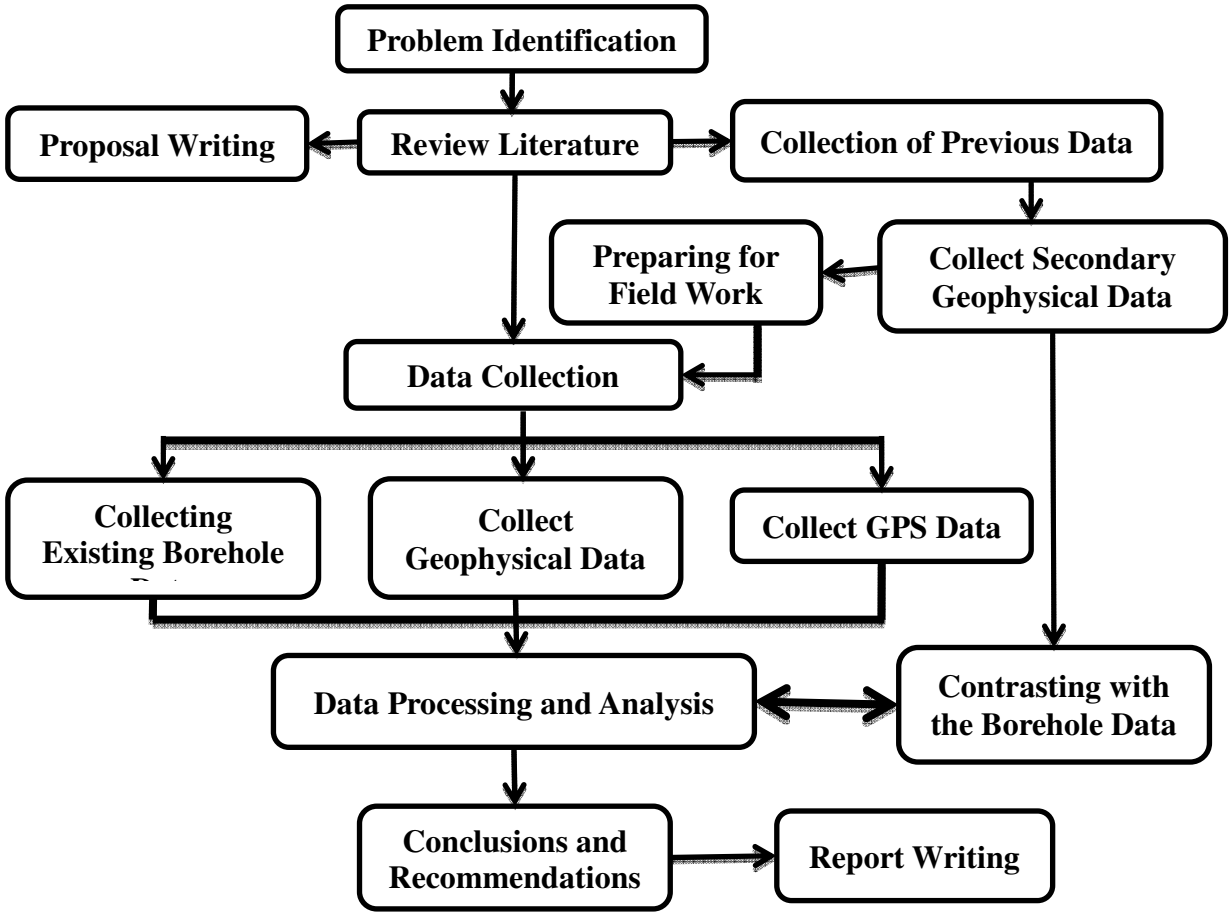

Figure 1-1: Flow model of the project.

1.6. Basic Research Question and Hypothesis

1.6.1. Basic Research Question

- How to map the location of faults and fractures?
- How to identify the groundwater table of the area?

- How to identify weak zones of the area?
- How to map the saturated zone of the area?
- Where to locate the drilling point?

1.6.2. Research Hypothesis

The potential of groundwater bearing horizons their depth and geologic structures can be obtained by measuring the electrical and magnetic properties of the subsurface.

1.7. Significance of the Study

The study has the following importance:

- It provides information about the aquifer zone, its depth as well as the drilling point of high potential zone of groundwater in the study area.
- It gives practical experience for the researcher and hence it is great resource for the respective sectors.
- Experience sharing had taken place with the researcher and the company on the use of geophysical methods for groundwater exploration and geological structure delineation and identification.
- The material can serve for the department and the company as a source document for the future researchers to continue their research in the similar areas.
- It takes in to application of theoretical concepts of the different subjects taken academically. Hence, it will be an input to review and to see the applicability of the subject matters.
- It develops the researcher's ability on geophysical software.
- It gives better understanding about the volcanic layers below the depth of 250 meters up to 1km depth.
- This study enhances the understanding of the geological structure of the area.
- It contributes some data set to the ongoing study of exploration of groundwater in the country.
- This research work fills the existing gap of detail information and its usage in the geophysical methods in the country.

- It gives a pure geological setting of the area for further scientific studies that needs the geology of an area for the investigation and interpretation of any geological problem.

1.8. Limitation of the Study

Like any other research works, this study has also faced number of limitations in this research. The main obstacles were:

- Severe financial and necessary field materials like transport and geophysical instrument,
- Shortage of software for analysis and interpretation of geophysical data,
- Non availability of previous geophysical work on the area, and
- The time bound set for the thesis work coupled with field constraint (transport and instruments).

1.9. Previous Works

There are a number of boreholes drilled on the site earlier based on geophysical investigation. In order to evaluate the transmissivity of the prospective site, resistivity logging was conducted in the existing boreholes. Except in some places, especially at the eastern part of the prospective site, the result of interpretation of the log shows that the deeper part has lower resistivity values showing higher saturation. In pilot production well designated as (WF03-PW1) a trachyte layer was encountered from 300 to 388m depth and this corresponds with the high resistivity value in the VES interpretation.In general the high apparent resistivity ranges in the VES could be due to the distribution of acidic volcanic rocks layers (pyroclastics rocks and trachytes) (WWDSE, 2011).

Lithological logs were used to classify the aquifer media, type of vadose zone and depth of soil profiles. An attempt has been made to evaluate the geological log, and resistivity log of the boreholes in the area. Since resistivity logging is only possible below the static water level, the evaluation of the upper parts of the borehole depends solely on the geologic log.

Four main different formations have been identified on the borehole logs. The alluvial deposits more or less up to 20m,the basalt that varies depending on the degree of weathered and fractured which continues to 200m.The third one is the trachyte that has a thickness of around 60m and the last one is the Tarmaber basalt which exists as fresh, weathered and fractured Earth material.

The geologic logs of the study area indicate that the major formation of the aquifer is basaltic in composition, while the water quality analysis revealed that the water is generally fresh. Therefore, the shape of the resistivity log curves depends mainly on the degree of fracturing and presence or absence of water. Correlation was found to be difficult due to the lenticular nature of the units, rapid lateral changes within units, and variable dips (due to different centers of volcanic activity depositing materials in different places in various periods). Since rocks of various ages are distributed in the study area aquifer characterization becomes a difficult and complex task (WWDSE, 2009).

1.10. Organization of the thesis

The thesis is organized in six chapters. Chapter one deals with the general introduction, objective, methodology and previous studies. Chapter two gives the physical description of the study area that includes the location, climate, topography, geology and hydrogeology of the site. Chapter three gives an overview of theoretical background of the geophysical methods employed in the work, i.e. Vertical Electrical Sounding (VES) and magnetic methods of prospecting. Chapter four presents the discussion on the selection of traverse, data acquisition and reduction, processing and presentation of the VES and magnetic data. Chapter five deal with the discussions and interpretations of the processed and presented data. The last (sixth) chapter deals with the conclusions and recommendations of the study.

CHAPTER TWO

2. DESCRIPTION OF THE STUDY AREA

2.1. Location

The study area is located at the western edge of the Main Ethiopian Rift. The site is situated near Akaki-Kality sub city, southeast of Addis Ababa within the Akaki catchment which is the part of upper Awash River Basin (Figure 2-1). It is bounded by geographical coordinates of approximately bounded between 8^0 47' 25.50" -8^0 53' 6.23" N latitude (973904-981863N) and 38^0 44' 00" – 38^0 49' 18.79" E longitudes (469812-480334E) with elevation ranging between 2050 and 2180m.a.s.l. The ground surface elevation increases generally towards north with major variations in the north eastern part of the area. The prospective site is bordered by Addis Ababa City on the north, by Furi Mountain on the southwest and by Guji Mountain on the southeast.

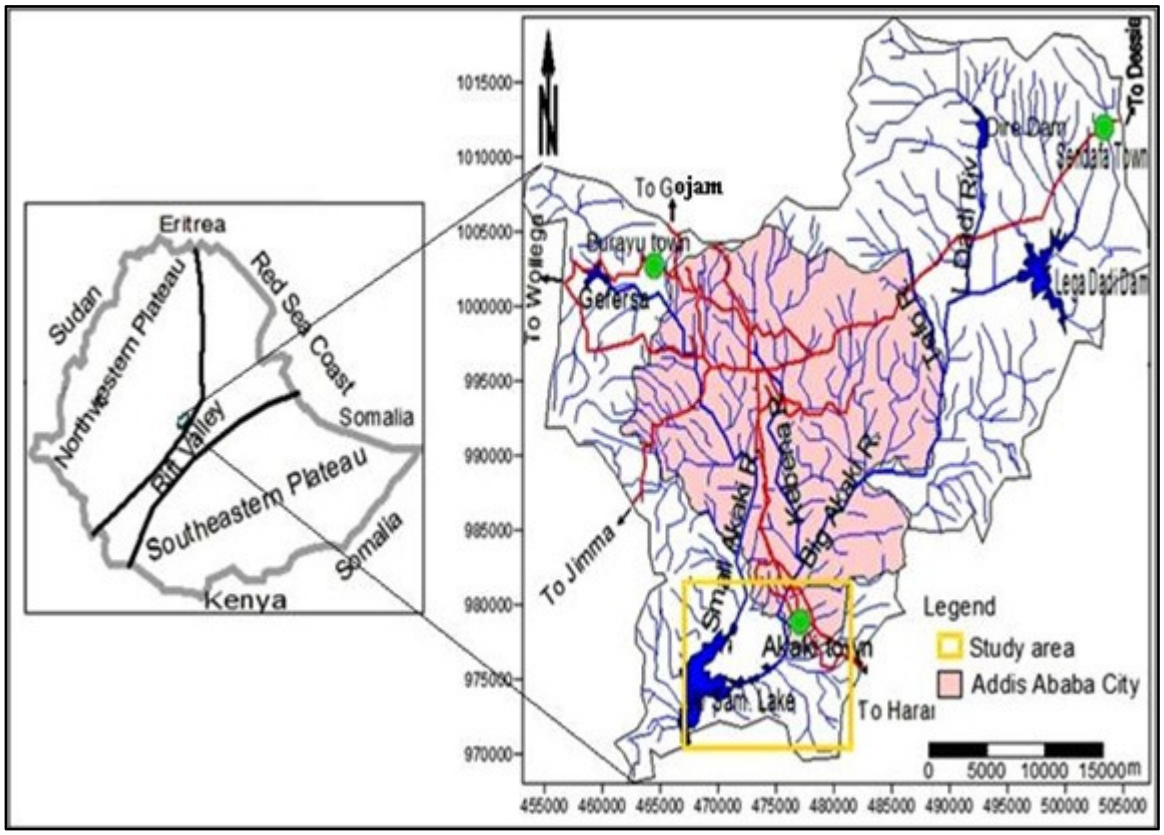

Figure 2-1: Location of the study area.

2.2. Topography and Drainage

Over all, the site ranges in elevation from 2050m in south and central part to 2180m in the northeastern corner. It is drained from northwest, north, and northeast towards the southeast and into Akaki River, in places losing itself among extensive seasonal swamps, but eventually discharging into the Awash River.

The area can be divided into three major physiographic regions. These are: (1) The Furi Ridge, (2) The eastern and (3) Akaki plain physiographic regions. The Furi ridge physiographic region, the south eastern part of the Furi volcano, is drained from northwest to southeast into the Akaki plain, part of the radial drainage of the Furi volcano. The creeks finally lose themselves into the extensive Akaki seasonal swamp area. The Furi Mountain rises from the surrounding area by about 700m.It is built of mainly trachytic flows and minor associated pyroclastics (WWDSE, 2011).

The northwestern, northeastern and southeastern areas are underlain by Quaternary age basaltic flows. These areas gradually slope due west into south central part. This is a large and relatively little modified basalt shield of recent origin. This large mound has been built by voluminous out pouring of basalt flows from east–northeast trending central fissures, now marked by speckles of numerous well preserved cinder and basalt cones. There are scattered cinder and basalt cones sticking out of the surrounding surface forming conspicuous topographic features in the site area.

The south central part of the site is a sediment depositional site, a NE–SW trending sort of graben structure now filled with recent alluvial sediments (WWDSE, 2011). It presents a flat lying not yet modified topography. The featureless alluvial plain is completely devoid of bed rock exposure and lies in elevation between 2060 and 2080m. Akaki River meanders southeastward across the plain, in places losing itself among extensive seasonal swamps, but eventually discharging into Awash River outside the site area. The river meanders through the alluvial sediment eroding its own depositions. Generally, the geomorphology of the study area is flat plain graben with scoria and vesicular basalt hills which is bounded by mountains NW and SE directions.

2.3. Climate

2.3.1. Rainfall

National Atlas of Ethiopia (1981) defined five climatic zones: "Kur" (Alpine), 3000m and above mean sea level; "Dega" (Temperate), 2300m to about 3000m; "Weina-Dega" (Sub tropical), 1500 to about 2300m; "Kolla" (Tropical), 800m to about 1500m and "Bereha" (Desert), less than 800m;having a maximum and minimum elevation range a little above 3000m and a little below 1500m and rainfall ranges 900-2200mm, 900-1200mm, 800-1200mm, 200-800mm, under 200mm per year respectively. Based on this classification, the study area is located within “Weyna-Dega” (sub topical) or midlands zone (Deressa Temesgen et al., 2008).

Accordingly, the climate of Addis Ababa area is typically characterized by two distinct seasonal weather patterns: the wet season which extends from June to September, contributing about 70% of the annual rainfall, and the dry season which covers the period from October to May with a minor rainy season in March and April well known for its frequent failure. Such climates which are characterized by alternating wet and dry seasons may favor. This seasonal variation of rainfall distribution within the study area is due to the annual migration of the inter-tropical convergence zone, a low-pressure zone marking the convergence of dry tropical easterlies and moist equatorial westerlies across the catchment (Ebasa Oljira, 2006). The climate is warming temperate to humid. The study area receives rainfall from Atlantic Equatorial Westerly during the main rainy season and from Gulf of Aden and Indian Ocean during March and April months. There is low to negligible amount of rainfall in the other months. Addis Ababa is located in the region where the rainy months are closely distributed weathering (Leta Guddisa, 2007).

2.3.2. Temperature

The highest and lowest mean maximum temperature over the record periods is 25°C in dry season (March) and 20°C in the wet season (August), while the variation of mean monthly temperature values fall in the range of 9°C (October) to 27°C (March) throughout the year. From these values one can observe that daily variation in temperature in the area is more pronounced than the annual variation and the calculated

mean annual temperature was around 23.32°C. In general, one can classify the climate in this area as warm temperate climate.

2.4. Vegetation

The types of vegetation in the study area are not as such diverse and consist mainly of Acacia, Eucalyptus, Fig/Shola, Tid/Junipers, Zembaba/Palm tree and small shrubs. The Eucalyptus trees are mostly found in homesteads/settlement areas. However, remnants of some of the tree types indicate that the area was once covered by indigenous trees at the time of this study the surrounding area is dominated by open grassland and farmland showing high anthropogenic impact (Abraham Hailemelekot, 2009).

2.5. Geology of the area

2.5.1. Regional Geology

Wide ranges of volcanic rocks of different ages characterize the area that covers the catchment of Akaki River including Addis Ababa and the well field (Morton et. al., 1979). The rocks in Addis Ababa are highly affected by the rift tectonics that is very common features of the Ethiopian Rift valley. The north and northeastern part of the catchment (the Entoto Mountain, the northern and north-eastern Addis Ababa) are covered with trachytes, rhyolites, basalts and several episodes of pyroclastic materials of older volcanism that occur on the upper part and foothill sides of Entoto ridge. The central and southern part of the Addis Ababa area is overlain by younger basaltic rocks 7-6.4My (Addis Ababa Basalt). Outcrops of ignimbrites have been observed in Bole (Eastern Addis Ababa) and Lideta areas (Central Addis Ababa) underlying the Addis Ababa basalt. Younger volcanic material of trachy-basalt, trachytes, ignimbrites and tuff belonging to the Wechecha, Furi and Yerer volcanoes are recognized overlying un-conformably on the Addis Ababa basalt in the western, southwestern and eastern part of the catchment. Akaki (including the well field), Dukem and Debre-Zeit area are covered with olivine basalt, scoria, scoriaceous basalts and vesicular basalts. In the upper part, in some places, intercalation of tuffs, sand and gravels are also recognized. In northeast, east and in smaller extent of the western part of Debre-Zeit, outcrops of trachytes, rhyolitic ignimbrites and tuffs are recognized covering the area (WWDSE, 2011).

The overburden covering the bedrocks includes soils, lacustrine and alluvial deposits. In the central, southeastern, northeastern, western (Kolfe-Keraniyo) and in northern (Gullelie) part of the catchment thick in-situ soil type cover is found. The lacustrine covers Bole, Lideta, Mekanisa, Akaki-Aba Samel area and Dukem-Debre Zeit area. Along Big and Small Akaki Rivers, in the southern and southwestern part of Addis Ababa, some alluvial deposits occur and minor deposits are also present along Kebena Rivers in the area northwest of Bole (Tadesse Yirga, 2004).

Most soils in this area are highly eroded and form thin soil cover. Most soil profiles are products of weathering of old basic and acidic rocks that outcrop in the central, western and southwestern parts of Addis Ababa. The detrital materials that are derived from elevated area of Entoto, Wechecha, Furi and Yerer are transported and deposited in the pediment and along the stream courses of Addis Ababa. The soils are black in color and their thickness varies from place to place primarily depending on the slope of the area. Clay is the dominant composition of the soil in the Akaki area. The thickness of the soils varies from 1m to 20m around the Akaki well field.

The alluvial sediments cover large parts of the Akaki River area along riverbanks. Along the Akaki River and the surroundings, the thickness of the exposed soil cover reaches up to 5m. Grain sizes are variable ranging from sand to gravel showing poor sorting. The alluvial sediments are characterized by high porosity and inter-granular permeability. These sediments constitute one of the potential aquifers in the Akaki area.

2.5.1.1. Stratigraphic Sequence

The area that covers the city of Addis Ababa and/or the Akaki river catchment consists of various volcanic rock units of different composition and age. Following a traverse from North (Entoto Mountain) to South (Kaliti-Akaki area), the geological formations change from the oldest volcanic sequences to the youngest. The volcanic stratigraphic sequence of Addis Ababa area has been proposed by many researchers. Haileselassie Girmay and Getaneh Assefa (1989) proposed the stratigraphy of the area starting from Sululta to Nazareth, based on Morton's geological map (Morton, 1974), unpublished student reports, K/Ar absolute age determination taken from different literatures and fieldwork to

clarify some geological uncertainties. They redefine the lithostratigraphic units and modified the existing stratigraphic sequence. Accordingly, the suggested Miocene-Pleistocene volcanic succession in the Addis Ababa area from oldest to youngest are: Alaji rhyolites and basalts, Intoto silicics, Addis Ababa basalts, Nazareth group, Bofa basalts and recent deposits.

a. ALAJI BASALTS

The Alaji group volcanic rocks (Alaji Rhyolite and Basalt) in this part of the escarpment were outpoured from the end of Oligocene until middle Miocene (Zanettin et al., 1974), extending from the crest of Entoto mountain (Northern part of Addis Ababa) towards the north (Haileselassie Girmay and Getaneh Assefa, 1989). This unit is composed of basalts, which show variation in texture from highly porphyric to aphyric with intercalations of gray and glassy welded tuff. This unit is underlain by tuffs and ignimbrites. The stratigraphic relationship of this unit with the Entoto silicics is difficult to determine as they occur in a fault contact. Mohr (1967) proved that the Entoto trachyte overlies the Alaji basalt. The age of the rock is 22.8My (Morton et. al., 1979).

b. ENTOTO SILICICS

These early Miocene age silicic volcanics could represent localized terminal episodes to massive Oligocene fissure-basalt activity in the Addis Ababa region (Morton et.al. 1979). The thickness of the flow becomes maximum on the top of Entoto ridge and thin both towards the plateau and the plain east of Addis Ababa. According to Zanettin and Justin-Visentin (1974) these lavas make up a thick pile of flows accumulated along east west fissures (east-west fault running from Kessem River to Ambo) and uplifted northwards. The unit is un-conformably overlain by Addis Ababa basalt on the foothill of Entoto and underlain by Alaji basalt.

The Entoto silicic is composed of rhyolite and trachyte with minor amount of welded tuff and obsidian (Haileselassie Girmay and Getaneh Assefa, 1989). The trachytic lava flow outcrops on the top of Entoto ridge and its foothills. The thickness varies and reaches the maximum of 30m nearby Kotebe covering the rhyolitic lava flows. It shows a quite uniform texture, and is constituted by phenocrysts of oligoclase, sandine and rebeckite

within a groundmass of plagioclase, iron oxide and minor quartz and mafic minerals. Two varieties of trachytic lava flows have been identified in the eastern side of the town, near Kotebe: a pale gray and a pink trachyte. The latter one is characterized by veins of hematized opal and by feldspar phenocrysts, which are often completely or partially altered with fine fractures filling of hematite (Varnier et. al., 1985).

The Entoto silicics are dated 21.5My by Morton (1974) and 22My by Morton et al. (1979). Thus from the general stratigraphy established by Zaneitin et al. (1974) both rhyolite and trachyte of the Entoto silicics belong to the "Miocene Alaji Rhyolite and Basalt" sequences.

c. ADDIS ABABA BASALT

The oldest rock, post-dating the Entoto silicics, is the Addis Ababa basalt. These units, which are mainly present in the central part of the town, are underlain by the Entoto silicics and overlain by Lower welded Tuff of the Nazareth group. It is porphyritic in texture, composed of labradorite, bytownite, olivine and augite as phenocrysts. The ground mass is made of andesine, labradorite, olivine, magnetite and pyroxene (Haileselassie Girmay and Getaneh Assefa, 1989). Olivine porphyritic basalts outcrop in the central part of the town that includes Merkato, Teklehaymanot and Sidist Kilo areas. The distribution of plagioclase porphyritic basalt is almost the same as that of the olivine prophyritic basalt, but only little more northwards. It outcrops in an area, which includes Sidist Kilo, General Wingate School and French Embassy. The thickness of the olivine porphyritic basalt varies from 1m or less in the foothills of Entoto, Lideta Airfield and Filwoha to greater than 130m at Ketchane stream (Morton, 1974; Varnier et. al., 1985).

The Lower Welded Tuff overlies both types of basalt nearby the Building College, the Kolfe Police School, the Kokobe-Tsebah School and Yeka-Mariam Church. On the other hand, only in the gorge of the Kechane stream the olivine pophyric basalt is overlain by the plagioclase porphyritic basalt, while elsewhere the relationship between them is very difficult to determine (Varnier et al., 1985). Age determinations for the Addis Ababa basalt give about 7My and seem to have no time/composition equivalent (Morton, 1974).

d. NAZARET GROUP

The units identified in this group denoted as Lower Welded Tuff, Aphanitic basalt and Upper Welded Tuff. The group is underlain by Addis Ababa basalt and overlain by Bofa basalts. The rocks outcrop mainly south of Filwoha fault and extend towards Nazareth.

i. Lower Welded Tuff

This rock outcrops as small discontinuous body in Filwoha, western parts of Addis Ababa and Sululta. It is glassy with abundant flame and has columnar joints. Generally, it is overlain by the aphanitic basalt and underlain by the olivine and plagioclase porphyritic basalt. The age of this rock as dated by Morton et al. (1979) at Addis Ababa and Sululta is 5.1 and 5.4My respectively. This age overlap with the period of the activity of Wechecha trachyte volcanoes, dated 4.6My. Wechecha is located 15km west of Addis Ababa and probably the sources of the Lower welded tuff at both localities (Morton et. al., 1979).

ii. Aphanitic Basalt

This basalt covers the southern part of the town, especially the areas of Bole International Airport and Lideta Airfield. The rock body shows vertical curved columnar jointing together with sub-horizontal sheet jointing. Kaolin, lenses are present at the contact of this basalt with the younger ignimbrite. This is a sure evidence for the hydrothermal alterations along a NE-SW fracture system, which may affect both the basalt and the Entoto trachyte. Moreover, the basalt is overlain by pumeacoues pyroclastic falls and the pyroclastic falls. It is underlain by a soil horizon that covers the plagioclase porphyritic basalt and overlain by soil horizon and tuff layers that lie below the young ignimbrite. It consists of labradorite, augite, rarely olivine and magnetite. The crystals of plagioclase show marked flow alignments. The age of the basalt in Addis Ababa ranges from 3.4 to 3.6My (Morton, 1974). Trachy-basalt outcrops around Repi and nearby General Wingate School. It is underlain by the plagioclase and olivine porphyritic basalt and overlain by the younger ignimbrite from which it is separated by tuffs and agglomerates. Its relation with the rocks of the group is not clear, but probably younger than the aphanitic basalt

(Getaneh Assefa et al., 1985). Moreover, phenocrysts that occur mainly in the rock are: sandine, labradorite, magnetite and augite.

iii. **Upper Welded Tuff**

This rock outcrops all over the southern part of the town including Bole, Nefas Silk and Railway station; nevertheless it is also present in the central and northern parts of the town. It is gray colored, vertically and horizontally jointed and composed of sandine, orthoclase, rebeckite, quartz, pumice and unidentified volcanic fragments (Getaneh Assefa et al., 1989). The welded tuff is underlain by aphanitic basalts and overlain by young olivine basalts. Age determinations made on a sample collected nearby Haile Gebreselassie road resulted 3.2My that overlap with the activity of Yerer trachytic volcanos (Morton et. al., 1979).

e. YOUNG TRACHYTIC FLOWS

This rock is predominating in the southwest part of the town towards Furi and Repi along the hills and foothills of Hana Mariam and Tulu Iyou. It is porphyritic with phenocrysts of plagioclase (albite-oligoclase) sandine, biotite within a groundmass of microlities of feldspar.

It is underlain by the tuff that covers the young ignimbrite and overlaying by alternating flows of plagioclase porphyritic basalt and rhyolite especially in the Repi hill. Its relation with the young olivine prophyrytic basalt is not clear as they outcrop in different parts of the areas; however, in a small outcrop nearby Aba Samuel Lake south, the trachyte underlies the olivine porphyritic basalt.

f. YOUNG BASALT AND ASSOCIATED SCORIA CONES

They outcrop southward from Akaki River where they appear in the form of boulders reaching a thickness of 10m. Vesicles are common features observed on these rocks. They are restricted and dominant in the southeast part of the town along the Debre Zeit Road. They contain phenocrysts of plagioclase, olivine that is partially and completely altered to iddingisite and augite within a groundmass composed of plagioclase, magnetite, pyroxene and olivine. This basalt is underlain by the tuffs, which cover the

welded tuff. The age of this basalt is 2.8My (Morton, 1974). The basaltic lava and cinder cones exist towards the southernmost part of the city along with the vesicular basalts. Some of them situated to the southeast and northeast of the Akaki well field seem to have erupted through these fractures as they are concentrated along the major NE-SW trending fault systems of Akaki and Dukem areas (Morton et. al., 1979)

g. BOFA BASALTS

This unit comprises of olivine porphyritic basalt, scoria, vesicular and scoriaceous basalt, and trachy-basalt lava flows. They extend in to the south from Akaki River and the unit is as thick as 10m (Anteneh Girma, 1994). They appear to have upper thick basalt of 20-40m over the Akaki well field but thinner to absent in other places.

h. RECENT DEPOSITS

These include alluvial, residual, and lacustrine deposits Quaternary to recent deposits. Lacustrine soils occur around Bole, Lideta, Mekanisa, between Aba Samuel Lake and Small Akaki River (WWDSE, 2011). Alluvial deposits are found in some places along Small and Big Akaki Rivers, especially South and South-West of the capital city. Thick alluvial deposit occurs in the area between Akaki Town and Aba Samuel Lake. The thickness varies between 5m and 50m in the south (AAWSA, 2000). It is often overlain by dark younger black cotton clayey soils. Residual soils are located in the central, southeast, northeast, and western flat plains (WWDSE, 2011).

Lithostratigraphy			Thickness	Age
Akaki Basalt		Olivine-phyric Basalt flows	>400m	Quaternary
Nazareth Group		Ignimbrite,tuffs agglomerate rhyolite,trachyte basalts	>300m	Late Miocene-Pliocene
Tarmaber Basalts		Basalt flows minor silicic rocks	>500m	Late Miocene
Alaji Formation		Mainly silicic rocks		Oligocene

Figure 2-2: Generalized stratigraphic column of the catchment (WWDSE, 2011).

2.5.2. Local Geology

In Figure 2-3 is given the 1:50,000 geological map of the study area. It is seen from the figure that the most extreme western and northwestern corners of the site area are underlain by silicic flows and pyroclastics rocks and by central silicic Furi volcano.

The silicic lava flows include light grey to greenish, strongly to moderately weathered, columnar jointed ignimbrite and minor trachyte and rhyolite flows, intercalated with variegated color tuffs, ash and agglomerates. The Furi trachyte includes the products the central silicic Furi volcano located southwest–west of Addis Ababa. The volcano is smaller center compared to Wechacha and Yerer volcanoes and rise only about 700m height relative to the surrounding plain. Radiometric ages of 4.0-3.7Ma have been reported for the Furi volcano (Mazzarini et. al., 1999). Furi volcano is built of predominantly trachytic lava flows and minor pyroclastics similar to Wechacha volcano. The trachyte is light grey–green in color, strongly layered, moderately to strongly weathered (white weathering), porphyrtic with phenocrysts of plagioclase and sanidine, pyroxene, rarely olivine generally altered to iddingsite. The map unit usually separates the overlying youngest map unit Olivine –Pyroxene Phyric basalt flows and the older underlying map unit basalt not exposed in the site area (WWDSE, 2009).

The south and southwest of Addis Ababa up to upper Awash and Debre Zeit (Bishoftu) is covered by Pleistocene age lava flows of akaki basalts. Numerous well preserved scoria and spatter cones stick out above the surrounding flow surface. The highest summit part of Yerer volcanic was affected by recent volcanism that produced scoria and spatters cones and associated basaltic lavas ascribed to the Akaki unit. The cinder cones and basaltic lava flows observed at the summit area of Yerer volcano probably belong to the same phase of volcanic activity (Gasparon et al., 1993).

Nazareth Group rocks covers the most northern, eastern and southeastern sectors of the site. In the central and western part of the site, it disappears underneath recent sediment cover. It represents the youngest volcanic episode in the site area. It is comprised specks of scoria cones and associated basaltic lava flows, alternating of basaltic flows and air fall pyroclastics is envisaged to have occurred as observed in places scoria pyroclastics

overlain by basaltic lava flow. They consist of pyroxene and olivine phyric basalts with phenocrysts of olivine, pyroxene and plagioclase. Age determinations have revealed 2.9 to 2Ma (Morton et al., 1979; Zanettin et al., 1980; W/Gabriel Giday et al., 1990).

The west central along the Akaki River representing a significant portion of the site area is covered by thick recent alluvial sediment deposits comprised of sand, silt and clay. It overlies the olivine-pyroxene phyric basalt lava flows map unit described before. The sediments are buff-brown to dark-brown in color and unconsolidated. The depositional basin appears to be a fault bounded northeast–southwest trending sort of graben now filled with thick alluvial sediments (WWDSE, 2011).

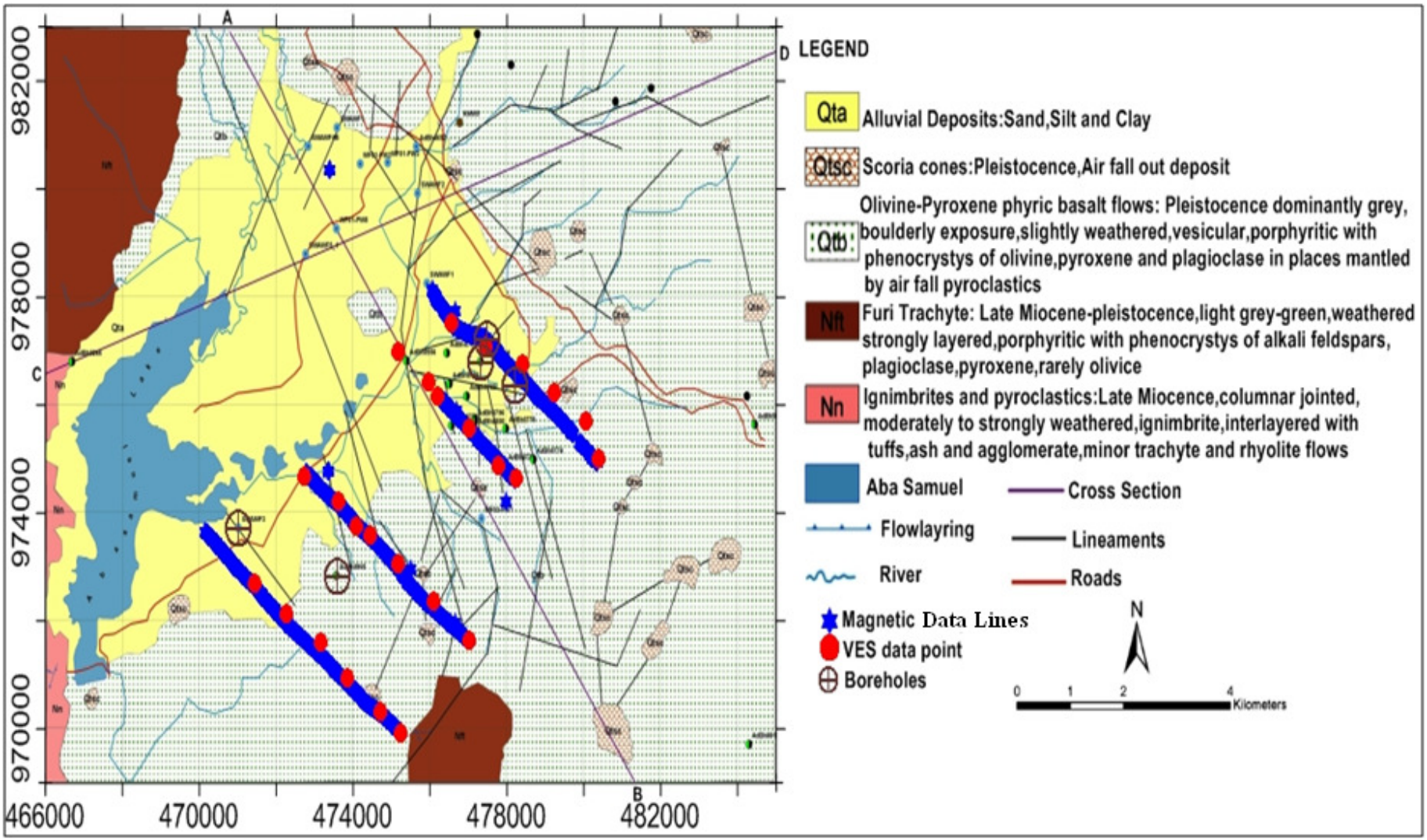

Figure 2-3: Geological map of the area with geophysical profile (Modified from WWDSE 2011).

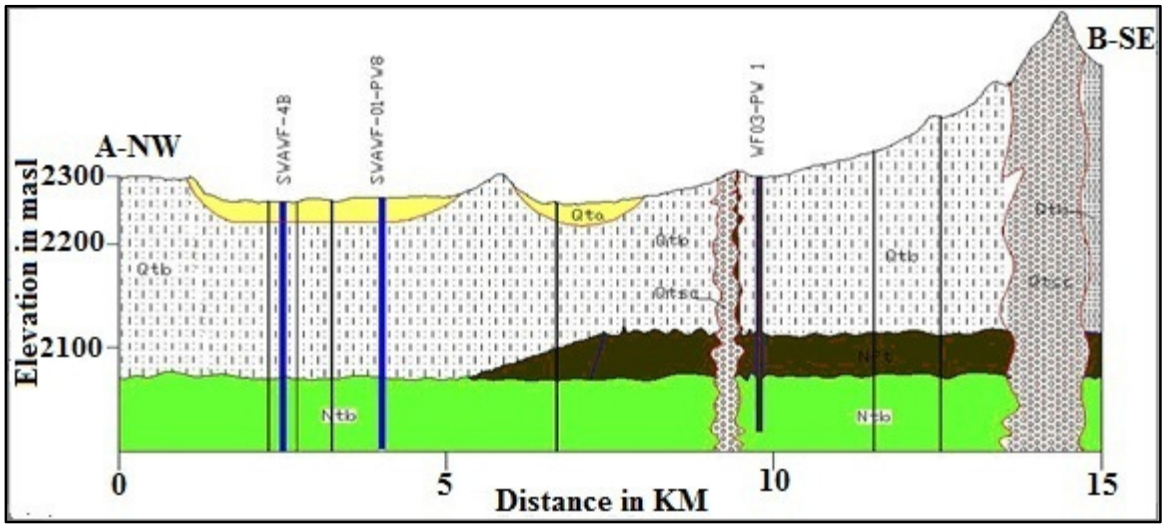

Figure 2-4: Geological cross-section along AB (NW-SE) (Adopted from WWDSE, 2011).

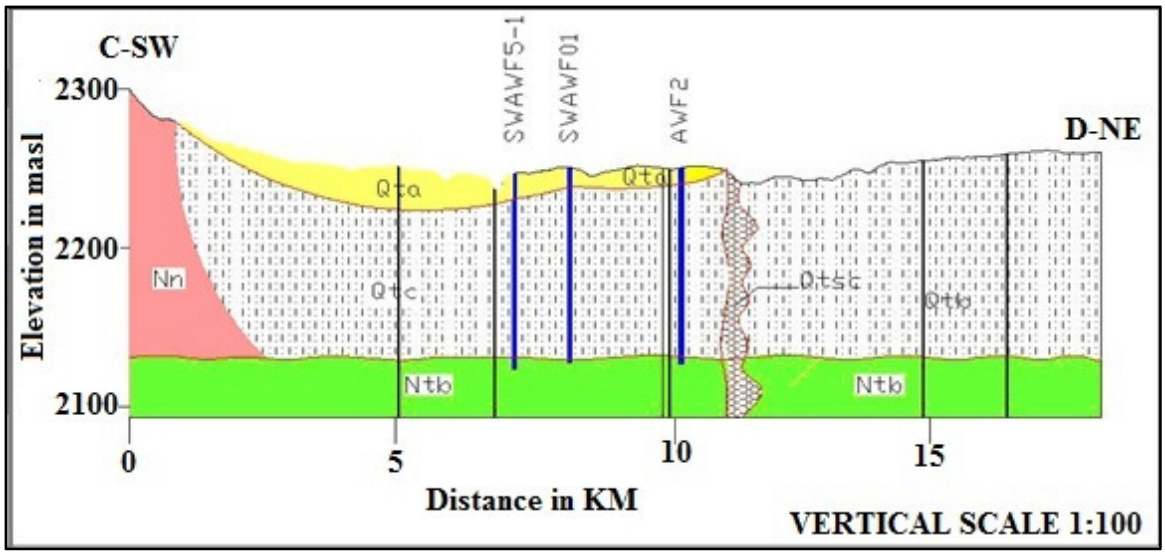

Figure 2-5: Geological cross-section along CD (NE-SW) (Adopted from WWDSE, 2011).

In the well field, thick soil cover of varying depth occurs especially in the part where agricultural activity exists. However, this decreases as one moves south of the well field, where the rocky outcrops and the agricultural activity eventually stops.

Basalts, rhyolites, trachytes, scoria, trachy-basalts, ignimbrites and tuff of varying ages form the main lithologies of the area. It is also overlain by fluvial and residual soils of varying depth (Girmay Kahsay, 2010).

2.5.2. Geological Structure of the study area

2.5.2.1. Lineaments

A number of conspicuous linear features (lineaments) have been recognized from topographic maps of the site area. The lineaments are marked by the rivers and streams that drain the site. They range in size from a few Kilometers to tense of kilometers. The major wide spread lineaments trend NE-SW and NW-SE, the less wide spread trend NNE-SSW and E-W (WWDSE, 2011).

2.5.2.2. Jointing

The Various rocks that make up the map units are affected by wide spread sets of joints, generally very closely spaced and display no visible displacement of the rocks on either side. They are a few centimeters to several meters long, tight and open, a few centimeters to half to one meters spacing. The strike of the joint sets is similar to that of the lineaments mentioned before. The main ones generally strike NW-SE (from 130^0-150^0 SE) and dip very steeply (85^0-90^0) and NE-SW (From 215^0-245^0SW) and dip steeply (75^0-90^0) (WWDSE, 2011).

2.5.2.3. Faults

The thick alluvial sediment occurs along Akaki River. This depositional basin appears to represent a fault bounded NE-SW oriented graben now filled with Quaternary basalt lava flows and recent alluvial material. The trend of the would be graben is similar to that of the MER system (WWDSE, 2011).

2.6. Hydrogeology of the area

The Akaki area groundwater prospective site is part of Adaa-Becho plains groundwater system which is found at the margin of the western part of the Ethiopian Rift Valley. The general hydrogeological set up of the basin is governed by the lithologic stratigraphy and tectonic of the area.

In the city scale for Addis Ababa, Tamiru Alemayehu et. al. (2005) characterized the rocks by ways of fracture porosity and interstitial porosity they exhibit and accordingly categorized the main aquifers into three groups:

a) Shallow aquifers: made of weathered volcanic rocks and alluvial sediments along the river courses,
b) Deep aquifers: made of fractured volcanic rocks that tap fresh groundwater, and
c) Thermal aquifers: those are located at the depths greater than 300m.

According to WWDSE (2008) the prospective site is recharged from large areas (Abay plateau and Upper part of Awash River basin). Part of the groundwater flow paths of the groundwater basin pass through Akaki area prospective site (SWAWF) and this makes the potential of the site prospective.

The Oligocene-Miocene Tarmaber basalts that cover the recharge zone of the groundwater basin, the pyroclastic rocks that cover most parts of the surroundings of Addis Ababa, the young basalt flows and scoria deposits that cover the surroundings of Akaki, the alluvial deposits along Akaki river flood plain and the fault lines which are all associated with the Ethiopian Rift system are the major geological phenomenon that are governing the hydrogeological conditions of the region in general (WWDSE, 2011).

A previous report (AAWSA and Seureca, 1991) had identified regional groundwater flow direction which is assumed to be north-south from Addis Ababa towards the Akaki well field. AGRA (1998) assumed groundwater flow direction in the well field is from the NE towards the SW. The groundwater flow system can be schematized with depth into two major categories: a shallow zone of active fast flow and a deeper zone of relatively slower flow and longer residence time. The shallow systems are confined to the upper permeable soil, sediment, and weathered rock zone (usually less than 50 meters). This zone is considered to be the phreatic near surface aquifer with high permeability supplying water to hand dug wells, low-discharge springs, and river base flows. Below this zone, there exists a fractured rock zone and volcano clastic deposits in places inter-bedded with paleosols (up to a maximum of 230 m depth). This zone is a major aquifer of the catchment dominantly confined in central and southern Addis Ababa. In the highlands, groundwater reserve is limited due to the absence of large faults and the existence of non-fractured massive volcanic forming the mountainous areas along the watershed boundaries. High flow exists in and around the Akaki well field where scoria

and fractured basalts provide the most productive aquifer (Tenalem Ayenew et. al., 2008). The groundwater flow direction within the prospective site do not flow along the Akaki River's flow direction, it flows almost perpendicular to the rivers flow direction (WWDSE, 2008). Groundwater in Akaki area prospective site exists in fractures of vesicular basalts and scoraceous basalts and in the pores of scoria.

The aquifers of the Akaki Well Field and its surrounding, the study area, are also of volcanic origin, largely related to processes of lava flow and tectonic fractures. Volcanic deposits of scoria, scoriaceous and vesicular basalts are the predominant rock types in the area. Tectonic activities in the region developed intensive and network fracturing/fissuring, which resulted in favorable conditions for groundwater circulation. In the study area and its surrounding, Anteneh Girma (1994) showed that there are four types of aquifers in the Akaki area. The first aquifer type, which is highly productive, is constituted by scoria deposits, scoracious basalt and alluvial sediments. The second type of aquifer comprises of highly fractured and fissured basalt while the third aquifer is of basalts with moderate productivity having fractures, vesicles and sparsely spaced joints, ignimbrite and agglomerates. The scoria cones and surge deposits form the last group of aquifer, which has low productivity.

CHAPTER THREE

3. THEORY OF GEOPHYSICAL METHODS

3.1. General

Geophysics, both solid earth or applied, is the scientific method that uses the science of physics with high degree of technological development employed to observe the hidden subsurface of the Earth. In applied geophysics, geophysical methods are developed to delineate the subsurface structure and to explore underground treasures. Nowadays, geophysicists are equipped with geophysical instruments which are capable of exploring up to several kilometers deep into the interior part of the Earth. Geophysics is not only applied for the subsurface studies but is also used to investigate the ocean and land surface of the Earth, which gives rise to the environmental application of geophysics.

Geophysical surveys greatly help in studying of groundwater potential in any hydrogeological setup and locate preferred borehole locations and determine the depth of aquifers. The property and thickness of various lithological units obtained from geophysical survey at different location has been given much attention in part by a desire to reduce the risk of drilling dry holes and also a desire to offset the cost associated with poor ground in groundwater. However, geophysical surveys are not always the most effective method of obtaining the information needed. For example, in some areas drill holes may be a more effective way of obtaining near-surface information than geophysical surveys. In some investigations a combination of drilling and geophysical measurement may provide the optimum cost benefit ratio.

Depending on the source signals, geophysical methods fall into two major groups: those that make use of natural fields of the Earth (passive methods), and those that require artificially generated energy as source signals (active methods).The passive methods utilize the Earth's natural fields which include like gravitational and magnetic. On the other hand, the active geophysical methods involve detection of responses for artificially generated local source fields and waves such as: electrical, electromagnetic and seismic. In general, the aim of geophysical prospecting is searching for local perturbations in the naturally occurring or artificial fields caused by obscured geological features.

Though, almost all geophysical survey methods have wider scope of utilizations, there is always one physical property for which a particular method is exceptionally sensitive and as such determines its specific range of applications. However, a number of geophysical methods may be applied simultaneously (integrated geophysical exploration) in solving certain geological problems and such approach greatly reduces the problem of ambiguity, which is the inherent drawback in the interpretations of results from one method, by complementing the information gap from the additional methods. Moreover, surface and drill hole geological information are of vital importance for the successful analysis and interpretation of geophysical data.

Of the number of geophysical methods that could measure variations in physical field of the Earth and its perturbations, the electrical and magnetic methods of prospecting have found major applications in groundwater investigations. This is because; the electrical methods are the most suitable to investigate the presence of saturated zones in the subsurface while the magnetic methods are, in addition to several advantages they offer, are the best tools that could map subsurface fractures detrimental for the movement of groundwater. These two methods have accordingly been used over the Akaki basin to investigate its groundwater potential and form the main methods used in this research work. The theoretical foundations of the methods are therefore briefly discussed in the following sections.

3.2. Theory of Electrical Surveys

The method of electrical survey is based on measurement of variations in electrical conducting properties of the Earth and as such measure variations in either resistivity or conductivity properties of the subsurface. Variation in resistivity is primarily caused by differences in the character of the subsurface rock and presence of water. Dry formations have poor electrical conductance and show very high resistivity. Increasing water saturation of the pores or cavities in the formation reduces its resistivity; the reduction in resistivity is partially controlled by the porosity. This occurs because water (in its natural condition) is an electrical conductor, and its presence in the interconnected cavities reduces the overall resistivity of the formation. There are, however, general differences in

the resistivity of various saturated formations. Silt, clay and shale have very low resistivity, sand and gravel with fresh water have moderate to high resistivity. In addition to aquifer material, water quality also affects resistivity. Formations filled with highly mineralized water show relatively low resistivity. Water in the fissures containing ions (e.g. Na^{+}, Ca_2^{+}, Mg_2^{+}, Cl^{-}, So_4^{2-}) reduces the resistivity of the rock. In contrast, those saturated with fresh water have relatively higher resistivity (Fletcher and Driscoll as cited in Aynalem Ali, 1999).

There are two procedures of measurement of variations in resistivity of the subsurface. These may be either sounding surveys or profiling surveys. The methods vary in the type of target they are looking for and their measurement layout. While sounding surveys, most commonly known as Vertical Electrical Sounding survey (or VES) measure the vertical variation of the subsurface at a point by assuming horizontal layer of the Earth while profiling surveys measure the lateral variation of the subsurface by assuming vertical variation in electrical properties of the Earth.

When it comes to the question groundwater resources potential studies, the method which is widely and commonly employed is the VES technique.

3.2.1. Vertical Electrical Sounding (VES) Principle

In Vertical Electrical Sounding (VES), the positions of electrodes are changed with respect to a fixed point (known as the sounding point) and the measured values reflect the vertical distribution of resistivity values on a geologic section.

Vertical electrical sounding consists of a symmetrical electrode array used to determine the resistivity of the subsurface which is assumed to be consisting of horizontally stratified layers. The procedure is used to determine the variations in resistivity in the vertical direction and is also called electrical drilling or commonly vertical electrical sounding (VES). By expanding symmetrically the distance between current electrodes about a point called the sounding point, while keeping the potential electrodes MN at the same position, provides a sounding curve corresponding to the apparent resistivity versus depth of the location. As the spacing between the current electrode increases, the

investigated depth will also increase. The two most commonly used arrays in electrical sounding survey are the Wenner and Schlumberger arrays. In this work, the data which was collected by using the Schlumberger electrode array techniques. When the Schlumberger array is used, the distance between the potential electrodes is not greater than one tenth of the current electrodes spacing. The advantage of this array is that initially only the spacing between the current electrodes is increased. However, at large current electrode spacing, the measured potential becomes very low and the distance between the potential electrodes is increased. Increasing the potential electrode spacing produces a 'step' in the apparent resistivity curve and it is good practice to obtain an overlap between the curve segments by obtaining two readings at different potential electrode spacing for two adjacent current electrode spacing. Segments obtained at larger potential electrode spacing can be shifted in order to produce a smooth curve (Gibson and George, 2003). In electrical prospecting to determine the depth and electrical resistivity of a series of horizontal or nearly horizontal ground, it is difficult to measure both parameters. In order to solve this problem, we should calculate the potential and the electric field, due to a point source of current, at any point on the surface of a stratified earth. This has advantages because of enables one to use axial symmetry of the potential filed about the vertical axis through the current source and the additive property of the potential is also be used.

Let us choose a cylindrical system of coordinate with the origin at the point source a direct current located on the surface. The subsurface consists of infinite number of layers separated by horizontal boundary planes, the deepest layer existing to infinite depth and the other layers have finite thickness $h_i = h_1, h_2, h_3 \ldots h_n$ and resistivities $\rho_i = \rho_1, \rho_2, \rho_3, \ldots, \rho_n$. Each of the layers is electrically homogeneous and isotropic.

The derivative of the potential based on the above conditions was first due to Stefanescu et al., 1930.

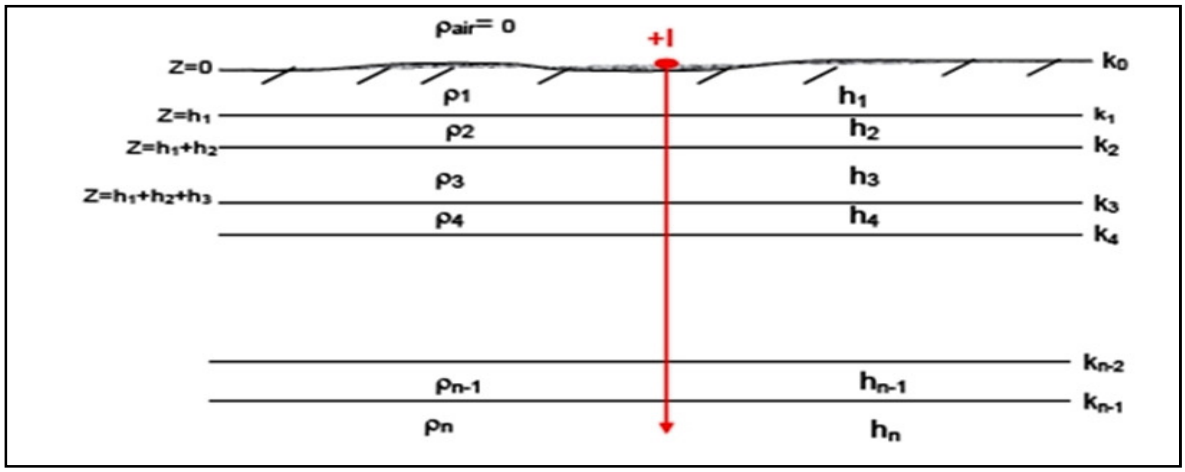

Figure 3-1: A multi-layer Earth and problem presentation for solution of the potential.

The electrical potential field V for direct current satisfies the differential equation of Laplace, which is

$$\frac{\partial^2 V}{\partial x^2} + \frac{\partial^2 V}{\partial y^2} + \frac{\partial^2 V}{\partial z^2} = 0 \tag{3.1}$$

The potential field has a cylindrical symmetry with respect to the vertical axis line through the current source. Therefore, Laplace equation in cylindrical coordinate is most appropriate.

For a solution symmetrical with respect to the vertical axis $\frac{\partial V}{\partial \theta} = \frac{\partial^2 V}{\partial \theta^2} = 0$ so,

$$\frac{\partial^2 V}{\partial x^2} + \frac{1}{r}\frac{\partial V}{\partial r} + \frac{\partial^2 V}{\partial z^2} = 0 \tag{3.2}$$

The particular solution of equation (3.2) can be obtained using the method of separation of variables and can be assumed to be of the form

$$V(r,z) = U(r)W(z) \tag{3.3}$$

Substituting equation (3.3) to (3.2) and divide throughout by the product U(r) W (z) gives

$$\frac{1}{U(r)}\frac{\partial^2 U(r)}{\partial r^2} + \frac{1}{rU(r)}\frac{\partial U(r)}{\partial r} + \frac{1}{W(z)}\frac{\partial^2 W(z)}{\partial z^2} = 0 \tag{3.4}$$

This equation is satisfied if and only if

$$\frac{1}{U(r)}\frac{\partial^2 U(r)}{\partial r^2}+\frac{1}{rU(r)}\frac{\partial U(r)}{\partial r}=\lambda^2 \quad (3.5) \quad \text{and} \quad \frac{1}{W(z)}\frac{\partial^2 W(z)}{\partial z^2}=-\lambda^2 \quad (3.6)$$

where **λ** is an arbitrary constant.

The solution of equation (3.6) may be given as

$$W(z)=c_1e^{-\lambda z} \quad \text{and} \quad W(z)=c_1e^{+\lambda z} \quad (3.7)$$

and that of equation (3.5) is given as

$$U(r)=c_3J_0(\lambda r) \quad (3.8)$$

where J_0 is the Bessel function of order zero.

The combination of equation (3.7) and (3.8) gives the particular solution of the differential equation given by equation (3.9), which is

$$\left.\begin{aligned} V(r,z)&=c_4e^{+\lambda z}J_0(\lambda r) \quad \text{and} \\ V(r,z)&=c_4e^{-\lambda z}J_0(\lambda r) \end{aligned}\right\} \quad (3.9)$$

where c and **λ** are both constants in the last of these equations.

Since, by theory of differential equation, every linear combination of the particular solution is also a solution, one can make **λ** to rough all possible values from zero to infinity and allowing the constant "c" to very independence of **λ** the general solution of equation (3.2) can be obtained as

$$V(r,z)=\int_0^\infty\left[\Phi(\lambda)e^{+\lambda z}+\Psi(\lambda)e^{-\lambda z}\right]J_0(\lambda r)d\lambda \quad (3.10)$$

Here $\Phi(\lambda)$ and $\Psi(\lambda)$ are arbitrary functions of the boundary conditions control the special form of these equations. From basic theory, the potential generated by a single point source of current intensity "I" located at the surface of an electrically homogeneous earth is given by

$$V=\frac{I\rho}{2\pi}\frac{1}{\sqrt{r^2+z^2}} \quad (3.11)$$

where **λ** is the resistivity of homogeneous Earth. Equation (3.11) can be written in integral form by using the so-called Lipchitz integral (also called the Weber Integral Formula) in theory of Bessel function as

$$\int_0^\infty e^{-\lambda z} J_0(\lambda r) d\lambda = \frac{1}{\sqrt{r^2 + z^2}} \tag{3.12}$$

So that equation (3.12) gives

$$V = \frac{I\rho}{2\pi} \int_0^\infty e^{-\lambda z} J_0(\lambda r) d\lambda \tag{3.13}$$

Equation (3.13) is also a solution of equation (3.2). Therefore, the combined solution will also be a solution to the equation, that is

$$V(r,z) = \frac{I\rho}{2\pi} \int_0^\infty \left[e^{-\lambda z} + \mathrm{X}(\lambda) e^{+\lambda z} + \Theta(\lambda) e^{+\lambda z} \right] J_0(\lambda r) d\lambda \tag{3.14}$$

where $\Theta(\lambda)$ and $\mathrm{X}(\lambda)$ are arbitrary function. Solutions of equation (3.14) are valid in all the layers of the subsurface. However, necessarily it is the same in different layers of the subsurface. Therefore, the potential due to a point source of current at the surface of a horizontally layered earth must in each layer satisfy

$$V_i = \frac{I\rho}{2\pi} \int_0^\infty \left[e^{-\lambda z} + \mathrm{X}_i(\lambda) e^{+\lambda z} + \Theta_i(\lambda) e^{+\lambda z} \right] J_0(\lambda r) d\lambda \tag{3.15}$$

This equation is called the Stefanescu Integral, with 'i' referring to the several layers of the subsurface.

Boundary conditions

For a potential set up by a single source of current at the surface of a horizontally stratified earth, the following boundary conditions are fulfilled.

1. At each of the boundary planes in the subsurface, the electrical potential must be the same

   $$V_i = V \text{ at } Z=h_i \tag{3.16}$$

2. The vertical component of the current density must be continuous on each boundary plane (the current density normal to the boundary planes …)

   $$(J_i)_N = (J_{i+1})_N$$

$$\frac{1}{\rho_i}\frac{\partial V_i}{\partial z} = \frac{1}{\rho_{i+1}}\frac{\partial V_{i+1}}{\partial z} \tag{3.17}$$

3. At the surface (z=0) the vertical component of the current density J_v (and hence that of the electric field intensity) must be zero everywhere except in the infinitesimal neighborhood around the current source. In air $J_{air} = 0$ and from condition (2), the vertical component of the current density at depth zero must be zero. Near the current source the potential must not approach infinity (must remain finite) as

$$V = \frac{I\rho}{2\pi}\frac{1}{\sqrt{r^2 + z^2}} \text{ at depth Z =0, as r } \rightarrow 0 \tag{3.18}$$

4. At infinite depth, the potential must approach zero, i.e. V $\rightarrow$0 as Z$\rightarrow\infty$

3.2.2. Basic Principles of Resistivity for Groundwater

Groundwater, through the various dissolved salt it contains, is ionically conductive and enables electric currents to flow into the ground. By measuring the ground and subsurface resistivity therefore gives the possibility to identify conditions necessary for the presence or absence of water. In resistivity surveying, especially in vertical electrical sounding (VES), conduction in rocks is mainly due to pore fluids acting as electrolytes. Water in its pure form is poor conductor but most water contains dissolved salts which facilitate current flow. Resistivities of rocks generally depend on the water content (porosity), the resistivity of the water, the clay content and the content of metallic minerals (Bernard, 2003). The following considerations help in the determination of the resistivity of rocks.

- A hard rock without pores or fractures is very resistive to the flow of electric current. This is generally observed in hard fresh Precambrian rocks.
- Dry sand without water is very resistive.
- Porous or fractured rock bearing free water has resistivity, which depends on the resistivity of the water and on the porosity of the rock.
- Impermeable clay layer, which is wet, has low resistivity but may not contain enough yields for successful groundwater exploitation.
- Mineral ore bodies (iron, sulphides) have very low resistivity due to their electronic conduction; usually lower or much lower than 1Ohm-m (Bernard, 2003)

To identify the conditions necessary for the presence of groundwater from resistivity measurements, the absolute value of the ground resistivity must be considered. Usual target for aquifer resistivity can be between 50 Ohm-m to 2000 Ohm-m (Bernard, 2003).

- In hard rock environment, which is considered very resistant to the flow of electric current, a low resistivity anomaly will be the target for groundwater.
- In a clayey or salty environment that is normally considered conductive, a comparatively high resistivity anomaly will most probably correspond to fresh water and thus will be the target in the case for groundwater exploration for domestic use.

Resistivity values of earth materials cover a wide range. The variety of resistivity has been the essential reason why the technique can be used for different applications (Loke, 2001).

In resistivity measurements, highest resistivities are associated with igneous rocks. Sedimentary rocks tend to be most conductive due to their high fluid content. Metamorphic rocks have intermediate resistivity (Table 3-1). Granites and quartzite have high resistivity ranges; sandstone and shale have intermediate resistivity ranges (Bernard, 2003). The resistivity therefore in a particular geological environment has an influence on the aquifer resistivity. Numerical values for various types of water are outlined (Table 3-2).

Table 3-1: Resistivity values for some common geological formations (Modified from Bernard, 2003).

Material	**Nominal resistivity (Ω-m)**
Sandstones	200 – 5000
Sandstone(weathered)	50-200
Clays	$1 – 10^2$
Gravel (saturated)	100
Basalt	$10\text{-}1.3*10^7$
Top soil	250-1700
Sand clay/clayed sand	30 – 215
Sand and gravel(saturated)	30 – 225

Table 3-2: Numerical values for various types of water (Modified from Bernard, 2003).

Type of Water	Resistivity (ohm-m)	Conductivity (micros/cm)	Salinity (mg/l)
Very fresh	200	50	35
Fresh	20	500	150
Salted	10	1000	700
Sea Water	0.3	30000	35000

In resistivity measurements current is injected into the ground via electrodes and the resulting potential is measured also by electrodes in the ground. The outer electrodes shows the current electrodes for injecting current into the ground and the inner electrodes are the potential electrodes connected to the voltmeter (Figure 3-2).

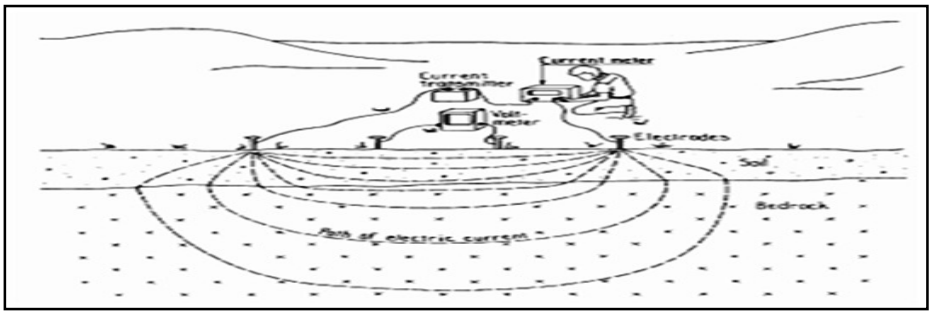

Figure 3-2: Sketch showing DC resistivity measurements (Modified from Robinson and Coruh, 1988).

Consider that a direct current of strength, I, is introduced in to a homogeneous and isotropic earth by means of two point electrodes as shown in the Figure 3-2. The potential difference between the two points P_1 and P_2 on the surface is given by using equation (3.19) as

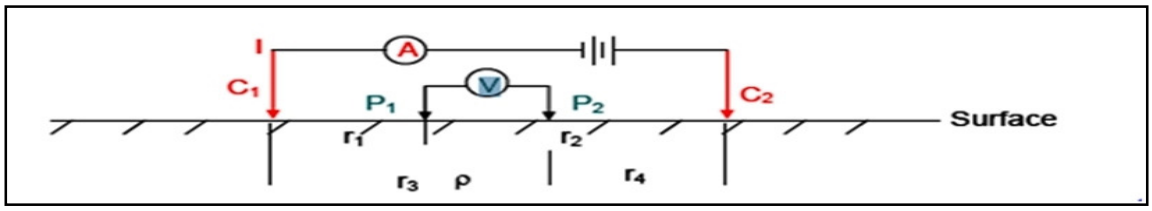

Figure 3-3: The arrangement of current and potential electrodes in a four-electrode system.

The Potential at P_1 $V_{P_1} = \frac{I\rho}{2\pi}\left(\frac{1}{r_1} - \frac{1}{r_2}\right)$

Similarly, the potential at $P_2 V_{P_2} = \frac{I\rho}{2\pi}\left(\frac{1}{r_3} - \frac{1}{r_4}\right)$

The potential difference $$\Delta V = \frac{I\rho}{2\pi}\left(\frac{1}{r_1} - \frac{1}{r_2} - \frac{1}{r_3} + \frac{1}{r_4}\right) \quad (3.19)$$

where the distances r_1,r_2,r_3 and $r_4$are all in meters. Therefore, after re-arranging the distances between the current and potential electrodes according to the well-known configurations, we can determine the resistivity of the homogenous ground.

The Apparent Resistivity

If the ground is homogenous, the potential difference measured is as a function of the true resistivity of the homogeneous earth and the geometric factor. But in reality the ground is locally in the homogeneous and the potential difference depends on the current applied, the resistivity of the subsurface medium and the geometrical factor (k) determined by electrode array or configurations types. The resistivity calculated from such non-homogenous ground is not a true resistivity rather it is called apparent resistivity (ρ_a) which can be related to the parameter as

$$\rho_a = k\frac{\Delta V}{I} \quad (3.20)$$

This apparent resistivity has to be interpreted using curve matching or inversion techniques to find estimated resistivity versus depth of the subsurface.

This are many type of electrode configurations used in ground surveys of which the most commonly used array are Wenner, Schlumberger and the Dipole-Dipole. Since, the electrode separation relate to the investigation depth and lateral solution power required, one can choose the best electrode configuration for planed survey at the initial of the survey. The expression for apparent resistivity in each of the array types will be different due to the difference in the geometrical factor (K) of each any type.

Take the Schlumberger array in which the electrodes are symmetrically placed a point at the center of the array as shown in the figure below.

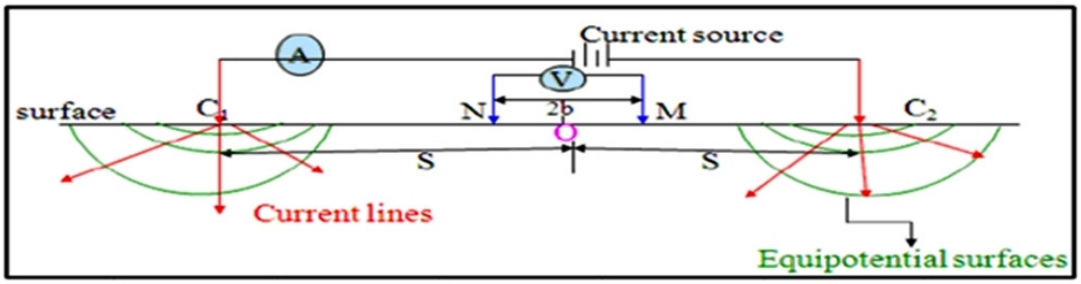

Figure 3-4: The electrode arrangement for the Schlumberger Array.

where r_1=s-b, r_2=s+b, r_3=s+b and r_4=s-b, 'O' is the center of the array (sounding point).

The potential difference ΔV using equation (3.19) is given by

$$\Delta V = \frac{I\rho}{2\pi}\left[\left(\frac{1}{s-b}-\frac{1}{s+b}\right)-\left(\frac{1}{s+b}-\frac{1}{s-b}\right)\right]$$

$$\Delta V = \frac{I\rho}{2\pi}\left[\frac{1}{s^2-b^2}\right]$$

$$\rho_a = \pi\left(\frac{s^2-b^2}{2b}\right)\left(\frac{\Delta V}{I}\right) \qquad (3.21)$$

where the geometric factor $k = \pi\left(\frac{s^2-b^2}{2b}\right)$ (3.22)

3.2.3. Interpretation of VES Data

The interpretation problem for VES data is to use the curve of apparent resistivity versus electrode spacing, plotted from field measurements on bi-log scale graph paper, to obtain the parameters of the geo-electrical section: the layers resistivity and thicknesses. From a given set of layer parameters, it is always possible to compute the apparent resistivity as a function of electrode spacing (the VES curve). Unfortunately, for the converse of that problem, it is not generally possible to obtain a unique solution. There is interplay between thickness and resistivity; there may be anisotropy of resistivity in some strata; large differences in geoelectrical section, particularly at depth, produce small differences in apparent resistivity; and accuracy of field measurements is limited by the natural variability of surface soil, rock and by instrument capabilities. As a result, different sections may be electrically equivalent within the practical accuracy limits of the field measurements.

To deal with the problem of ambiguity, VES field curves can be interpreted qualitatively using simple curve shapes, semi-quantitatively with graphical model curves, or quantitatively with computer modeling.

Master Curves

Layer resistivity values can be estimated by matching to a set of master curves calculated assuming a layered Earth, in which layer thickness increases with depth. For two layers, master curves can be represented on a single plot.

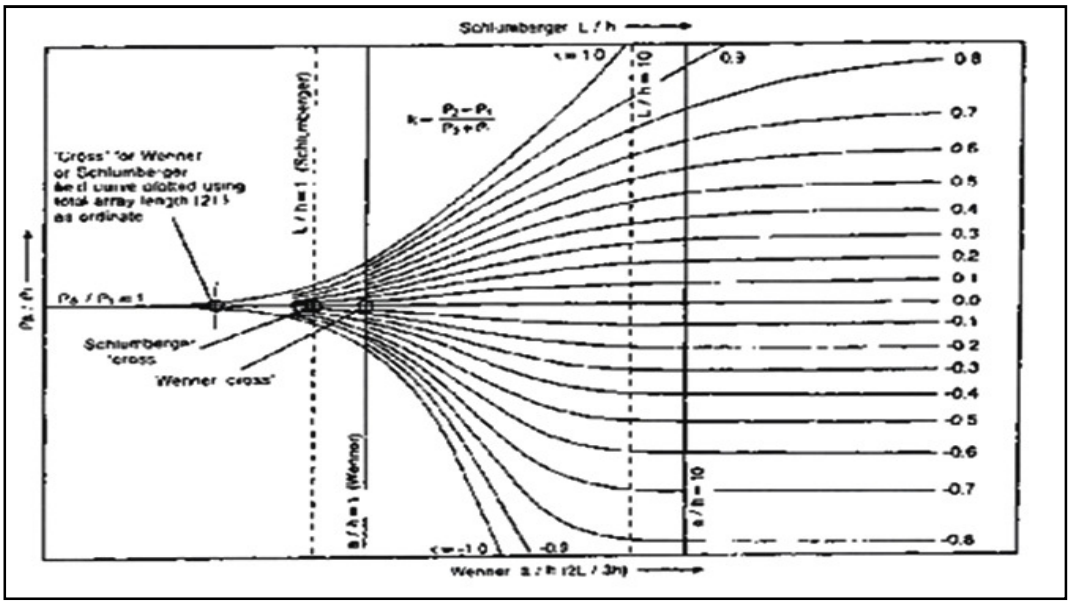

Figure 3-5: Master curve of the two layer Earth model.

Master curves: log-log plot with ρ_a/ρ_1 on vertical axis and a/h on horizontal (h is depth to interface)

- Plot smoothed field data on log-log graph transparency.
- Over lay transparency on master curves keeping axes parallel.
- Note electrode spacing on transparency at which (a/h=1) to get interface depth.
- Note electrode spacing on transparency at which (ρ_a/ρ_1 =1) to get resistivity of layer 1.
- Read off value of k to calculate resistivity of layer 2 from the formula given below:

$$k = \frac{\rho_2 - \rho_1}{\rho_2 + \rho_1}$$

Inversion

Curve matching is also used for three layer models, but book of many more curves. Recently, computer-based methods have become common:

- Forward modeling with layer thicknesses and resistivities provided by user, and
- Inversion methods where model parameters iteratively estimated from data subject to user supplied constraints.

Example (Barker, 1992)

Start with model of as many layers as data points and resistivity equal to measured apparent resistivity value.

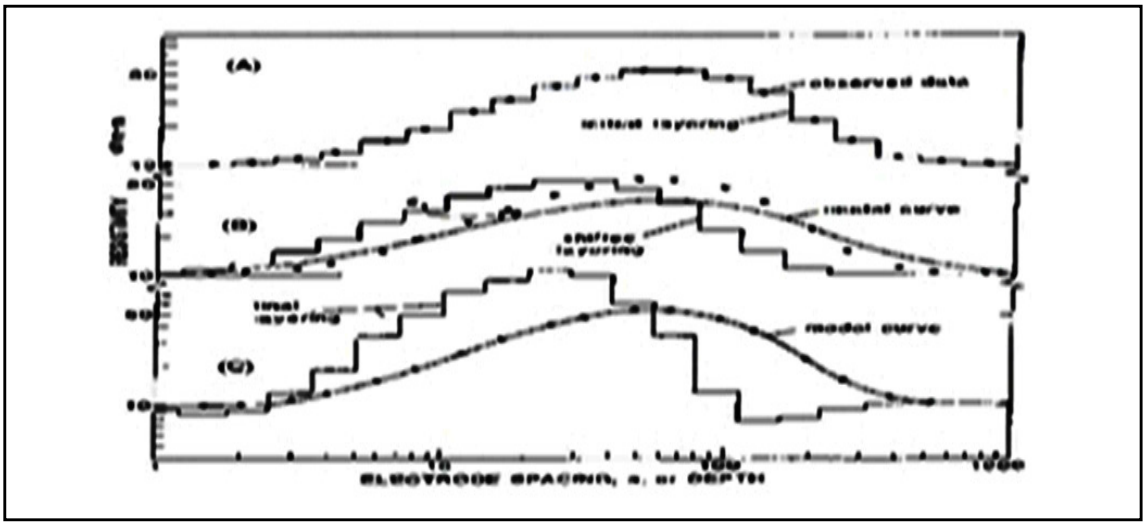

Figure 3-6: Curve matching (Adopted from Barker, 1992).Calculated curve does not match data, but can be perturbed to improve fit.

3.3. The Magnetic Method

The Earth's magnetic field resembles the field of a large bar magnet situated near the center of the Earth. Many geological formations, by virtue of their magnetic minerals content, will behave like large buried magnets and will then have a magnetic field associated with them. These local magnetic fields will be superimposed on the magnetic field taken, in the locality of such geological formations, and show deviations from the undisturbed Earth's magnetic field.

These changes or anomalies could be large or small in magnitude, and could either increase or decrease the Earth's main field. Their influences on the main field depend on

the geometry, orientation, depth of burial and magnetic properties of the body and the direction and intensity of the inducing Earth's field.

Magnetic surveys are used to locate and delineate:

- Magnetic iron ore deposits,
- Metallic ore deposits which may have either magnetite or pyrrhotite associated with them, and
- Geological structures like contacts, faults, dykes, etc.

Magnetic surveys are used in groundwater studies to map the depth to the magnetic basement rock and also it provide a valuable aid to lithological mapping, as the character of a magnetic anomaly is indicative of the rock. Moreover, it can also be applied in mapping structural features, which often provide a conduit for the accumulation of groundwater and, at times, act as barriers.

3.3.1. Principle of Magnetic Method

Magnetic force

The force between two poles of strength m_1, and m_2, situated a distance 'r' apart is given by:

$$F = \frac{m_1 m_2}{\mu r^2}\vec{r} \qquad (3.23)$$

Where, $\vec{r}$=unit vector from m_1 to m_2

μ= permeability = $\mu_r\mu_0$

μ_r= relative permeability (~ 1 for air and many rocks)

μ_0= permeability of free space =$4\pi\times10^{-7}$ henry/m

r = separation between m_1 and m_2

Flux density/Magnetic induction

A magnetic field strength gives rise to a magnetic flux, just as electric field strength can give rise to an electric charge flux (current). The magnetic flux density that is the flux per unit area, also called magnetic induction, is denoted by **B,** and the field strength by **H**. The magnetizing force (field strength) gives rise to the flux density, i.e. the cause of the magnetic field is the magnetizing force, thus

$$B = \mu H \tag{3.24}$$

where, μ is the absolute permeability of the medium on which **H** is acting. In SI units, the magnetizing force or field strength (**H**) is measured in ampere per meter [Am^{-1}]. The unit of magnetic flux is volt-second (V-s), also named Weber [Wb].Hence, the unit of flux density **B** is [Vsm^{-2}] or [Wbm^{-2}] which is also called tesla[T]. The magnetic fields that we measure in practice are flux densities. For most geophysical purposes, the tesla is too large as a unit and flux densities are more conveniently expressed in nanotesla [nT =10^{-9} T]. One nT is equals the basic unit of **B**, namely gamma [γ]. The absolute permeability (μ), being equal to **B/H** has its dimensions from:

$$\mu = \frac{B}{H} = \frac{v.\sec}{m^2}\frac{m}{A} = Ohm\ \frac{\sec}{m} = \Omega.\sec .m^{-1}$$

The absolute permeability of vacuum is denoted by μ_0, its value in SI unit is:
$4\pi \times 10^{-7}\Omega.sec.m^{-1}$, thus in vacuum the flux density due to a magnetizing force **H** will be

$$B = \mu_0 H \tag{3.25}$$

For most practical purposes, the absolute permeability of air, and even most rocks, may be taken to be μ_0.

The Earth's Magnetic Field

The Earth's magnetic field is akin to that of a dipole situated at the center of the earth with its magnetic moment pointing towards the Earth's geographical south. The Earth's magnetic field vector **F** is completely specified at any point by its elements. Figure 3-7 shows the elements of the Earth's magnetic field.

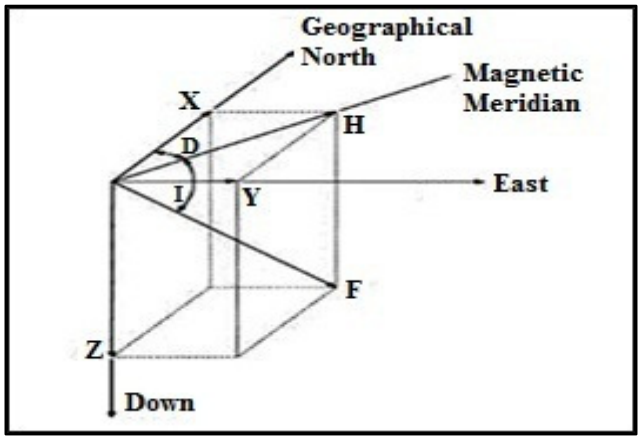

Figure 3-7: Elements of the Earth's magnetic field.

According to Figure 3-7, the Earth's total field is **F** makes an angle I (the inclination) with the horizontal plane. It can be measured by a dip needle and is also called magnetic dip. The angel D is the angle between geographic north and magnetic north, or the declination of **H** (here, **H** is the horizontal component of the total field vector, **F**) east or west of true north. In the northern hemisphere the magnetic field is directed downwards towards the north magnetic pole and in the southern hemisphere it is directed up wards and away from the south magnetic pole. At the magnetic equator the magnetic field is horizontal and at the magnetic poles the field is vertical i.e., the strength of the Earth's field varies from 25,000-30,000nT in the equatorial regions while 60,000-70,000nT, in the Polar Regions.

The amplitude of total field varies more rapidly along the N-S direction as compared to the east-west. On Figure 3-7, **Z** is the vertical component of the total field (**F**). It is directed downwards in the northern hemisphere (positive) and upwards (negative) in the southern hemisphere. **H**, which is the horizontal component of **F**, is directed towards magnetic north for both the Southern and Northern hemispheres.

Relative permeability, susceptibility and magnetization

It for a medium other than vacuum we write $\mu = \mu_r \mu_0$we get from equation (3.24)

$$B = \mu H$$
$$B = \mu_r \mu_0 H$$
$$B = \mu_0 H + \mu_0 (\mu_r - 1) H$$
$$B = \mu_0 H + \mu_0 k H \qquad (3.26)$$

where, we have put, $k = \mu_r - 1$, that is $\mu_r = 1 + k$

μ_r is a ratio of the two permeabilities: ($\mu_r = \frac{\mu}{\mu_0}$) and therefore is a pure number.

It is called the relative permeability of the medium, and κ is called susceptibility which is a dimensionless quantity. For a vacuum, μ_1=1 and k= 0.

From equation 3.26, to obtain in vacuum a flux density equal to the density μ**H** in the medium under consideration, we would need an additional magnetic field strength KH.

This additional field strength that may be said to be present at points of space occupied by a medium subject to a field strength H is known as intensity of magnetization M induced by H. The direct relation is given by:

$$M = kH \tag{3.27}$$

Since K is a pure number and M is measured in Am^{-1}. Further B and H are vectors we can state equation-3.26 more generally as magnetic induction (total field within a body) and written as:

$$B = \mu_0 (H + M) \tag{3.28}$$

Then, for the x, y and z components of **B**, in an orthogonal coordinate system, we have

$$\begin{aligned} B_X &= \mu_0 (H_X + M_X) \\ B_Y &= \mu_0 (H_Y + M_Y) \\ B_Z &= \mu_0 (H_Z + M_Z) \end{aligned} \tag{3.29}$$

Equation (3.27) implies, a magnetic body placed in a magnetic field becomes magnetized by induction. The magnetization (M) is proportional to the inducing external magnetizing force. The constant of proportionality K is the magnetic susceptibility. It is a dimensionless quantity.

Magnetic susceptibility is a measure of the degree to which a material gets magnetized. The larger the susceptibility the greater the intensity of induced magnetization (M) and hence the bigger will be the anomaly produced relative to the Earth's field. The susceptibility of rocks is almost entirely controlled by the amount of ferromagnetic minerals, their grain size, and mode of distribution and hence is highly variable.

Table 3-3: Magnetic susceptibility of different rocks.

Earth Material	**Susceptibility*10^{-3}(SI)**
Limestone	0-3
Sandstones	0-20
Rhyolite	250-37700
Basalt	0.2-175

3.3.2. Noise and Correction

All magnetic data sets contain elements of noise and will require some form of correction to the raw data to remove all contributions to the observed magnetic field other than those

caused by subsurface magnetic sources. In ground magnetic survey, it is always advisable to keep any magnetic objects like high electric power cable, railway and keys etc., which may cause magnetic noise, away from the sensor.

In all magnetic data, diurnal and IGRF correction can be applied. The most significant correction is for the diurnal correction in the Earth's magnetic field. Base station readings taken over a survey period of facilitate the compilation of diurnal correction.

$$DC = \left(\frac{BS_2 - BS_1}{T_2 - T_1} \right)(T_r - T_1)$$

Where DC=Diurnal Correction.

BS_2=Reading of Base Station-2.

BS_1= Reading of Base Station-1.

T_2=Observation time of Base Station-2.

T_1= Observation time of Base Station-1.

T_r= Observation time of each measuring points.

In order to produce a magnetic anomaly, the data have to be corrected to take into account the effect of latitude and, to a lesser extent, longitude. As the Earth's magnetic field strength varies from 25000nT at the magnetic equator to 69000nT at the poles, the increase in magnitude with latitude needs to be taken into account (Reynold, 1997).Survey data at any given point can be corrected by subtracting the theoretical filed value obtained from IGRF, from the measured value.

3.3.3. Interpretation of Magnetic Data

Once magnetic data have been corrected and reduced to their final form, they are usually displayed either profiles or as maps and interpretation procedures are different for the two cases.

A single magnetic anomaly can have the form of positive peak only, a negative peak only or a doublet consisting of both positive and negative peaks. In addition, the single largest unknown is whether there is any remanent magnetization and, if there is, its intensity and direction (J_r) need to be ascertained. It must also be remembered that many geophysical interpretation may not be unique. For this reason, it is always useful to use other

geophysical methods in the same area to help constraint the interpretations. If some geological information already exists for the area, then this should be used to help with the geophysical interpretations. There are two ways of interpretation: qualitative and quantitative techniques.

Qualitative interpretation

For qualitative interpretation the following profile curves and maps were prepared:

Profile Curves help to see the changes of the anomalous structure of the subsurface.

Statistical Filters such as averaging (Moving average) and median filters used to remove spurious noise or to smooth anomalies to make them more interpretable.

Contour Maps have traditionally been a popular way of presenting gridded data. These maps have largely been replaced by images in recent years. Like stacked profiles it can be difficult to choose a single contour interval suitable for all the data. Where recognition of absolute amplitudes of anomalies is important these presentations are important. Many interpreters continue to use contours because they are superior to images when gradients of anomalies are to be used in determining dips of structures.

Vertical and Horizontal Derivatives quantify the spatial rate of change of the magnetic field in vertical or horizontal directions. Derivatives essentially enhance high frequency anomalies relative to low frequencies.

Analytic Signal transformations combine derivative calculations to produce an attribute that is independent of the main field inclination and direction of magnetization as well as having peaks over the edges of wide bodies. Thus a simple relationship between geometry of the causative bodies and the transformed data are observed.

Tilt Derivative Filter (*TDR*): Magnetic data alone gives an idea about the general structure of the area. Filtering the magnetic data enhances and sharpness the anomalies and trends of the data and helps in the interpretation. The TDR and its total horizontal derivative are useful for mapping shallow basement structures.

Horizontal and Vertical Gradient: The main advantage of the horizontal gradient method is that it is least susceptible to noise in the data, because it only requires the

calculations of the two first-order horizontal derivatives of the field (Phillips, 1998). This method is also robust in delineating both shallow and deep sources while, the vertical gradient delineate shallow structures.

Reduction to Pole (RTP): The reduction to the pole operation is a data processing technique that recalculates total magnetic intensity data as if the inducing magnetic field had a 90^{o} inclination. This transforms dipolar magnetic anomalies to monopolar anomalies and converts asymmetric shape to symmetric shape that centered over their causative bodies which can simplify the interpretation of the data.

The guideline of qualitative interpretation of a given anomaly is given in the next table:

Table 3-4: Guideline of qualitative interpretation of magnetic profiles and maps (Adopted from Reynold, 1997).

Applies to	Magnetic character	Possible cause
Segments of a profile and areas of maps	Magnetically quite	Low k rocks near surface
	Magnetically noisy	Moderate-high k rocks near surface
Anomaly	Wavelength	Short=near surface feature
		Long=deep-seated feature
	±Amplitude	Indicative of intensity of magnetization
Profile*	Anomaly structure† and shape	Indicates possible dip and dip direction
		Induced magnetization indicated by negative to north and positive to south in northern hemisphere and vice versa in southern hemisphere, if the guidelines does not hold, it implies significant remanent magnetization present
Profile and maps	Magnetic gradient	Possible contrast in k and/or magnetization
Maps	Linearity in anomaly	Indicates possible strike of magnetic feature
Maps	Dislocation of contours	Lateral offset by fault
Maps	Broadening of contour interval	Down-throw of magnetic rocks

*Can be determined from maps also; †Structure=composition of anomaly, i.e., positive peak only, negative peak only or doublet of positive and negative peaks; k=magnetic susceptibility.

Quantitative interpretation

The essence of quantitative interpretation is to obtain information about the depth to particular magnetic body, its shape and size and details about its magnetization in two

possible ways. One is direct, where the field data are interpreted to yield a physical model. The other is the inverse method, where models are generated from which synthetic magnetic anomalies are generated and fitted statistically against the observed data. The degree of detail is limited by the quality and amount of available data and by the sophistication of either the manual methods or the computer software that can be used.

Depth estimation based on magnetic method

The depth estimation methods were used to determine the depth of the basaltic intrusions, basement complex and calculated the thickness of the sedimentary section in the studied area. These methods of interpretations are Euler deconvolution and 2D magnetic modeling. The advantage of these methods is to delineate any geological structures such as faults, dykes-like structures and volcanic basaltic intrusions, etc.

Euler Deconvolution Method

The Euler deconvolution method is a new tool used in interpretation of the potential methods (gravity and magnetic), for determining the depths of the contact between sedimentary rocks and basement rocks. This method depends on the structural index, level of the magnetic data and sampling rate. This method uses both horizontal and vertical gradients, to calculate the location and the depth of the anomaly sources (Keating, 1998 and Valeria, 1999).

The Euler deconvolution method uses the first order derivative to determine the magnetic sources and estimate their depths, but it requires an assumption about the nature of the source or structural index (Blakely, 1995). If (x_0, y_0, z_0) is the position of a magnetic source whose total field T is measured at (x, y, and z) and the total field has a regional value of B then Euler's equation reduces to:

$$(x - x_0)\frac{\partial T}{\partial x} + (y - y_0)\frac{\partial T}{\partial y} + (z - z_0)\frac{\partial T}{\partial z} = N(B - T) \qquad (3.30)$$

where (x_0, y_0, z_0) is the position of a source whose total field T is detected at any point (x,y,z), B is the background value of the total field and N is the degree of homogeneity,

interpreted physically as the attenuation rate with distance and geophysical as a structural index (SI).

The degree of homogeneity N is interpreted as a structural index (SI) (Thompson, 1982) which represents the source type and measure of the rate of change of field with distance. The choice of a proper structural index is crucial in order to attain correct depths and converging solutions over magnetic contacts. An index that is too low gives depths that are too shallow and too high gives estimates that are too deep. The correct index for a particular feature gives the best solution clustering and consequently the best depth estimates.

2D Modeling

The 2D modeling method was done to create the type lithology of the area with their respective thickness by constraining with the geoelectric section and the existing boreholes. The model was prepared along the profile and it indicates the faults and fractures of the study area. The model was carried out on GMSYS program on Oasis Montaj software.

CHAPTER FOUR

4. DATA ACQUISITION AND PROCESSING

4.1. Survey Traverse Selection

The water works design and supervision enterprise (WWDSE) selected an area south east of AA and Finfinne surrounding Oromia special zone to be studied in detail for groundwater resources potential based on previous detailed geological and hydrogeological and previous VES surveys (WWDSE, 2008, 2009). The area was planned to be studied for detailed investigation to understand the different lithologic units, ground water potential zones, geological structures and the physical properties of subsurface rocks. The methods chosen for the survey consist of VES and magnetic geophysical technique. The area was basically selected due to the presence of thick alluvial sediments that occur along Akaki River course. Moreover, this depositional basin appears to represent a fault bounded NE-SW oriented possible graben now filled with Quaternary basalt flows and recent alluvial material both factors suggesting a good groundwater resource potential. The trend of this graben is said to be similar to that of the MER.

The geophysical observations have been carried out all along the transect lines. The layout of the geophysical observation points and lines is shown in Figure 4-1.

4.2. Data Acquisition and Instrumentation

4.2.1. Vertical Electrical Sounding

VES survey was carried out along four transect lines oriented approximately northeast-southwest within the area and observations were made at around 1km sounding station spacing. A Schlumberger array using current electrode spacing 1500m (AB/2=1500m) was generally used to the maximum depth of interest. A total of twenty five VES distributed on four different lines were surveyed in the study area with transect separation ranging from 1km to 2.7km. Some of these VES were located near previously drilled boreholes to obtain control during interpretation. The VES observation points were generally located at 1km interval, however at places these positions were shifted

approximately up to 0.5km in line and sometimes off the transect lines to find suitable measurement ground.

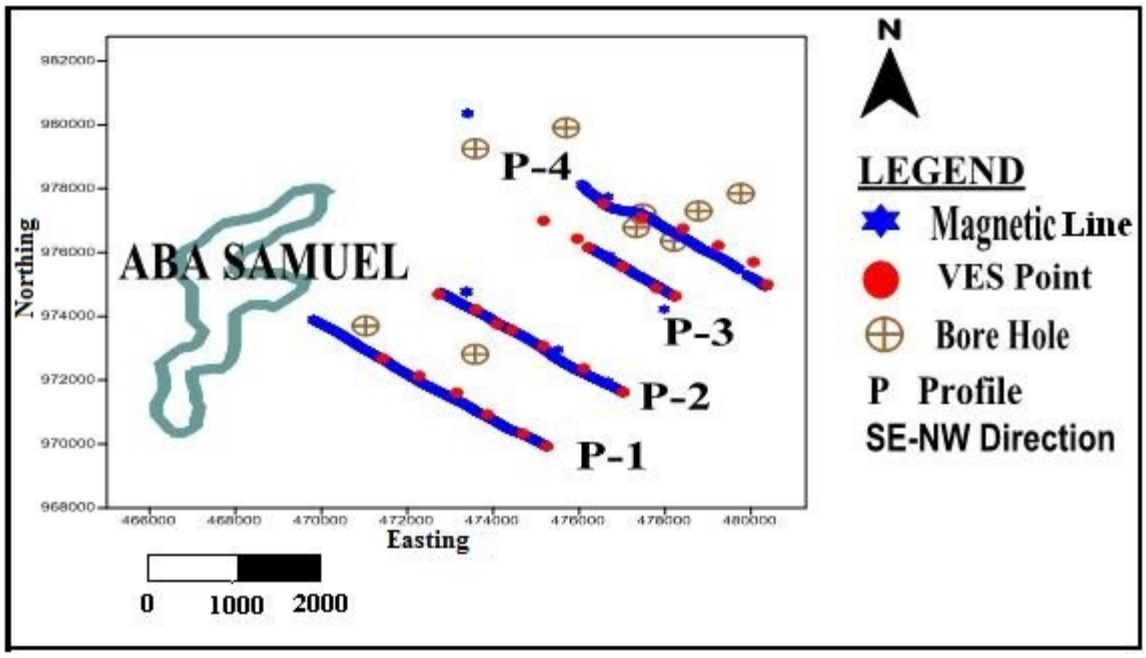

Figure 4-1: Location map of geophysical survey traverses and boreholes.

The instrument employed for the Vertical Electrical Sounding (VES) survey was the AGI Super Sting R1 electrical resistivity unit having a maximum current output of 2A. Handheld GPS was used to record the sounding point locations.

The apparent resistivity for different electrode spacing and the location of VES points were recorded. Data quality was controlled by concurrently plotting and examining the VES data in the field. The spread directions were dully recorded and these were used during data processing session for anisotropic correction purposes.

4.2.2. Magnetic Survey

A total field magnetic survey was carried out along VES lines and observations were made every 20m along all transect lines of the VES. A total of one thousand one hundred twenty four point data were acquired, with transect separation similar to that of the VES, i.e. ranging from 1km to 2.7km. The profiles where oriented about northwest-southeast in order to cross and so to detect the possible structure related to groundwater occurrence. Very few of these magnetic data were surveyed near to the previously drilled boreholes.

The total magnetic intensity, the time, date and the location of data points were recorded. Data quality was controlled by measuring the data three times to take the average and taking base station readings at the beginning and end of a 1km interval of the magnetic survey for the profile to overcome diurnal variation. In addition to this, the data was recorded from early morning to 11:30a.m to minimize the effect of diurnal fluctuations.

The magnetic survey was carried out using the G-856AX Portable Proton Precession Magnetometer, which is a versatile and rugged tool for such a survey and, handheld GPS was used for recording the time and position of the measured point.

4.3. Data Reduction and Processing

4.3.1. VES Data Reduction and Processing

4.3.1.1. VES Data Reduction

The apparent resistivity values are plotted on logarithmic transparent paper. In processing of the collected data, the apparent resistivity value on the ordinates and the electrode separation (AB/2) on the abscissa. The resistivity measurements were made by progressively increasing the potential electrode distance (MN) for relatively large increment of the current electrode distance (AB/2). In most cases the sounding curve is segmented due to overlap measurement and cannot be interpreted as it is. To have precise interpretations the segmented curves were shifted to the small MN curve points, so that the effect could be quantified and corrections could be made in order to obtain a single smooth curve that could be processed with the computer using IP2WIN and then WIN RESIST software (Velpen, 1995).

4.3.1.2. VES Processing

The field results of the study are presented in both qualitative and quantitative interpretations. In the qualitative interpretation the shape of the field curve is observed to get an idea qualitatively about the number of layers and resistivity of layers. The segmented curves were shifted to the small MN curve points to have precise interpretation. The results of this method of interpretation involved slice stacked of electrical resistivity maps and geo-electrical pseudo-sections. The VES data collected in the field were plotted on a bi-log paper and interpreted by using IP2WIN software to find

out initial model parameters of possible layers. Those parameters obtained from IP2WIN software were arranged and analyzed with the lithological units of existing boreholes to use as an initial model in RESIST inversion software which resulted and reliable electrical parameters of the layers with tolerable error ranging 1.5-4.5%. In the quantitative method geo-electrical parameter, i.e. true resistivity and layer thickness were obtained to make geo-electrical section using the software AutoCAD 2007.

The type of the curve and model parameters for the first curves of each profile are obtained from the software are presented on Figure 5-1.

A slice stacked map for different value of AB/2 reflects the lateral variation of apparent resistivity over a horizontal plane at a certain depth. In other words, these maps indicate distribution of apparent resistivity in the area against distance of current electrodes. The maximum depth penetration of the AMNB method is 1/3 to 1/4 of the maximum distance of current electrodes (Frohlich et al., 1996). These apparent resistivity contour maps for different values of AB/2 are illustrated in the Figure 5-2.

Pseudo-section qualitatively reflects the apparent resistivity distribution within the subsurface versus electrode spacing values (AB/2). These pseudo-sections are given in the Figure 5-3, 5-5, 5-7 and 5-9.

Geo-electric sections, in general, show the distribution of layer resistivities and thicknesses and are believed to give a closer approximation to the actual geoelectrical setting in the subsurface. In practice, most of the quantitative interpretation would be based on these sections. In order to prepare the geoelectric sections, the final model parameters (thickness and resistivity), in this work, are determined by an inversion software, RESIST. The geoelectric sections of all profile are presented in the Figure 5-4, 5-6, 5-8 and 5-10.

4.3.2. Magnetic Data Reduction and Processing

4.3.2.1. Magnetic Data Reduction

Data reduction and processing is the series steps taken to remove both signal and spurious noise from the data that are not related to the geology of the site. This process thereby

prepares the dataset for interpretation by reducing the data to only contain signal relevant to the task. These steps are summarized below:

i. **Data checking and editing:** involves the removal of spurious noise and spikes from the data that was caused by high tension power cable.
ii. **Diurnal removal:** corrects for the temporal variation of the Earth's main field which was achieved by subtracting the time synchronized signal, recorded at a stationary base magnetometer from the survey data.
iii. **IGRF removal:** removes the strong influence of the Earth's main field. This was achieved by subtracting a calculated of main field using Oasis Montaj from the diurnal corrected survey data.

4.3.2.2. Magnetic Processing

The processing of the total intensity map revealed a set of processes such as residual map, analytic signal, vertical derivative, horizontal and vertical gradient, tilt derivative filter (TDR) of analytic signal, RTP and the difference map between residual map and upward continuation map at 1000m (which shows the anomalies between the surface up to 500m depth and used for 2D modeling construction). All processed map are used for qualitative interpretation. The qualitative interpretation for the constructed magnetic maps, aims to get a clear view of the subsurface structures, estimation of the relative depth of the magnetic anomalies sources. The quantitative interpretation has been used to determine the depth of shallow subsurface structures (faults and dykes), fractures and contacts of the studied area. These methods of interpretations are Euler deconvolution and 2D magnetic modeling. The analysis and processing were done by specialized computer program (Oasis Montaj V.6.4.2, 2007). All processes of magnetic data are represented by profile curve, maps and 2D model in the next chapter.

CHAPTER FIVE

5. DISCUSSIONS AND INTERPRETATIONS

5.1. General

As discussed in the preceding section, the results of resistivity sounding survey are presented in the form of interpreted VES curve, pseudo-depth slice map and apparent resistivity pseudo-sections for the purpose of qualitative assessments and vertical geo-electric section, permitting quantitative interpretations. Again, the results of the magnetic survey also presented as curve and different maps. IGRF corrected map, analytic signal map, TDR map, and vertical derivative map, horizontal and vertical gradients of analytic signal, and RTP map for qualitative interpretation and differenced grid between residual and upward continuation map for 2D modeling. Then, Euler deconvolution and 2D model for quantitative assessments. In this section, the results will be presented and discussed profile-wise except the slice map for VES and magnetic maps.

5.2. Discussions and Interpretation of VES

5.2.1. Interpreted VES Curves

Apparent resistivity versus electrode spacing plotted on a bi-log scale is interpreted using the IP2Win to obtain the initial model parameters to be entered in to inversion software (RESIST) by constraining it further with the existing boreholes. It is seen from the interpreted field curves that a very good correlation between the field data and the interpreted model sections are obtained for all the four VES points. This is attested by an RMS error of 1.5 to 4.5% obtained for the sounding data. An illustration is made using four interpreted VES curves, one each from each of the survey traverses and these are given in Figure 5-1. In the four sounding curves, a 4 to 7 layer of the subsurface is seen too well represents the subsurface (with the AB/2 of 1500m used for the survey). The rest of interpreted VES curves are found in Annex-1.

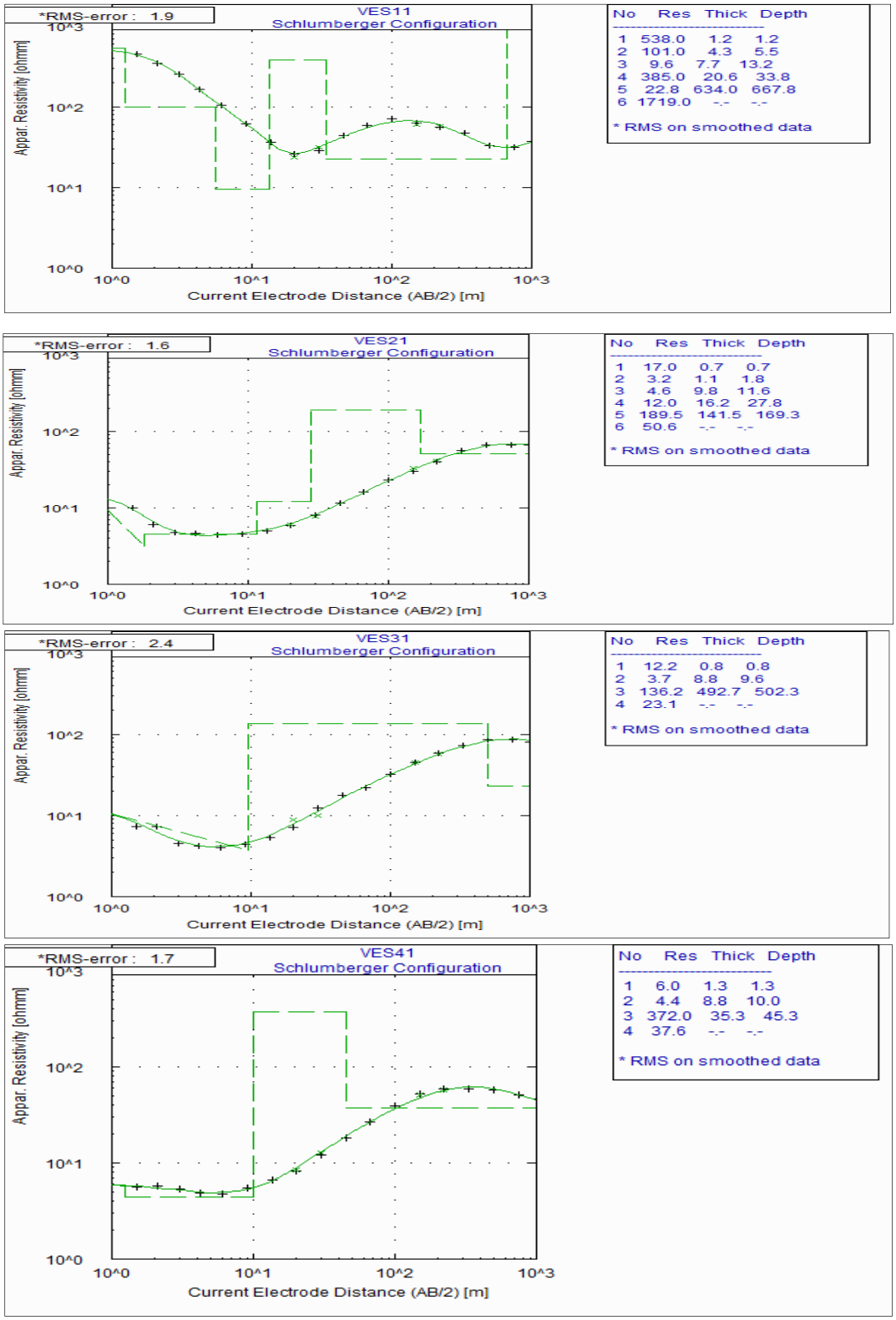

Figure 5-1: Interpreted VES curves of the four sounding points.

5.2.2. Sliced-Stacked Section

The apparent resistivity sliced pseudo-depth map shown in Figure 5-2 is prepared by superimposing the two dimensional apparent resistivity plan maps for selected AB/2 values of 1.5, 20, 45, 100, 220, 5500, 1000, and 1500. All VES points are used for qualitative assessments of the electrical nature of the geologic medium. The sounding points are almost evenly distributed so it is believed to give a good representation of the ground overall.

5.2.2.1. Sliced-Stacked for different AB/2.

In the figure below, the slice stacked maps were constructed for AB/2=1.5, 20, 45, 100, 220, 500, 1000 and 1500m. The choice of such spacing depends on the variability between them and to show the lateral variations of resistivity at different pseudo depth. These maps reflected the lateral variations of the electric resistivity over a horizontal plane at a depth of about 0.75, 10, 22.5, 50, 110, 250 and 750m respectively. Specifically, the map shows the relative variation of the apparent resistivity value of the whole area laterally as well as vertically at different depths of the spacing of current electrodes. It is found that the apparent resistivity value varies considerably from 0-460 Ohm-m. According to Figure 5-2 the most interesting feature of this sliced plot is the low resistivity zone, (<120Ω-m) that occupies the vast portion of the survey area. The value of the high apparent resistivity value zone decreases as the investigation depth increases. The value of the low apparent resistivity zones observed in the west, northwest and southeast parts of the area for all selected AB/2. On the other hand, the relatively very high resistivity response, (>200 Ω-m) that is found in the northeast and eastern part of the area for all AB/2 except AB/2=20m and high resistivity response (>100 Ω-m) that is found in northeast part at all AB/2. However, both high resistivity zone decreases with depth up to AB/2=500m and finally low resistivity zone dominates in all AB/2.

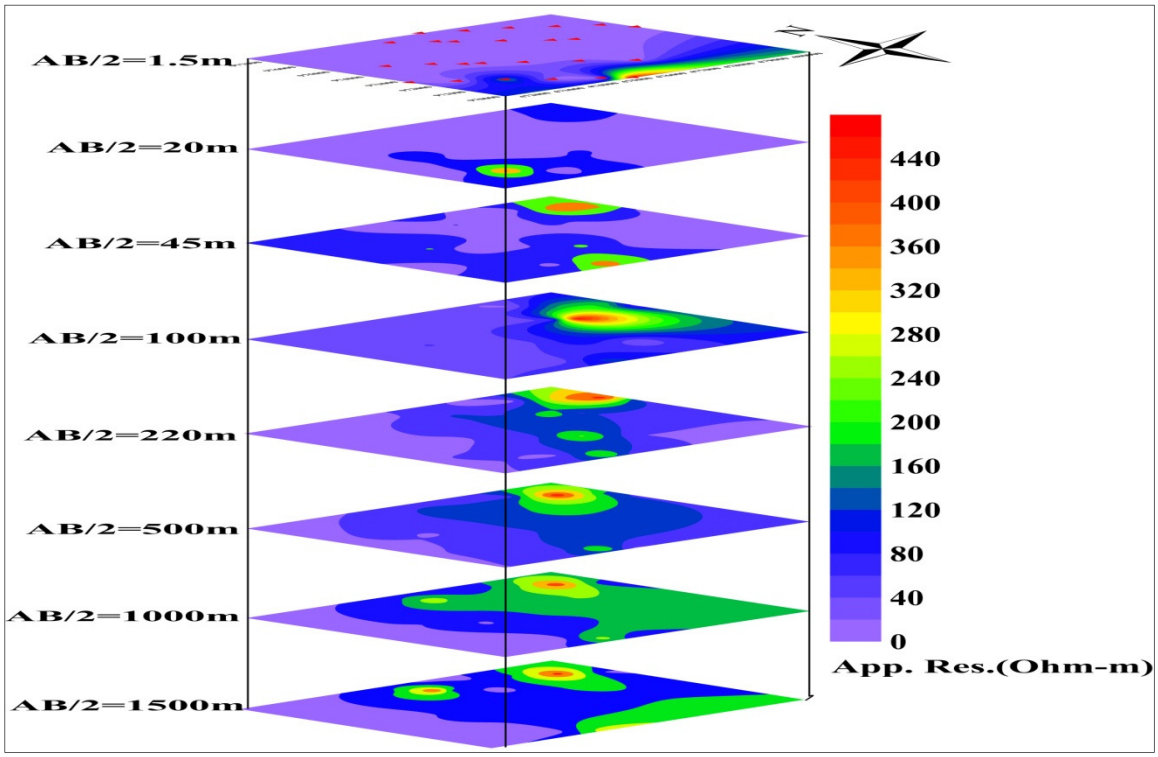

Figure 5-2: Sliced stacked map for different AB/2.

5.2.3. Pseudo depth section and Geoelectric Section of the Profiles

The data after reduction and filtering of VES data along all survey lines were used to construct the pseudo-sections in order to identify the distribution of different resistivity values in the lateral and vertical direction. The softwares which were used for the construction of pseudo-section of the VES data were SURFER (Version 10) software. The qualitative interpretation of pseudo-section gives preliminary idea for identification of high potential of groundwater and examination to see relative resistivity variation for preparing geo-electric sections.

The final result from one dimensional inversion of VES data along all survey lines were used to construct the geoelectric sections in order to identify the distribution of different lithologic units in the vertical direction. The softwares which were used for the inversion of the VES data were IP2WIN and WIN RESIST whereas the plotting was carried out by using AutoCAD (V 2007). The lithologic logs from boreholes that are lying on these profiles were used to fix the thickness of each layer by grouping the rock samples based

on their type and degree of weathering and fracturing. The pseudo-depth sections along these survey lines were examined to see the relative resistivity variations when preparing geo-electric sections.

5.2.3.1. Profile One

Pseudo depth section

The pseudo-depth section constructed for VES-11, 12, 13, 14, 15 and 16 that lie on the survey traverse line-1 are given in Figure 5-3. According to this figure, there is a lateral variation in resistivity in the top most part of the section with prominent high resistivity top zones mapped between VES-11 and VES-12. This high resistivity zone is not extending to large depth. Otherwise, the vast region under the section shows extensive coverage of the low resistivity zone. The resistivity ranges (0 to 100 Ohm-m) of this low resistivity region are indicative of potential water saturation.

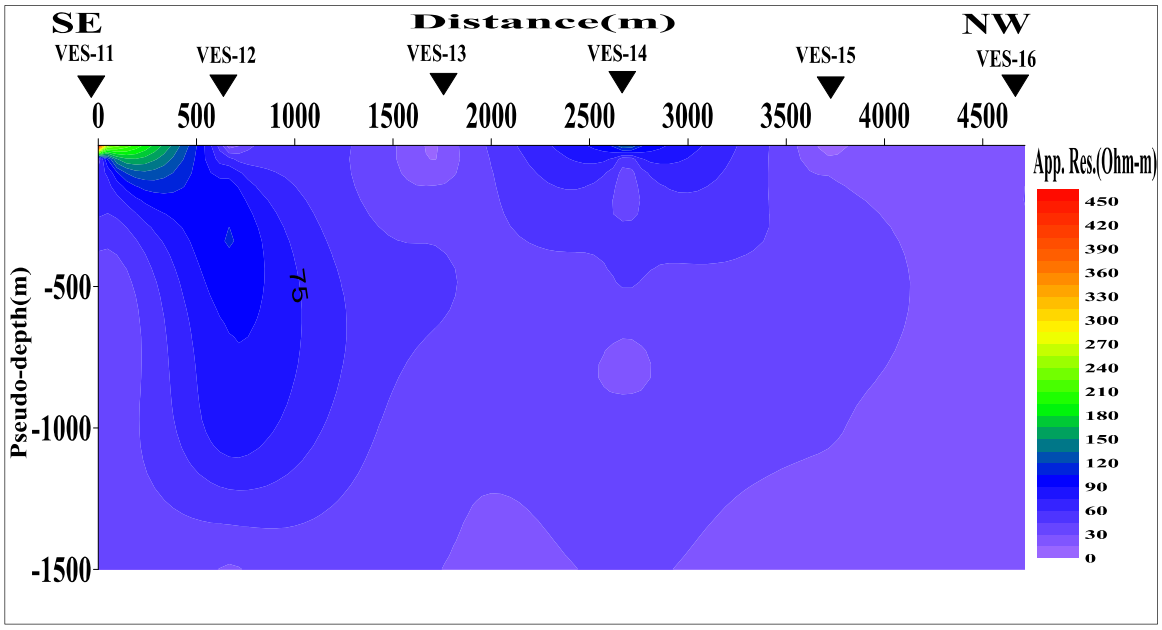

Figure 5-3: Pseudo depth section of Profile one.

Geoelectric Section

The resulting geoelectric section constructed from the interpreted layer parameters of the six VES lying on this traverse is given in Figure 5-4. A borehole SWAWF3 (WWDSE, 2011) is located near profile-1; especially close to VES-16 was also used to constrain the depth and identify the lithological units beneath these VES points during modeling. In

essence, the lithological description of the borehole depth section (given in Annex 2-A) with their resistivity parameters from each interpreted VES were used to prepare the geoelectric section shown below (Figure 5-4).

Near-surface geoelectric layer that has highly variable resistivity ranging from about 19-580 Ohm-m. The difference in the resistivity values is due to the variation in the amount of grain size. Areas with high resistivity values indicated the presence of gravel and sand as top soil, while those with relatively low resistivity values indicated the presence of clay intercalation with sand and the thickness variation are about from 0.5-1.3m and may be attributed to the top soil with alluvial cover (sand, clay and silt).

The second geoelectric layer is marked by resistivity values ranging from 4 to 242 Ohm-m. The thickness variation is from 4.8-17m. This layer likely reflects clay and slightly weathered basalt.

The third geoelectric layer that corresponds to the moderately saturated layer manifests resistivity value varies highly, i.e., 15-442 Ohm-m with thickness variation from 8.5-368.5m and may be represented clay intercalated with sand and silty, vesicular basalt with boulder sand slightly and highly weathered and fractured basalt. This layer has little potential of groundwater due to its resistivity of 112 Ohm-m under VES-14 and 16 as compared to the other.

The resistivity of the fourth geoelectric layer that corresponds to moderately saturated layer varies from 20-169 Ohm-m and its thickness also varies from 6.3m-infinite for VES-13 and 57.6-347.5m to the rest VES. The type of lithologies of this layer may be volcanic ash, silty clay and slightly weathered, moderately to highly fractured and weathered basalt. From the section, this layer has relatively good potential of groundwater especially under VES-13, 14 and 16 with the resistivity ranging from 37-67 Ohm-m.

The thickness of the next layer varies from 313.2m-582.3m with lateral variation of resistivity from 16-71 Ohm-m and the layer may be moderately to highly weathered and fractured basalt. From geoelectrical point of view, the fifth layer in the sequence seems to

be more promising for its high potential of ground water. The resistivity signature, within this section, ranges from 16 to 71 Ohm-m is a thought to be a response of a conductive basaltic rock. The likely litho-compositional interpretation is that; this layer may comprise highly weathered and fractured scoraceous basalt with a possible intercalation of clay materials.

The bottom resistive layer is detected intermittently at the location of VES-11(5031 Ohm–m) and most probably represents dry and fresh basaltic bed rock. And for VES-12, 15 and 16, the resistivity is 12 which may be representing fine grain sediment like clay, sand, silt and moderately fractured basalt which has potential of groundwater.

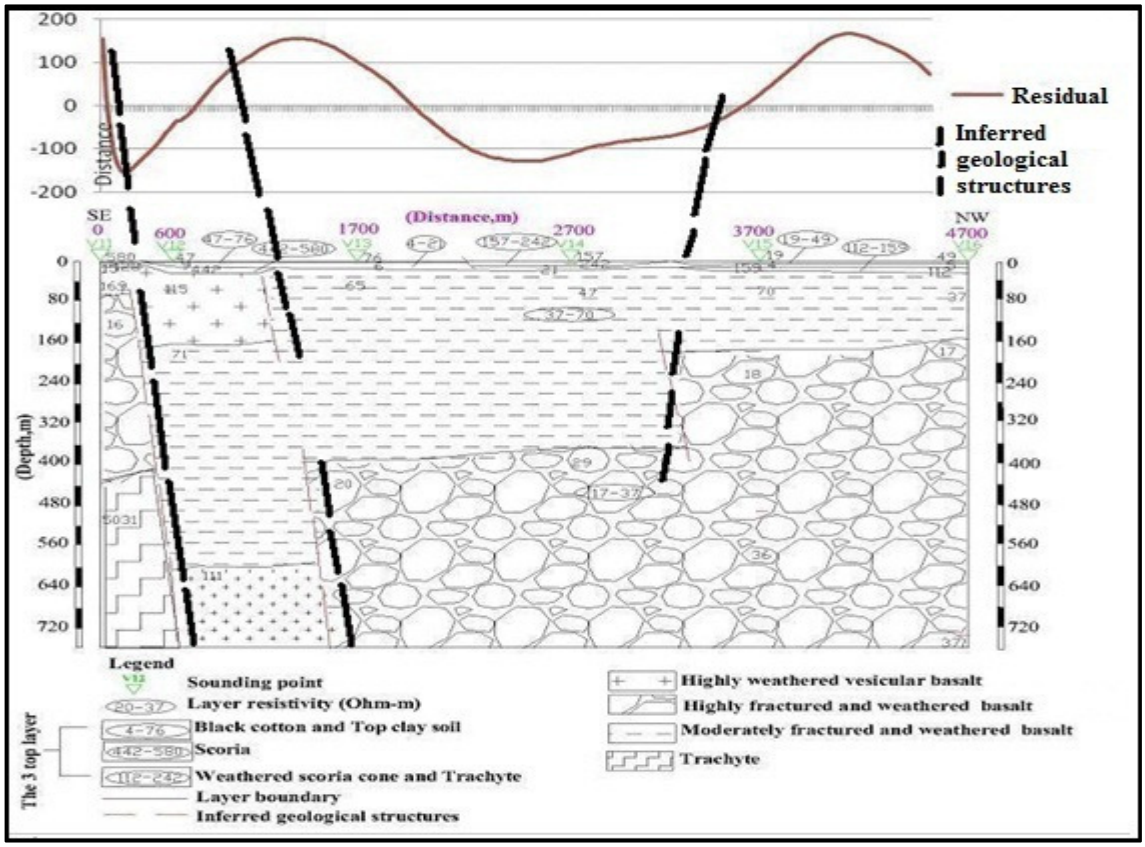

Figure 5-4: Magnetic profile plot and geo-electric section of Profile one.

From the above Figure 5-4, the magnetic curve and geoelectric section shows the same pattern in geological structures which may be concluded as discontinuities of geological structures like contact, fractures or faults. The inferred geological structures exist at an approximate horizontal distance of 300m, 1100m and 3400m on magnetic and electrical analysis.

5.2.3.2. Profile Two

Pseudo depth section

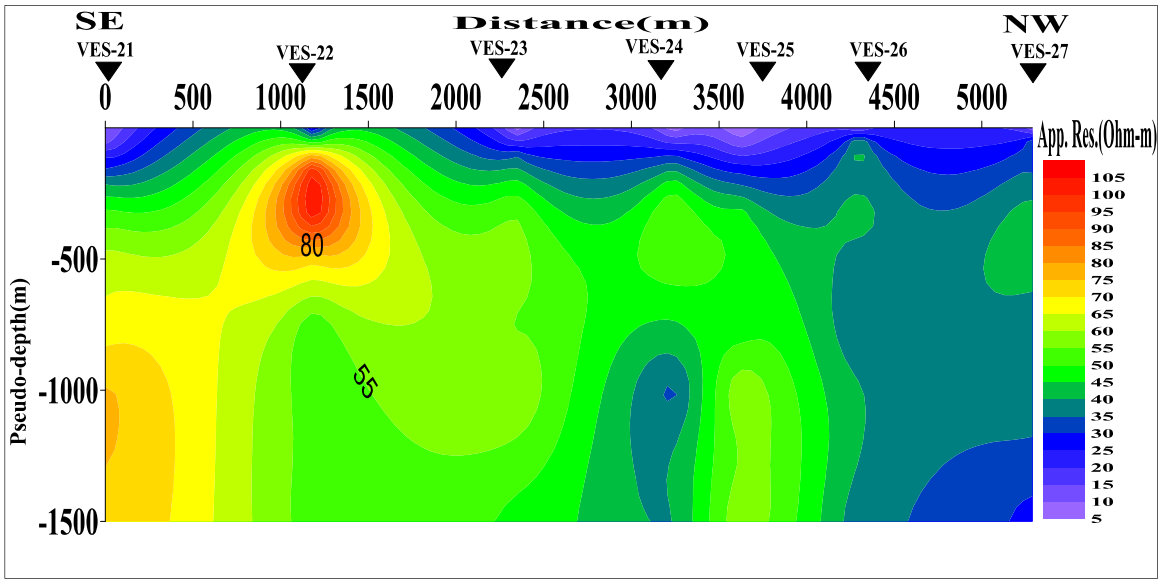

Figure 5-5: Pseudo depth section of Profile two.

The pseudo-depth section constructed for VES-21, 22, 23, 24, 25, 26 and 27 that lie on the survey traverse line-2 are given in Figure 5-5. According to this figure, there is a lateral variation in resistivity in the section with prominent high resistivity away from the top zones mapped between VES-21 and VES-23 but relatively high resistivity exists near to the top zone mapped at VES-22. This high resistivity zone is extending to large depth at VES-21. Otherwise, the right side of the section has relatively small resistivity near to VES-26 and 27. The large area of the top of the section has small resistivity (<45 Ohm-m) and the deep depth of VES-27 small resistivity value. The vast region under the section shows extensive coverage of the low resistivity zone. The resistivity ranges (5 to 75 Ohm-m) of this low resistivity region are indicative of good potential water saturation.

Geoelectric section

The resulting geoelectric section constructed from the interpreted layer parameters of seven VES lying on this traverse is given in Figure 5-6. A borehole Dewara Guda (UNEP, AA report, 2003) is located near profile-2; especially close to VES-25 was also used to constrain the depth and identify the lithological units beneath these VES points during modeling. In essence, the lithological description of the borehole depth section

(given in Annex 2-B) with their resistivity parameters from each interpreted VES were used to prepare the geoelectric section shown below (Figure 5-6).

The top geoelectric layer that has resistivity ranging from about 11-38 Ohm-m and the thickness variation are about from 0.4-1m and may be attributed as black cotton soil. The second geoelectric layer is marked by resistivity values ranging from 3 to 14 Ohm-m. The thickness variation is from 2-15.9m. This layer likely reflects top clay soil. The third geoelectric layer manifests resistivity value varies moderately, i.e., 78-81 Ohm-m with thickness variation from 13.1-13m and may be represented moderately weathered vesicular basalt and 267-287 Ohm-m with thickness variation from 33.3-47.3m and may reflects weathered scoria.

The resistivity of the fourth geoelectric layer that corresponds to moderately saturated layer varies from 33-95 Ohm-m and its thickness also varies from 101-119.9m. The type of lithologies for resistivity variation of 33-38 Ohm-m, and 72-95 Ohm-m may be highly, and moderately fractured and weathered basalt respectively. From the section, this layer has relatively good potential of groundwater with the resistivity ranging from 33-95 Ohm-m.

Subsequently, the thickness of the geoelectric layer varies from 86.7-131.8m with lateral variation of resistivity from 14-78 Ohm-m and the layer may be sand and highly weathered and fractured basalt. This geoelectrical layer in the sequence seems to be more promising for its high potential of ground water. The resistivity signature, within this section, ranges from 14-78 Ohm-m is thought to be a response of a conductive basaltic rock. The likely litho-compositional interpretation is that; this layer may comprise highly weathered and fractured scoraceous basalt with a possible intercalation of fine grain sand materials.

The bottom relatively conductive layer is detected with lateral resistivity variation ranges from 26-72 Ohm-m and most probably represents moderately to highly fractured and weathered basalt. This layer has good potential of groundwater.

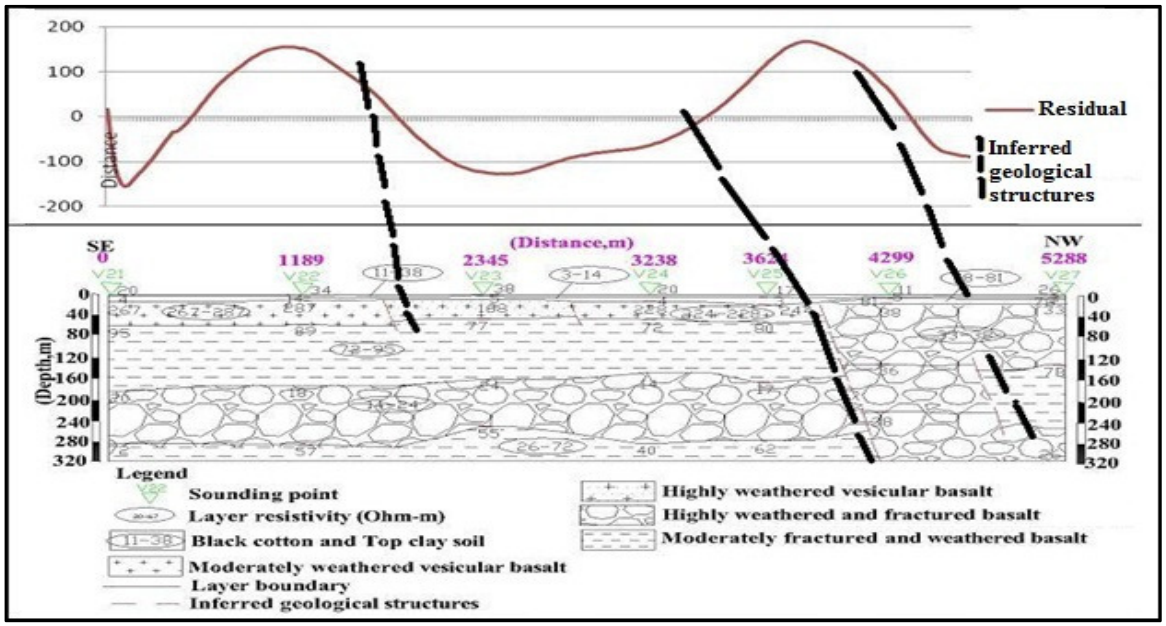

Figure 5-6: Magnetic profile plot and geoelectric section of Profile two.

From the above figure, the discontinuities of geological structures are identical in horizontal position in the curve and plausible Earth model. The magnetic curve and geoelectric section shows the same pattern in geological structures which may be concluded as contact, fractures or faults. The inferred geological structures (discontinuities) exist at an approximate horizontal distance of 1850m, 3750m and 4600m on magnetic and electrical result.

5.2.3.3. Profile Three

Pseudo depth section

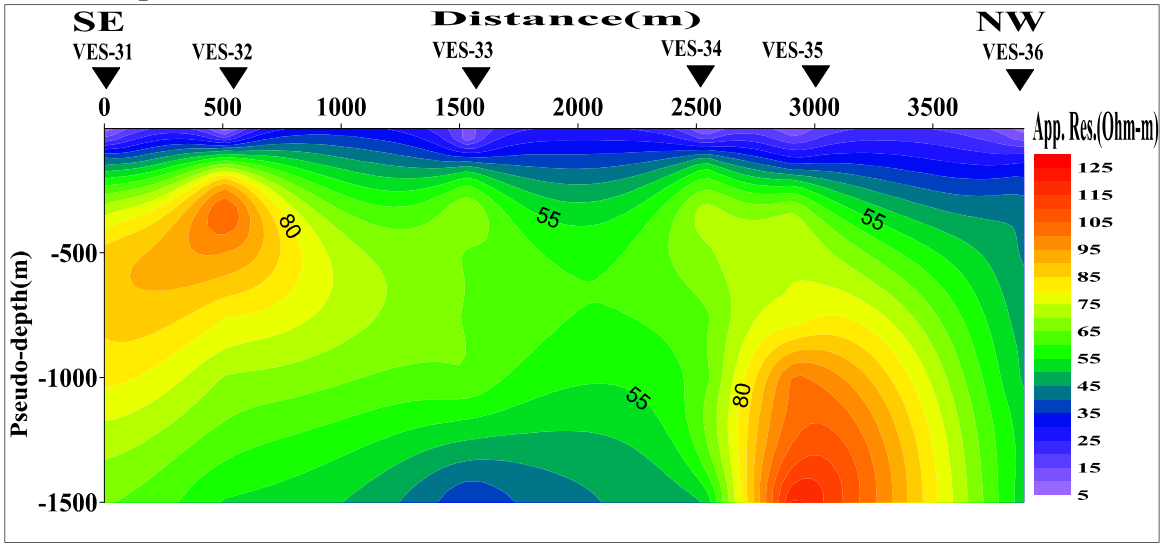

Figure 5-7: Pseudo depth section of Profile three.

The pseudo-depth section constructed for VES-31, 32, 33, 34, 35 and 36 that lie on the survey traverse line-3 are given in Figure 5-7. According to this figure, there is no lateral variation in resistivity in the section at the top zones mapped for all VES point. The resistivity of the section between VES-34 and 36 is increases with depth. The middle portion of the section (between VES-32 and 34 has relatively small resistivity than the other side of it). This region under the section shows good coverage of the low resistivity zone. The resistivity ranges (5 to 70 Ohm-m) of this low resistivity region are indicative of good potential water saturation.

Geoelectric section

The resulting geoelectric section constructed from the interpreted layer parameters of six VES lying on this traverse is given in Figure 5-8. A borehole BH24 (Alema Tesfaye, 2009) is located near profile-3; especially close to VES-36 was also used to constrain the depth and identify the lithological units beneath these VES points during modeling. In essence, the lithological description of the borehole depth section (given in Annex 2-C) with their resistivity parameters from each interpreted VES were used to prepare the geoelectric section shown below (Figure 5-8).

The top geoelectric layer that has variable resistivity ranging from about 34-48 Ohm-m and the thickness variation are about from 0.2-0.6m and may be attributed as black cotton soil.

The second geoelectric layer is a combination of three layers from the interpreted VES curve due their negligible resistivity variation which marked by resistivity values ranging from 1-14 Ohm-m. The thickness variation is from 0.7-2 m. This layer likely reflects top clay soil.

The third geoelectric layer manifests two distinct regions of resistivity value varies from 53-57 Ohm-m and 105-226 Ohm-m with thickness variation from 142.1-174.2m and 179.7-348.9m respectively. This layer may be represented weathered scoria and moderately weathered and fractured scoracious basalt. This layer has potential of groundwater at under VES-35 and 36 with resistivity ranging from 53-57 Ohm-m.

The fourth geoelectric layer resistivity varies from 13-74 Ohm-m and its thickness also varies from 90.9-326.1m. The type of lithologies of this layer may be moderately to highly fractured and weathered basalt. From geoelectrical point of view, this layer in the sequence seems to be more promising for its high potential of ground water. The resistivity signature, within this section, ranges from 12-46 Ohm-m is a thought to be a response of a conductive basaltic rock intercalated with clay.

The bottom resistive layer is detected intermittently at the location of VES-35 (179 Ohm–m) and most probably represents weathered basalt. The rest part of the layer has resistivity variation ranges from 49-88 Ohm-m which may represent moderately fractured and weathered basalt.

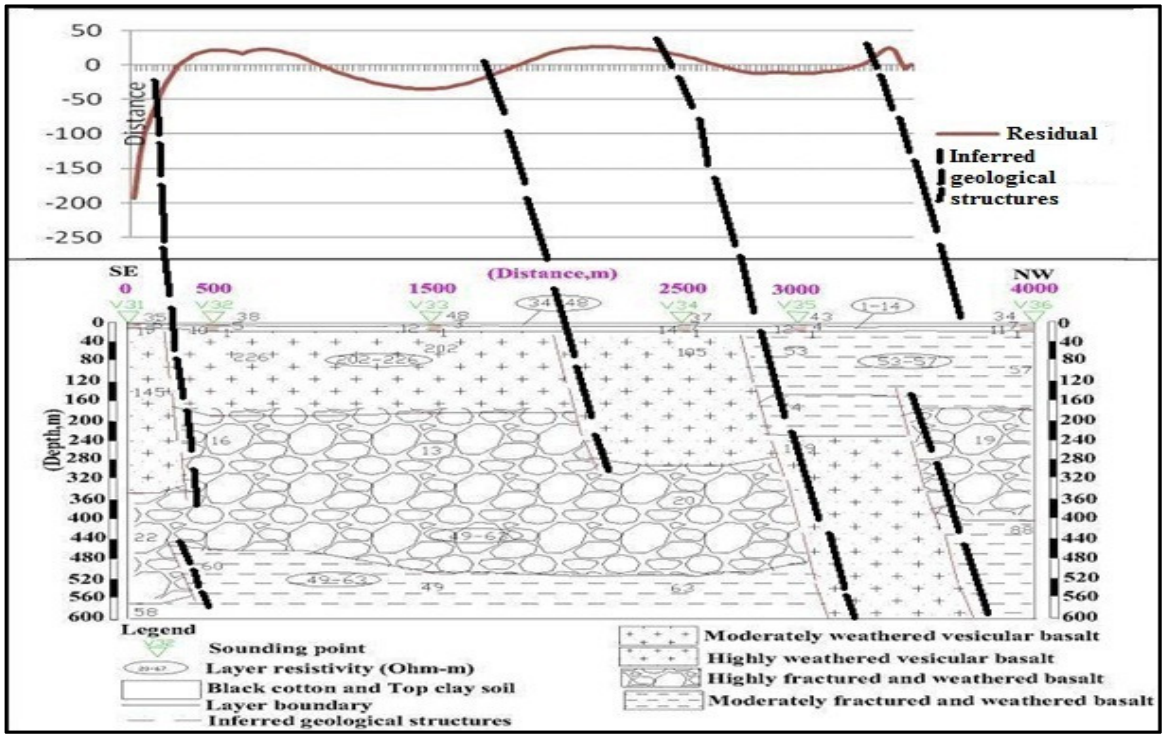

Figure 5-8: Magnetic profile plot and geo-electric section of Profile three.

From the above figure, the discontinuities of geological structures are identical in horizontal position in the curve and plausible Earth model. The magnetic curve and geoelectric section shows the same pattern in geological structures which may be concluded as contact, fractures or faults. The inferred geological structures (discontinuities) exist at an approximate horizontal distance of 300m, 2000m, 2800m and 3500m on magnetic and electrical result.

5.2.3.4. Profile Four

Pseudo depth section

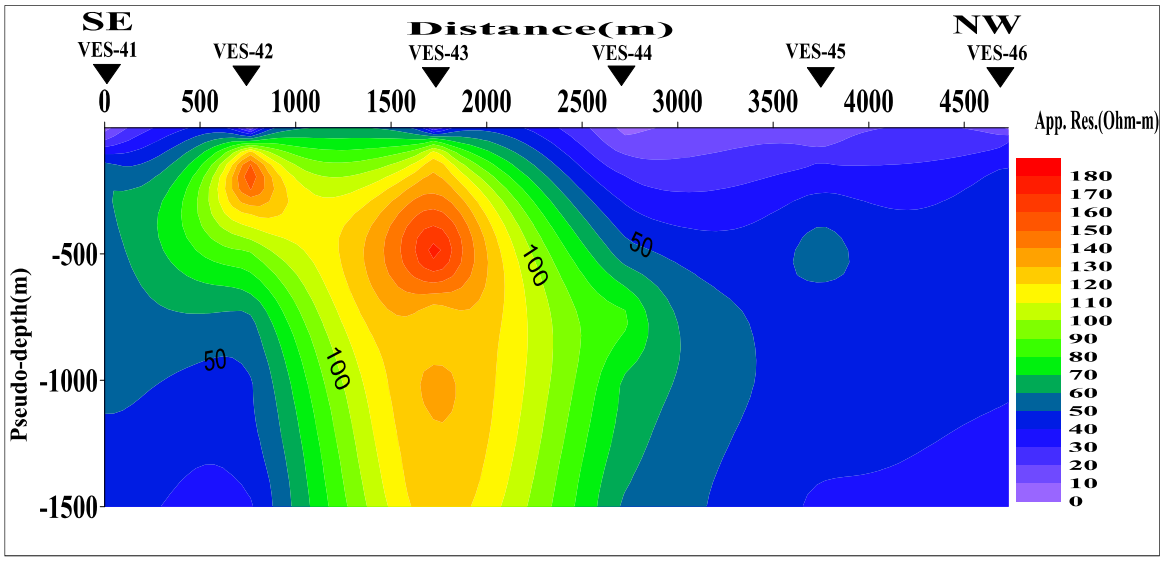

Figure 5-9: Pseudo depth section of Profile four.

The pseudo-depth section constructed for VES-41, 42, 43, 44, 45 and 46 that lie on the survey traverse line-4 are given in Figure 5-9. According to this figure, there is a lateral variation in resistivity in the section with prominent high resistivity away from the top zones mapped between VES-42 and VES-43 but relatively high resistivity exists near to the top zone mapped at both VES point. This high resistivity zone is extending to large depth at VES-43. Otherwise, the right side of the section has relatively small resistivity near to VES-45and 46. The large area of the bottom of the section has small resistivity (<120 Ohm-m) and the deep depth of VES-45 and 46 has small resistivity value. The vast region under the section shows extensive coverage of the low resistivity zone. The resistivity ranges (0 to 100 Ohm-m) of this low resistivity region are indicative of potential water saturation.

Geoelectric section

The resulting geoelectric section constructed from the interpreted layer parameters of the six VES lying on this traverse is given in Figure 5-10. A borehole BH23 and BH17 (Alema Tesfaye, 2009) is located on profile-4 that was also used to constrain the depth and identify the lithological units beneath these VES points during modeling. In essence, the lithological description of the borehole depth section (given in Annex 2-D and E)

with their resistivity parameters from each interpreted VES were used to prepare the geoelectric section shown below (Figure 5-10).

The top geoelectric layer is the combination of three interpreted VES curve for simplification of the model. It has high resistivity variation ranging from about 2-83 Ohm-m with thickness variation from 0.4-15.6m and may be attributed as expansive (which may vary in grain size) and top clay soil.

The second geoelectric layer is marked by high resistivity variation ranging from 15-179 Ohm-m. The thickness variation is from 7-281.6m. This layer likely reflects clay, slightly weathered vesicular and moderately weathered and fractured basalt. From the geoelectric section, this layer has good potential of groundwater under VES-44 and 45 with resistivity variation 50-74 Ohm-m.

The third geoelectric layer that corresponds to the moderately saturated layer manifests resistivity value varies highly, i.e., 29-1602 Ohm-m with thickness variation of 18.3 399.4m and may be represented as moderately weathered and fractured trachyte (fresh basalt), sand, gravel and clay, slightly weathered and highly fractured and weathered basalt. At VES-45 and 46, there is good potential of groundwater due to their resistivity values ranging from 29-51 Ohm-m under as compared to the other VES on this profile.

The underneath and highly saturated geoelectric layer is detected at the location of VES-41, 42, 44, 45 and 46with resistivity variation ranging from 28-35Ohm–m and most likely represents highly fractured and weathered basalt. This layer has good potential of groundwater as compared to the above layer.

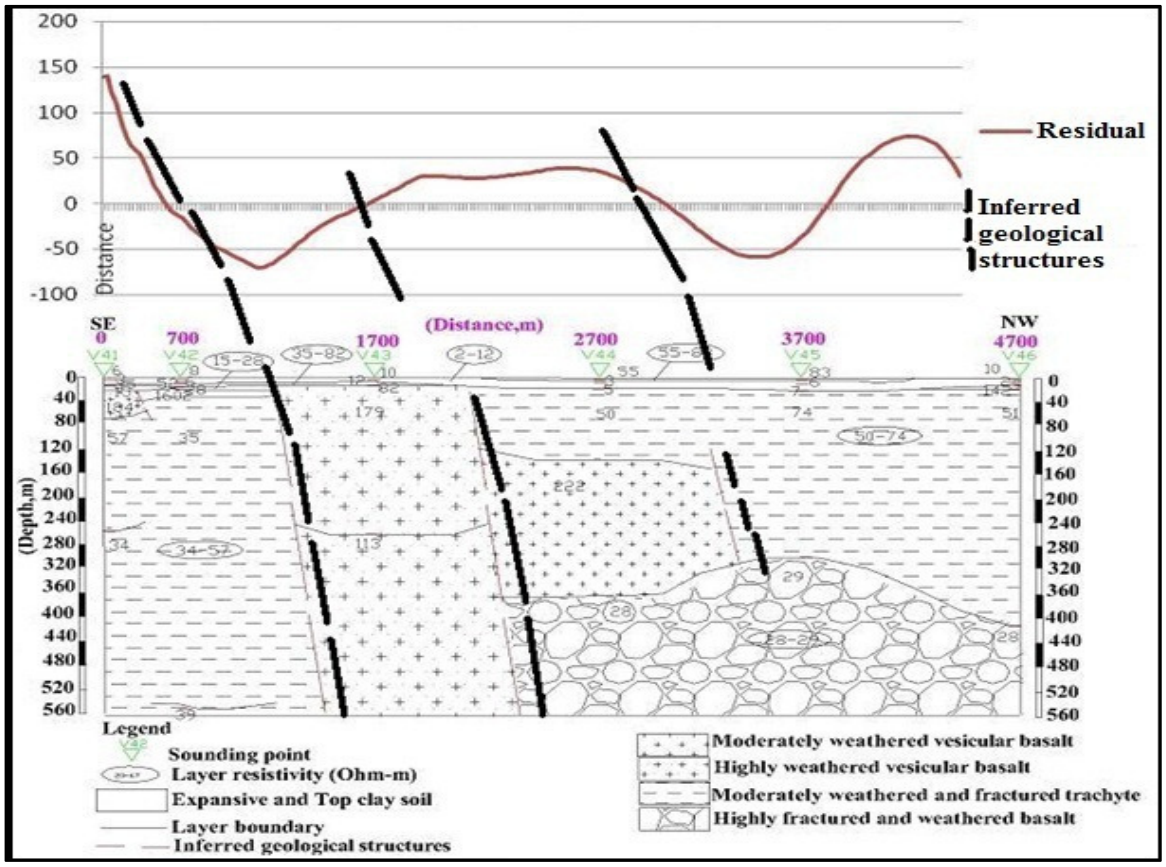

Figure 5-10: Magnetic profile plot and geo-electric section of Profile four.

From the above figure, the discontinuities of geological structures are identical in horizontal position in the curve and plausible Earth model. The magnetic curve and geoelectric section shows the same pattern in geological structures which may be concluded as contact, fractures or faults. The inferred geological structures (discontinuities) exist at an approximate horizontal distance of 1000m, 2100m and 3200m on magnetic and electrical result.

5.3. Discussions and Interpretations of Magnetics

5.3.1. Magnetic Data Presentation

After the removal of diurnal variation and IGRF, the observed total magnetic field anomaly data were processed and plotted on 2D gridding, contouring and mapping software: Oasis montaj (V4.6.2). The results are presented in contoured forms for visualization and further interpretation. For 2D visualization, the total magnetic field intensity data were gridded using minimum curvature gridding method with 15m cell size

and 1200 blanking distance. For effective interpretation of the magnetic data, further enhancements were carried out using various transformations such as, analytical signal, horizontal/vertical derivative and gradient, RTP and tilt angle derivative. The transformations are made using a mathematical property of potential fields that allows 2D maps of any component of a field to be transformed into maps of the same component or into maps of another component, or into maps of the gradients.

5.3.2. Interpretation of IGRF Corrected Curve of a Profile.

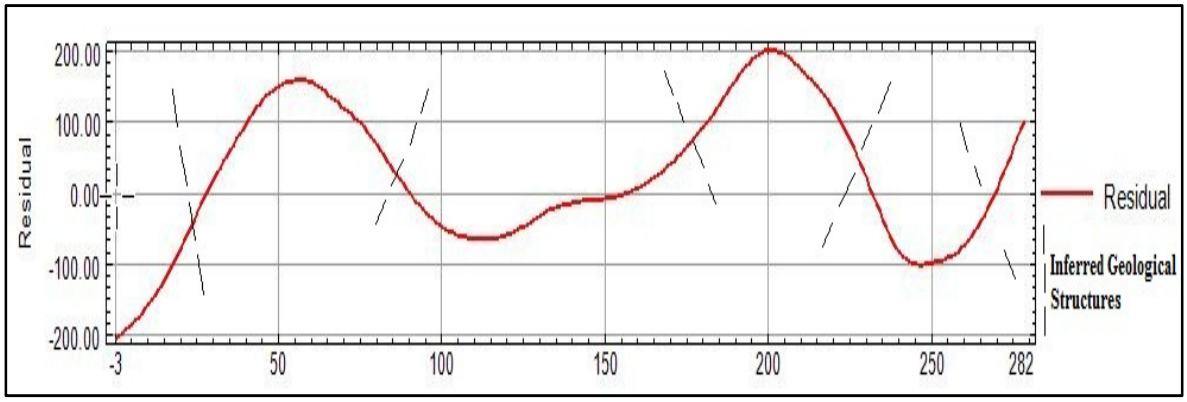

Figure 5-11: IGRF corrected and elevation curve of Profile two.

At both 50 and 200 of horizontal axis of the profile, Figure5-11, double-peak magnetic high are observed. The contrast in character between these two anomalies may suggest either a difference in magnetic properties of the rock producing the anomalies or a variation in depth of burial of the causative body.

This anomaly is characterized by higher magnetic intensity and uniform pattern. High magnetic variation may reflect the presence of a volcanic unit (relatively basalt) within a few meters of the surface, i.e. the closer the level of observation to a magnetic body, the steeper the magnetic gradients and the smaller the extent of major features on the anomaly.

On the anomaly located towards the SE and NW end of the profile, the strength of the magnetic field relatively declines with high magnetic gradient, which may be an indication of the existence of a geologic contact (fault) between volcanic units, between the more magnetic and thus more basic lithology (basalt) occurring towards south western end of the profile and less magnetic vescicular and scoracious basalt.

5.3.3. Results and Interpretations of Different Anomaly Maps

The carefully and thoroughly processed geophysical data were used to produce different anomaly maps, which show contrast in the susceptibility, magnetization direction and remanence of the subsurface rocks. The following section will show the results and interpretation of magnetic anomaly maps.

Observed Total Magnetic Field Anomaly Map

The observed total magnetic field anomaly map was created after the diurnal corrections and removal of the IGRF model field from the field-collected data, Figure 5-12.

The total magnetic field anomaly map depicts low anomalies in north, east, northwest central and isolated very low magnetic anomaly is observed at south of the study area. The intermediate magnetic anomaly over study area encloses the low magnetic anomaly of northern and eastern part and high magnetic anomaly observed at the western, southeastern and northeastern part of the map.

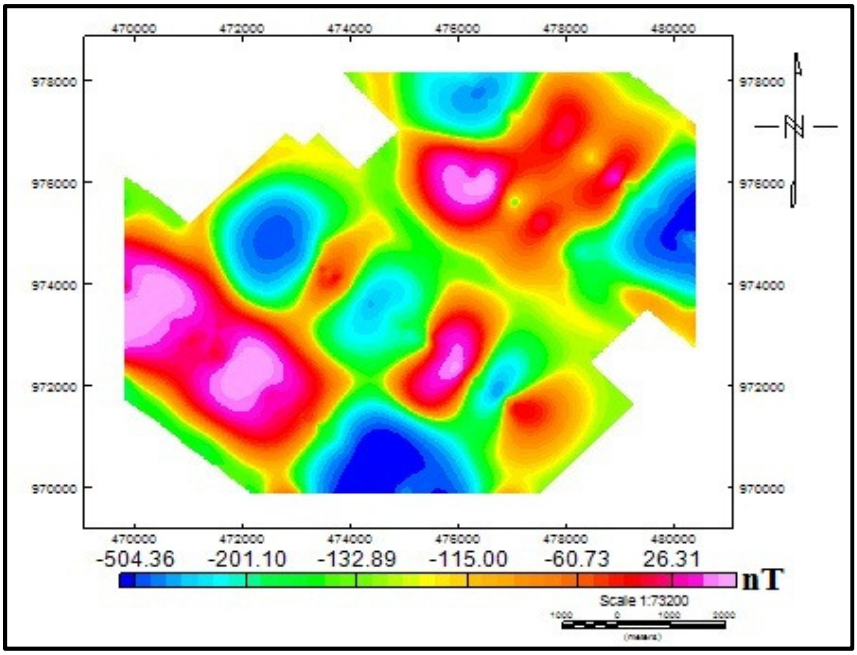

Figure 5-12: Observed total magnetic field anomaly map.

Residual Anomaly

The residual magnetic field anomaly map was created after subtracting third order trend of the regional magnetic map, Figure 5-13.

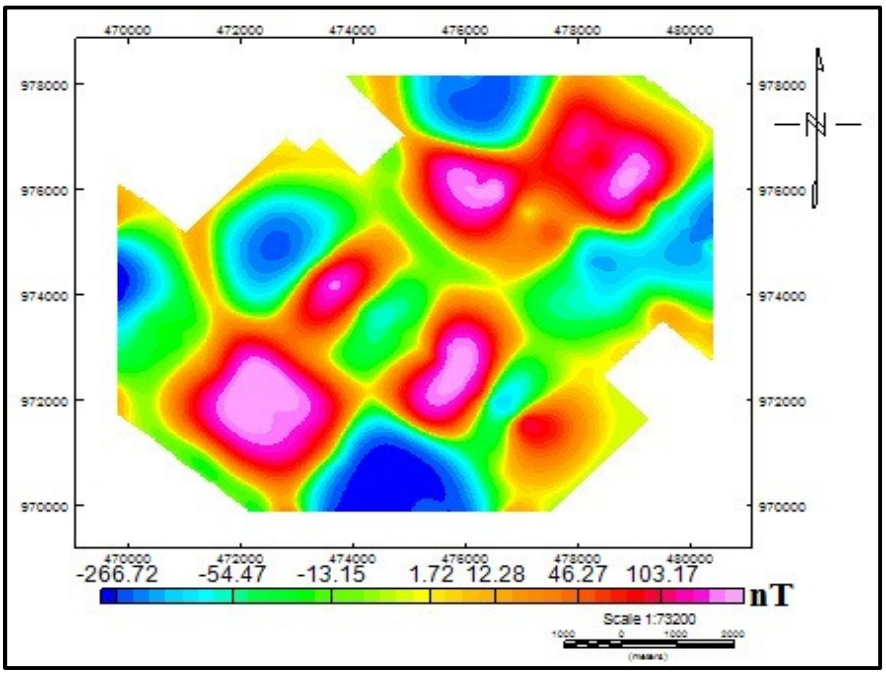

Figure 5-13: Residual anomaly map.

As shown in the map, the residual magnetic anomaly varies from -269.26 to 133.074. An interpretation difficulty with residual anomalies is that they are dipolar (anomalies having positive and negative components) such that the shape and phase of the anomaly depends in part on the magnetic inclination and the presence of any remnant magnetization. This anomaly complexity makes interpretation more difficult because the body and its edges do not necessarily coincide with the most obvious mapped feature.

Hence, in order to accentuate the magnetic signature of the linear geologic structures, analytic signal has been calculated from residual values and interpretations were made based on this map. In addition, horizontal gradient to the East and North, first order vertical derivative, TDR (Tilt Derivative) and RTP maps were prepared from analytic signal values.

Reduction to Pole of Residual

In this way the interpretation of the data is made easier as vertical bodies will produce induced magnetic anomalies that are centered on the body symmetrically.

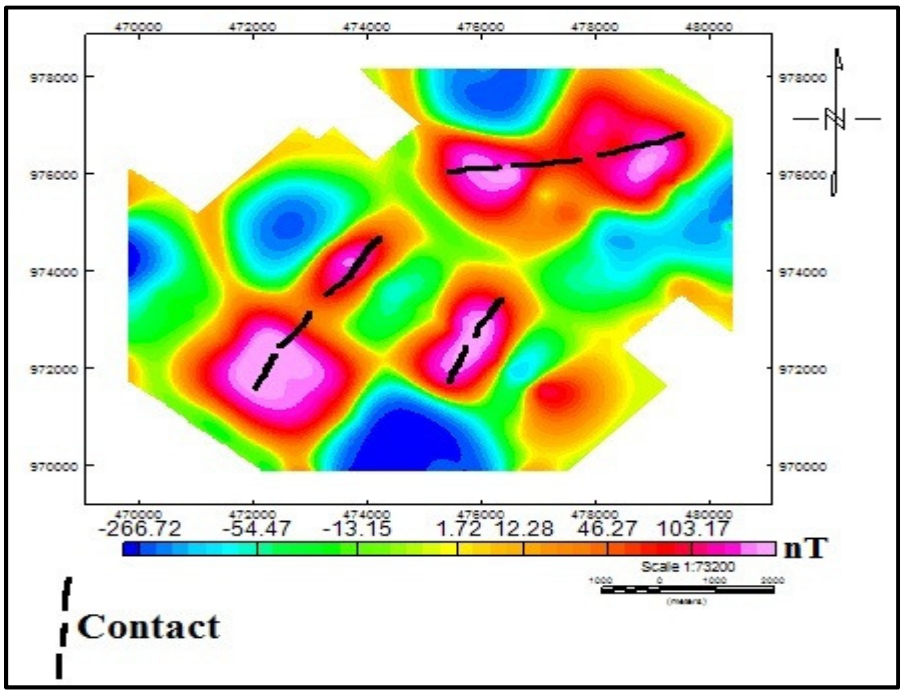

Figure 5-14: RTP map of the residual.

This method entails removing the dependence of magnetic data on the magnetic inclination i.e. converting data which were recorded in the inclined Earth's magnetic field to what they would have been if the magnetic field had been vertical. This method simplified the interpretation because for sub-vertical prisms or sub-vertical contacts (including faults), it transforms their asymmetric responses to simpler symmetric and anti-symmetric forms. The symmetric "highs" are directly centered on the body, while the maximum gradient of the anti-symmetric dipolar anomalies coincides exactly with the body edges. This operation is usually required for magnetic data at low latitude. The map (represented by the broken lines) shows the contact between alluvial deposits and basalt flow of the study area which is perfectly shows on the geological map.

Analytic Signal Map

When the analytic signal applied to the observed (residual) magnetic field, the method generally generates good horizontal locations for contacts and sheet sources regardless of their geologic dip or geomagnetic latitude.

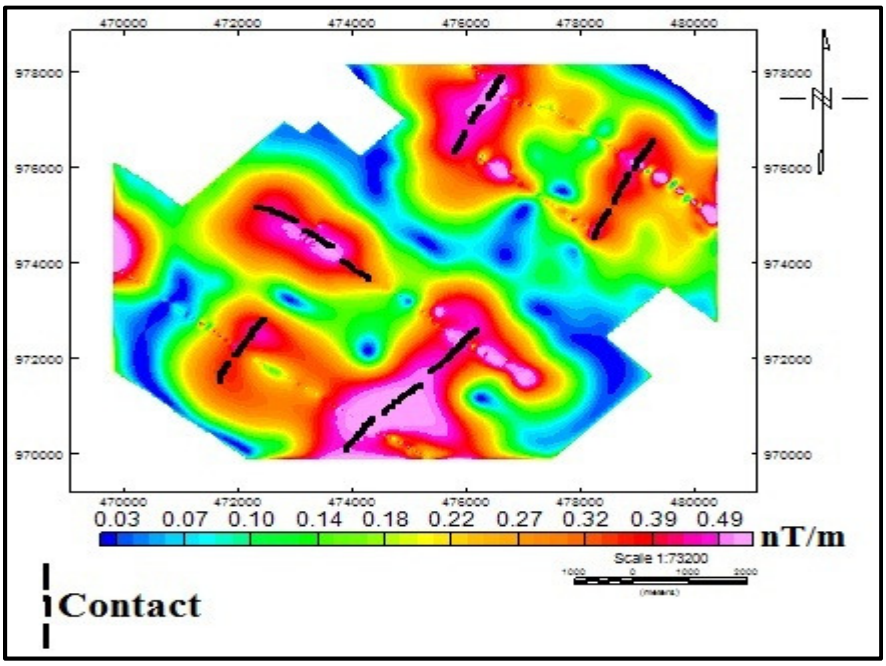

Figure 5-15: Analytic signal map.

The total magnetic intensity map has been subjected to the analytic signal algorithm (Figure 5-15).Since analytic signal map shows the response of anomalous bodies from their upper portions, it is supportive to give a picture of the near subsurface conditions. It is also known that the maximum amplitude is exactly located over a magnetic contact which depends on the locations of the body (horizontal coordinate and depth) but not on the inclinations of magnetization.

It is evident that the study area is dominated by two main structures perpendicular to each other; namely: NE-SW and NW-SE. Figure 5-15 indicating presence of NE-SW and NW-SE bodies causing relatively high magnetic anomalies.

The high amplitude of the analytic signal at the southern and northern region shows discontinuities from south to the north, this discontinuity might be due to shearing effect.

First Order Vertical Derivative Map of Analytic Signal

The first order vertical derivative of the analytic signal sharpens the image resolution and defines the positions of anomalies clearly. These features, together with enhancement of the signal from shallow sources, make it potentially of valuable in interpreting the sources.

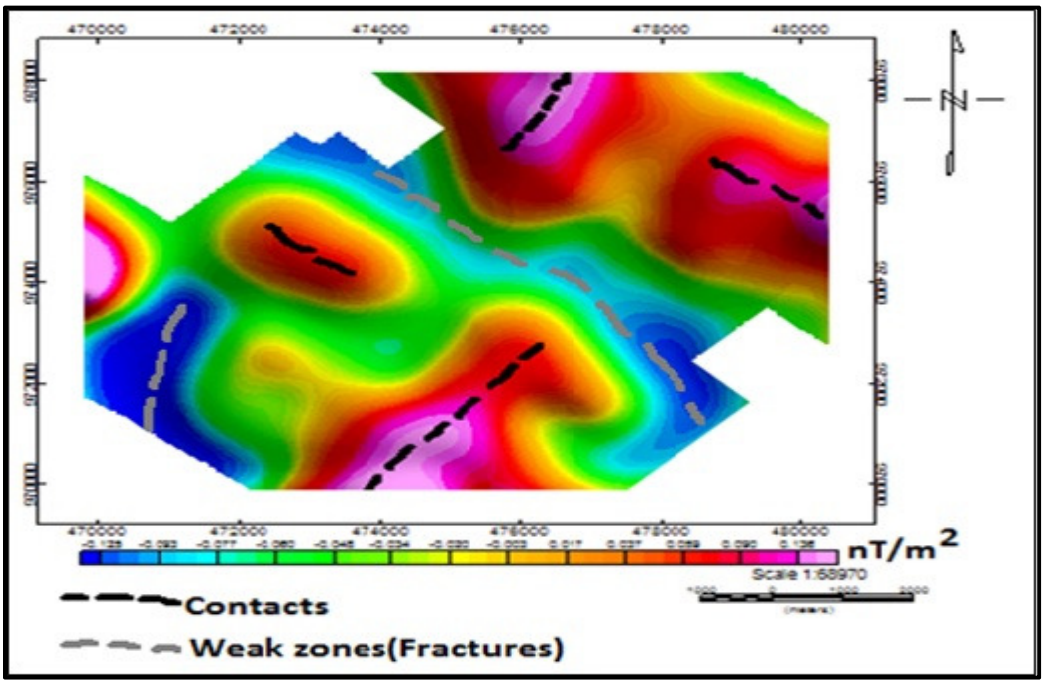

Figure 5-16: First order vertical derivative map of analytic signal.

It is the derivative of the analytic signal in the Z-direction and as such outlined the near surface high amplitude in the NW-SE and NE-SW trend at the northeastern and southern flanks of the map. The map shows a minimum magnetic response that runs NW-SE and NE-SW direction due to the fracture or weak zones at the center and southwestern of the area.

Horizontal Gradient of Analytic Signal

The main advantage of the horizontal gradient method is that it is least susceptible to noise in the data, because it only requires the calculations of the two first-order horizontal derivatives of the field (Phillips, 1998). This method is also robust in delineating both shallow and deep sources.

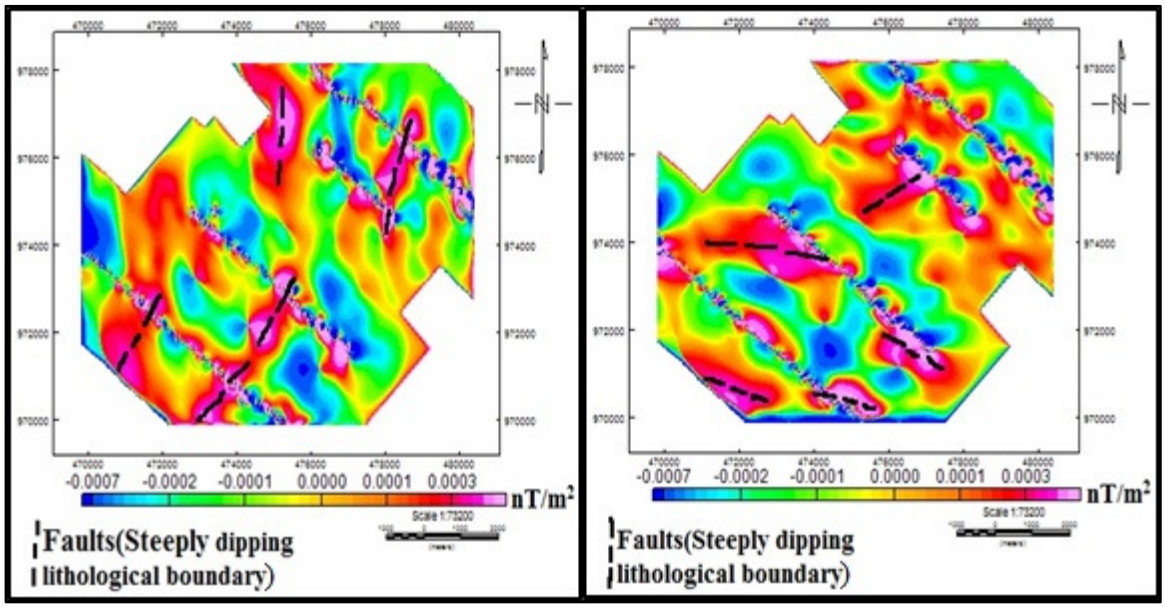

Figure 5-17: Horizontal gradient map of analytic signal to E-W (Left) and N-S (Right).

The maximum magnitudes of the horizontal gradient to the East and North related with the faults that exists in the study area. This implies that the steeply dipping lithological boundaries (faults/contacts) generally occur in the NW-SE and NE-SW direction at the study area. The existing steeply dipping lithological boundaries may be shallow and deep in the subsurface.

Vertical Gradient of Analytic Signal

This method is robust in delineating the shallow sources.

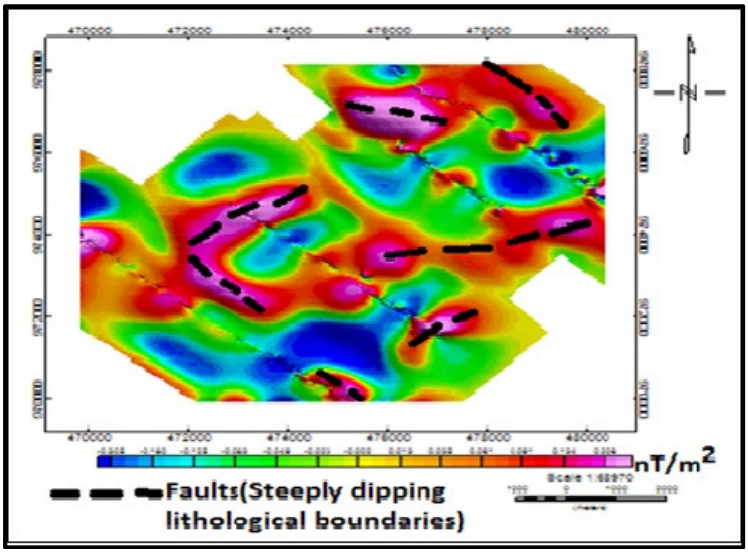

Figure 5-18: Vertical gradient map of analytic signal.

The map shows the direction of the shallow steeply dipping lithological boundaries (faults) that run from NW to SE and NE to SW direction. These lithological boundaries and discontinuities may act as the guide for the flow of groundwater in the study area.

Tilt Angle Derivative of Analytic Signal

The magnetic images are used to indicate areas of considerable magnetic contrast and to visualize features such as faults and dykes, which are depicted as lineaments. Because the amplitude of magnetic anomalies depends on magnetic field strength and depth of anomalous sources, lower amplitude, anomalies may be suppressed at the expense of higher amplitudes. For this reason, the edge detection filters are presented for delineating linear features without diminishing the long wavelength information. One of the most important filters is TDR which is proposed by Miller and Singh (1994).

Miller and Singh (1994) have shown that TDR crosses through zero at or near the edges of a vertical-sided source and is negative outside the source region.

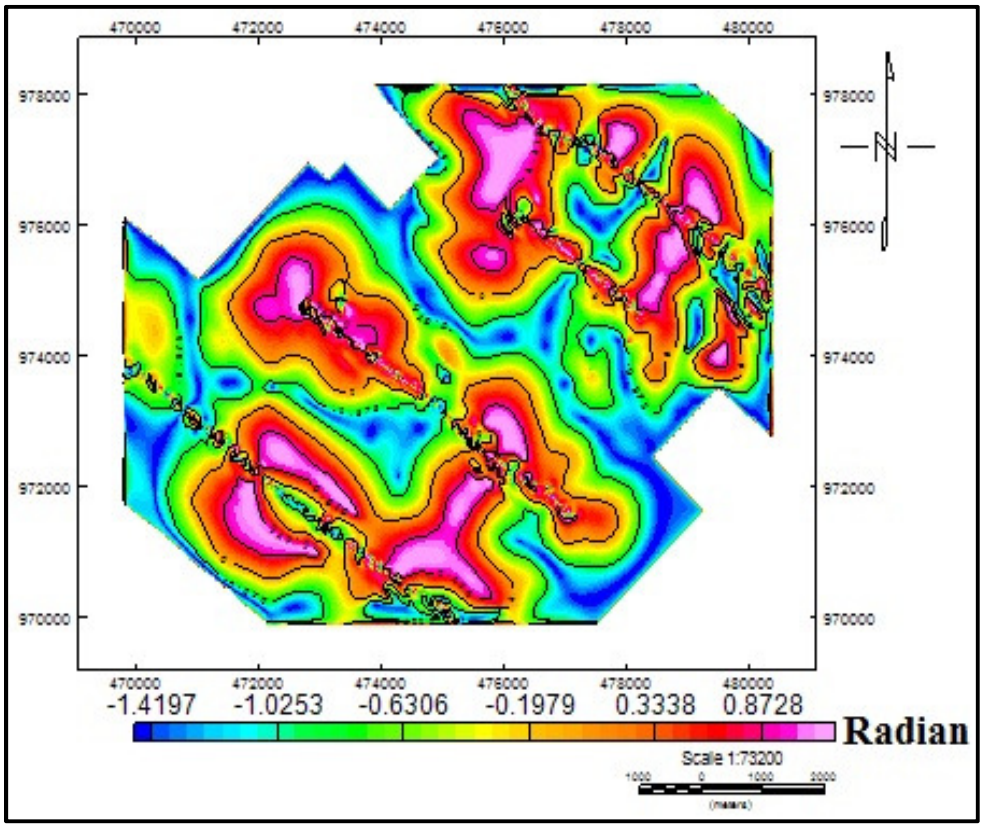

Figure 5-19: Tilt angle derivative map of analytic signal.

The above figure shows that the recognition of the horizontal location and extent of edges of anomalous sources assuming between vertical contact model. The zero contoured that exists between the lines on the map estimates the horizontal location of abrupt lateral changes in susceptibility. The TDR map accentuates short wave lengths and reveals the presence of magnetic lineaments. As shown in Figure 5-19, the structural elements are improved simply by inspecting the alignment of anomalies and by distinguishing the noticeable abrupt change between positive and negative anomalies in Figure 5-13, particularly at the location of sharp gradients.

The strike direction in the study area is NW-SE and NE-SW; it is likely to observe these features clearly on the map (Figure 5-19). The anomaly features interpreted as faults and fractures (weak zones). As a result, these magnetic responses showed that how much lateral movement affects the area geology.

Euler Deconvolution Depth Map

For this study, Euler deconvolutions with different structural indices (SI = 0, 0.5, 1, 1.5, 2, 2.5 and 3) were used to get converging solutions over magnetic contacts. Furthermore, from these structural indices, the best solution over the magnetic contact is determined (in this case, SI = 0) and shown in Figure 5-20. The Euler depth map depicts that the north and east sides show relatively high clustering of solutions at different depths than the south and west side. This is probably due to the presence of contacts (fractures) in the north and east parts of the surveyed site than the rest side. The line formed by the symbols may be interpreted as contacts (fractures) with the orientation of SE-NW which act as the conduits for the groundwater flow. Based on Euler depth solution, the depth to the contact is ranging from mainly 300-400m and 200-300m in some area of the study area.

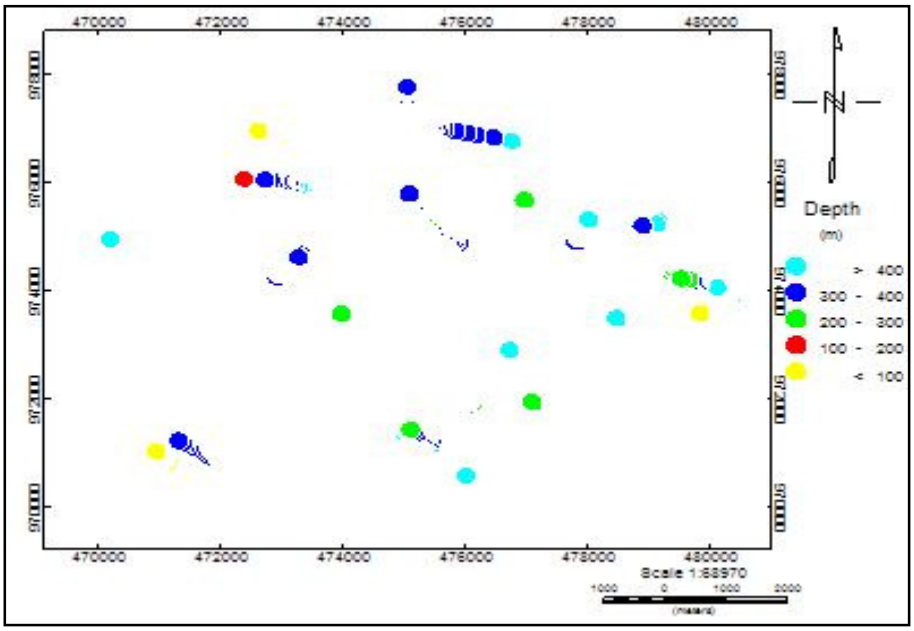

Figure 5-20: Euler deconvolution depth map of the site.

2D Modeling

Modeling is done using the GM-SYS modeling software. It is an interactive forward modeling program which calculates the magnetic response from a user defined hypothetical geological model. Any difference between the model response and the observed magnetic field are reduced by refining the model structure. It should be noted that magnetic models are non-unique, i.e. many earth models can produce the same magnetic response, and similarly, several geological lithologies may be interpreted from a given model block's susceptibility properties. It is therefore importance to use as many independent source of information as possible to constrain the model. The 2D model created by GM-SYS extends to depths of 50km by default and it changes with depth (Z direction) and along the profile (X direction, perpendicular to strike) (GETECH Group plc., 2007).

Accordingly 2D magnetic modeling is developed along all profiles from the difference map between the residual (Figure 5-13) and upward continuation of residual at 1000m (Figure 5-21) as shown in Figure 5-22.

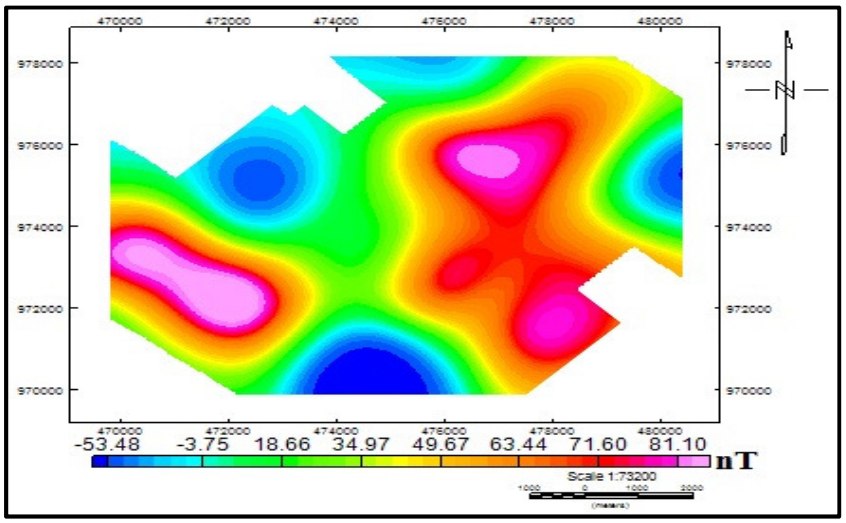

Figure 5-21: Upward continuation of the IGRF corrected to the height of 1000m.

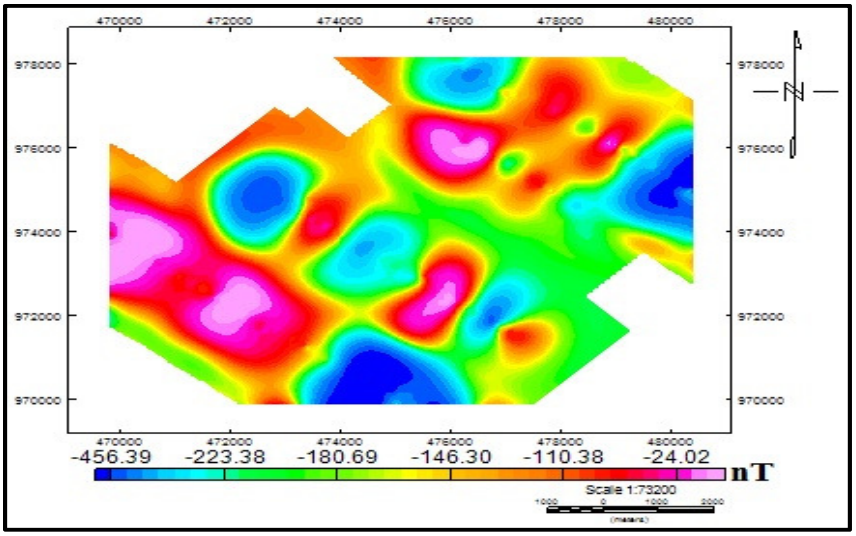

Figure 5-22: Difference map of IGRF corrected and its upward continuation to the height of 1000m.

This model is developed based on the information from the borehole (for Profile 1 and 4) and geo-electric section of VES (for Profile 2 and 3). The developed model has an error of 4.5% and it perfectly matches with all the maps and curves developed along the profiles from the different methods in displaying the layering, fault and contact location. Based on this model, the faults and contacts are located around 65m and 150m, and this is consistent with all the maps and models discussed above.

Profile-1

The magnetic 2D profile model is developed from the interpreted layer parameters of the VES, geologic cross-section and borehole data (SWAWF3 which is found in the Annex-2A) and picked from Figure 5-22. The model shows that the existence of faults below a depth of 45m and extend vertically up to 350m and a basaltic intrusion. From the geoelectric section, the basalts are varying in their degree of weathered and fracture. Again the remanence of the basalt also varies of each layer.

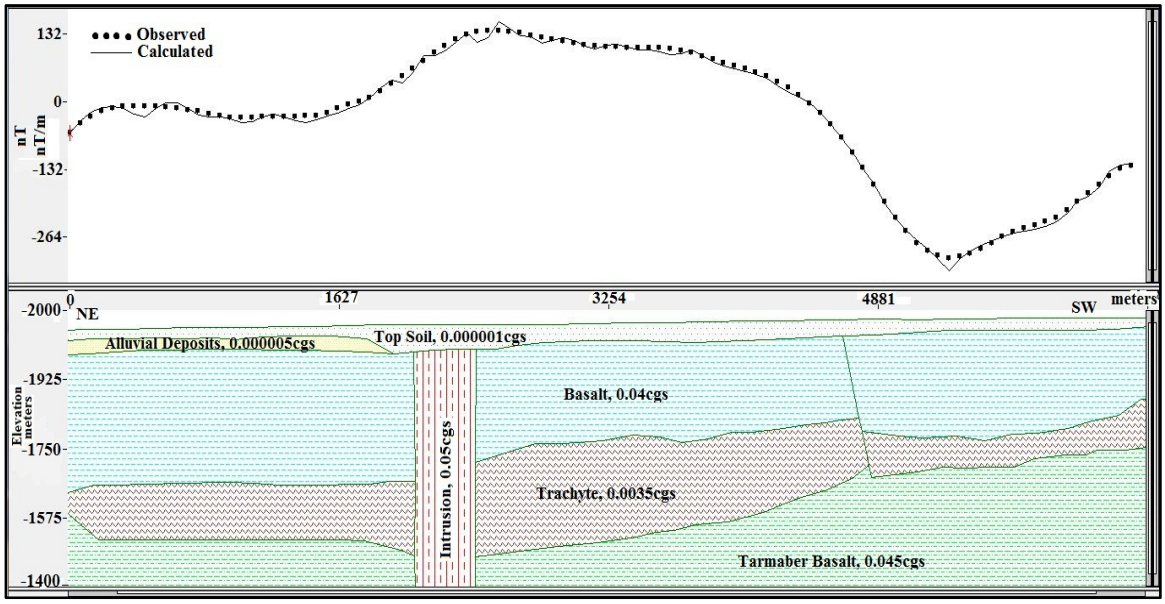

Figure 5-23: 2D magnetic modeling of Profile-one.

Profile-2

The magnetic 2D profile model is developed from the interpreted layer parameters of the VES, geologic cross section and borehole data (Dewara Guda which is found in the Annex-2B) and picked from Figure 5-22. The model shows that the existence of faults below a depth of 25m and extend up to 300m and basaltic intrusions. From the geoelectric section, the scoria and vesicular basalts are varying in their degree of weathered and fracture. Again the remanence of the basalt also varies of each layer.

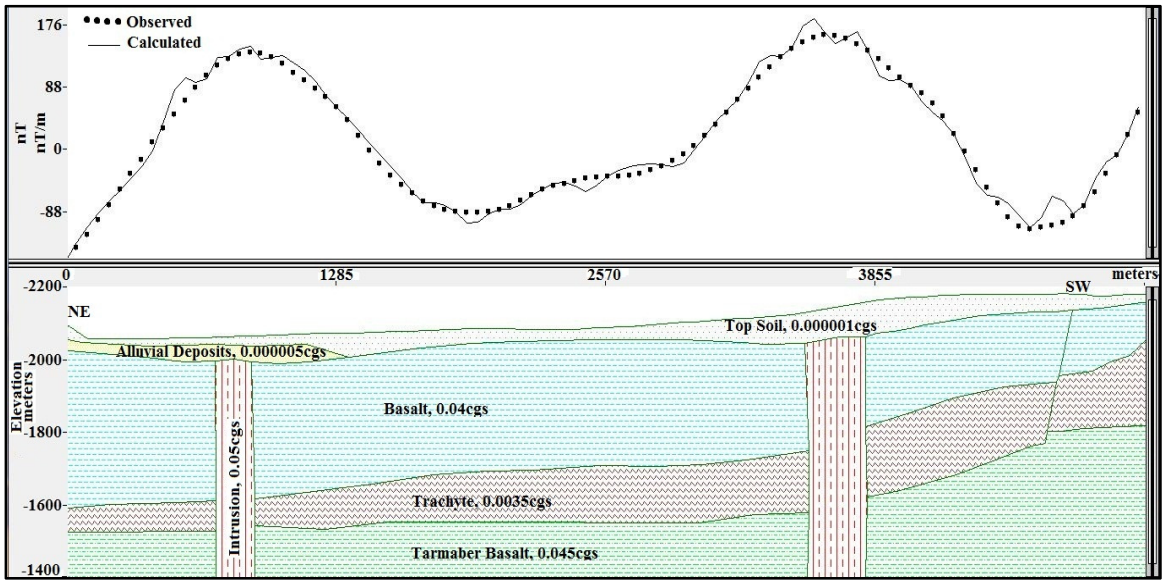

Figure 5-24: 2D magnetic modeling of Profile-two.

Profile-3

The magnetic 2D profile model is developed from the interpreted layer parameters of the VES and borehole data (BH24 which is found in the Annex-2C) and picked from Figure 5-22. The model shows that the existence of faults below a depth of 25m and extend vertically up to 450m and a basaltic intrusion. From the geoelectric section, the scoria and basalts are varying in their degree of weathered and fracture. Again the remanence of the basalt also varies of each layer.

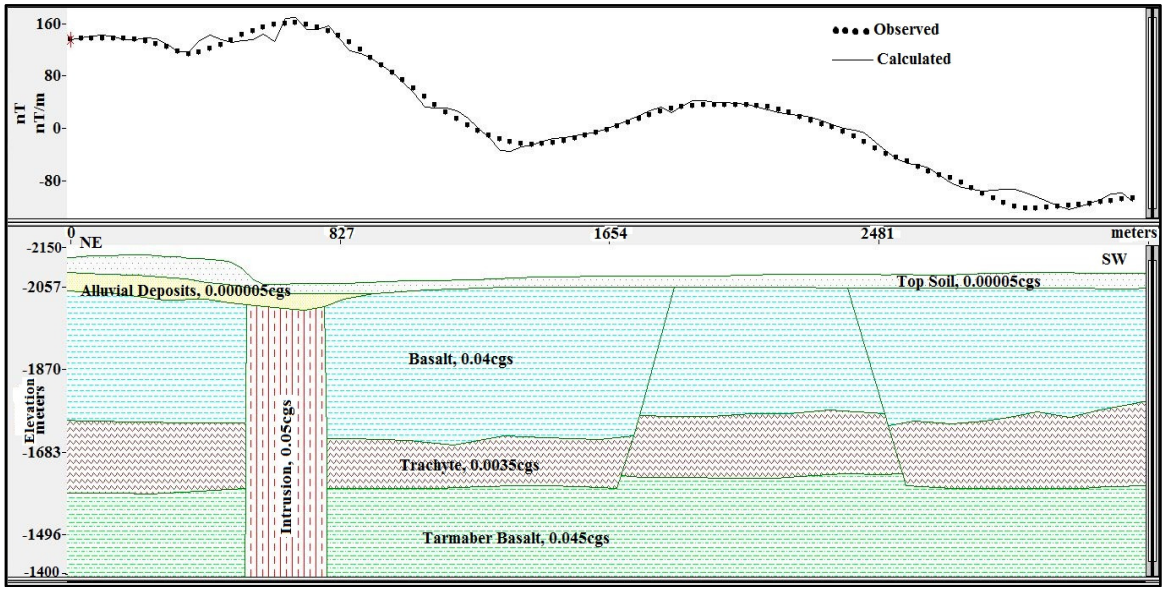

Figure 5-25: 2D magnetic modeling of Profile-three.

Profile-4

The magnetic 2D profile model is developed from the interpreted layer parameters of the VES and borehole data (BH23 and BH17 which is found in the Annex-2D and 2E) and picked from Figure 5-22. The model shows that the existence of faults below a depth of 50m and extend vertically up to 450m and a basaltic intrusion. From the geoelectric section, the basalts are varying in their degree of weathered and fracture. Again the remanence of the basalt also varies of each layer.

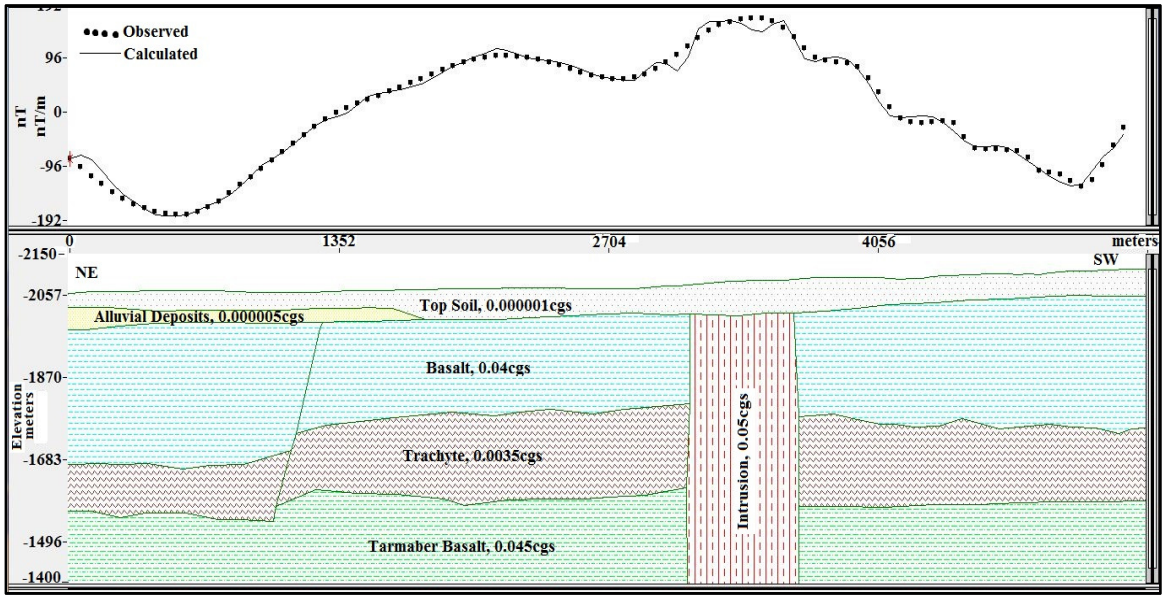

Figure 5-26: 2D magnetic modeling of Profile-four.

CHAPTER SIX
6. CONCLUSIONS AND RECOMMENDATIONS

6.1. Conclusions

Based on the result discussions and interpretations, the following conclusions have been drawn using the combination of data presentation approaches:

1) The apparent resistivity pseudo-depth sections and the true resistivity geoelectric sections show the presence of shallow as well as deeper low resistivity horizons which are potential zones of groundwater saturation. The low resistivity and large thickness of these horizons is an indicator of high groundwater potential in the study area.
2) From the result of the electrical resistivity and magnetic surveys, it is also seen that the area is highly affected by tectonic forces that have resulted in local fracturing and faulting of the rock units at varying depths. These faults (contacts) and fractures are believed to control the flow of groundwater. The fractures and weak zones are the major controls for the flow of ground water over the area. Most of basaltic rocks (for all traverse lines) are highly fractured and weathered which expected to be the water-bearing zones at different depths.
3) The geological structures (fractures, faults and contacts) play a great role in the movement and occurrence of the groundwater in the study area. The highly to moderately weathered and fractured basalts and sand layer contribute more for the recharge and movement of the groundwater through the faults and wake zones.
4) Comparison of the geophysical interpretations with drilled borehole results show that the results of geophysical survey are good correlation with the borehole lithologic logging results.
5) The main geologic units encountered over the survey area that are likely to bear groundwater (based on the degree of fracturing and weathering) are basalts and sand.
6) The water table of the study area varies from 20 to 60 meters deep that increases towards the northwest of the study area.

7) From the magnetic modeling, the fault may found below a depth of 25m and extend vertical up to 180m and 450m due to the tectonic effect of the Main Ethiopian Rift.
8) Some of the important locations and depths to water bearing horizons over the survey traverse lines are as follows:
    - Traverse Line-1: As shown in Figure 5-4, the water-bearing horizon is mapped to be at the depth below 160m and a borehole preferably drilled to a depth of range between 200m and 400m.
    - Traverse Line-2: A borehole preferably drilled to a depth below 80m and between VES-26 and VES-27 may yield high volume of groundwater (Figure 5-6).
    - Traverse Line-3: From Figure 5-8, the depth of the water-bearing horizon is at the depth 300m for VES-31, 32, 33 and 34 but for VES 35 it ranges from 40m to 180m For VES-36, the depth is below 100m. The borehole preferably drilled to a depth range between 340m and 480m under VES-31, 32, 33 and 35.
    - Traverse Line-4: As shown in the Figure 5-10, at the depth below 320m has the water-bearing horizon. The borehole preferably drilled to a depth below 300m for VES-41 and 42 but for VES-44, 45 and 46 drilling will be taken at a depth below 360m.

These have been indicated as preferred locations for the sinking of boreholes to extract good amount of groundwater. A drilling program- both test and productive- is suggested to focus on these areas.

6.2. Recommendations

Based on the outcome of this study, the following thoughts are recommended.

1) Three boreholes are recommended for drilling in the following order. The first borehole is recommended at or around VES-12, VES-33 and VES-44 with UTM coordinates (474700, 970323), (477008, 975560) and (478411, 976755) respectively.
2) Additional VES survey is recommended in the perpendicular direction of the existing traverse for detail investigation for the extension of low resistivity zones.

3) Similar detailed magnetic survey outside of the area is recommended to identify the extension of faults that are behaved to serve as conduit for groundwater flow.
4) It is highly recommended that to study detailed time domain electromagnetic survey and geochemistry for the investigation of additional drilling point and the quality of the groundwater in the area.
5) It is recommended that to study detailed structural geological investigations for mapping the orientation of faults, fractures and weak zones as well as their natures like dip, strike and their extension.
6) Further regional hydrological and hydro-geological investigations are recommended to understand the basin, amount of precipitation and evaporation which are used to estimate the percolation of surface water to the groundwater.

References

1. **AAWSA and SEURECA, (1991).**Addis Ababa water supply project stage III, detail report, and Groundwater resource, **4**. Addis Ababa Water and Sewerage Authority, Addis Ababa, Ethiopia.
2. **AAWSA, (2000).** Addis Ababa water Supply project. Stage-IIIA Groundwater-Phase II, Modeling of Akaki Well field, **1**, main report, Addis Ababa Water and Sewerage Authority, Addis Ababa, Ethiopia.
3. **Abraham Hailemelekot, (2009).** Determination of Spatio-Temporal differences of water Hyacinth and Its effects in Lake Aba Samuel, South East of Addis Ababa, Ethiopia. Unpublished thesis.pp:13
4. **AGRA (1998).** Hydrogeology of Akaki well field.
5. **Alema Tesfaye, (2009).** Steady-state groundwater flow and contaminant transport modeling of Akaki well field and its surrounding catchment (Addis Ababa, Ethiopia). Unpublished MSc thesis, International institute of Geo-Information Science and Earth Observation, Netherlands.
6. **Anteneh Girma (1994).** Hydrogeology of Akaki Area. Addis Ababa University, Addis Ababa, Ethiopia, Unpublished Master Thesis.
7. **Aynalem Ali, (1999).** Water Quality and Groundwater/River water Interaction in the Akaki River Basin (Sekelo). MSc Thesis, Addis Ababa University, Addis Ababa.
8. **Barker, (1992).** Cited on Lecture notes on Electrical and electromagnetic exploration (GPH 221) [http://www.a-alamri.com/index/download/id/78/lang/ar, accessed on Mar 24, 2013.]
9. **Bernard, J. (2003).** Short notes on the principles of geophysical methods for groundwater investigations.
10. **Blakely R.J. (1995).** Potential theory in Gravity and Magnetic applications. Cambridge University Press, Australia, pp.: 461.
11. **CIA (2012).**CIA World Fact Book. URL: https://www.cia.gov/library/publications/the-world-factbook/geos/et/html,accessed on Oct 29,2012

12. **CSA Ethiopia, (2012).** National statistics on population.URL: http://www.csa.gov.et/index.php/2013-02-20-13-43-35/national-statistics-abstract/141-population, accessed on Feb 8, 2013.
13. **Deressa Temesgen, Hassan RM, Ringler C., (2008).** Measuring Ethiopian farmers' vulnerability to climate change across regional states. IFPRI discussion paper No. 806. Accessed online on URL: http://www.ifpri.org/pubs/dp/ifpridp00806.asp, Washington, DC.
14. **Ebasa Oljira,(2006).**Numerical Groundwater Flow Simulation of Akaki River Catchment, unpublished, Addis Ababa University, Ethiopia, 2003 (Addis Ababa report)
15. **Ethiopian Reporter, (2013).** Ato Asegid Getachew on ethiopianreporter.com, accessed on March 07, 2013; 12:31pm.
16. **Ewusi Anthony, (2006).**Groundwater Exploration and Management using Geophysics: Northern Region of Ghana, PhD thesis.
17. **Frohlich RK, Fisher JJ, Summerly E, (1996).** Electric-hydraulic conductivity correlation in fractured crystalline bedrock: Central Landfill, Rhode Island, USA. J Appl. Geophy 1996; 35: 249-59.
18. **Gaspron, M. Innocenti, F. Manetti, p., Peccerillo.A. and Tsegaye, A., (1993).** Genesis of the Pliocene the recent Giomadel mafic-felsic volcanism in the Debre-Zeit area, central Ethiopian volcanological and geological constraints .J. Afar Earth science. **17**:45-165.
19. **GETECH Group plc., (2007).** Advanced processing and interpretation of gravity and magnetic data, pp.: 24-26, accessed from www.getech.com at 10:30a.m on July 30, 2013.
20. **Gibson, P.J. and George, D.M., (2003).** Environmental applications of geophysical surveying techniques. Nova Science Publishers, Inc. New York.
21. **Girmay Kahsay, (2010).** The Impact of Low cost Sanitation on Groundwater Contamination in the City of Addis Ababa, PhD thesis, University of South Africa,pp:57

22. **Haileselassie Girmay and Getaneh Assefa, (1989).**The Addis Ababa Nazareth Volcanical Miocene-Pleistocene Volcanic Succession in Ethiopian Rift. SINET, **12(1),** Addis Ababa.
23. **Igor S. Zektser and Lome G. Everett, (2004).** Groundwater resources of the world and their use, UN. pp:20
24. **Keating, P., (1998).** The fractal dimension of gravity data sets and its Implication for gridding: Geophys. Prosp. **41**:983-993.
25. **Leta Guddisa, (2007).**Analysis of Subsurface Contaminant Transport in Akaki Well Field and surrounding areas, Central Ethiopia, Unpublished, Addis Ababa University
26. **Loke, M. H., (2001).** Electrical imagine survey for environmental and engineering studies: A practical guide to 2D and 3D surveys.
27. **Mazzarini, F, Abeba, T, Innoccentti, F., Manetti, P, and Parethi, M.T, (1999).** Geology of the Debre Zeit area (Ethiopian), with accompanied geological map at 1: 100,000 made Adama volcanological map at 1:100,000 rate Volcanological, **11**, **No.1**: 31-141.
28. **Miller, H.G. and Singh, V., (1994).**Potential field tilt—a new concept for location of potential field
29. **Mohr P.A., (1967).** The Ethiopian Rift System. Bulletin, Geophysical Observatory. Addis Ababa, Ethiopia
30. **Molla Demlie, (2007).** Groundwater Recharge, Flow and Hydro-geochemical Evolution in a Complex Volcanic Aquifer System, Central Ethiopia [Electronic Version]. Hydrogeology Journal, pp.: 1169-1181.
31. **Morton W.H., (1974).** Geological map of Addis Ababa. Addis Ababa University, Ethiopia
32. **Morton, W.H., Rex, D.C., Michell. I.G and Mohr, P.A., (1979).** The rift word longing of volcanic units in the Addis Ababa region, Ethiopian Rift valley: Nature **280**:284-288
33. **Mulugeta Chanie, (2011).** Application of integrated geophysical techniques to map groundwater potential zones and geological structures at Gelchet area, Borena zone, South Ethiopia. Unpublished MSc thesis, Addis Ababa University.
34. **Ethiopian Mapping Agency, (1981),** National Atlas of Ethiopia.

35. **Orellana, E., and Money, H.M., (1966).** Master Tables and Curves for Vertical Electrical Sounding over Layered Structures. Interciencia, Costanilla de Los Angeles, 15, Madrid, Spain.
36. **Oseji and Ujuanbi, (2009).**Hydro-geophysical investigation of groundwater potential in Emu kingdom, Ndokwa land of Delta State, Published, Nigeria.
37. **Peter G. Cook, (2003).**A guide to regional groundwater flow in fractured rock aquifers, CSIRO Land and Water, Glen Osmond, SA, Australia.
38. **Phillips, J.D., (1998).** Processing and Interpretation of Aeromagnetic Data for the Santa Cruz Basin – Patahonia Mountains Area, South-Central Arizona. U.S. Geological society.
39. **Reynold, (1997).** An Introduction to Applied and Environmental Geophysics. John Wiley and Sons limited, England, UK, pp.: 160.
40. **Roset, W. Veroef, J. and Plikinton, M., (1992).**Magnetic interpretation using the 3-D analytical signal. Geophysics, **57**: 116-125.
41. **S.S. Stefanescu,C., (1930).** Schlumberger Distribution of electric field in potential horizontals layers, homogeneous and isotropic, J.Phys. radium,**7**:132-141
42. **Second World Water Forum, The Hague, (17–22 March, 2000).** URL: http://www.waternunc.com/gb/secWWF.htm, accessed on Jan 5, 2013.
43. **Solomon Tale ,(2000).**The Extent of Surface and Groundwater Pollution in Addis Ababa, Unpublished, Addis Ababa University
44. **Tadesse Yirga, (2004).**Groundwater Modeling. A case study on volcanic water supply aquifer(Akaki well field) of the city of Addis Ababa,pp:21
45. **Tamiru Alemayehu, (2000).** Water pollution by natural inorganic chemicals in the central part of the Main Ethiopian Rift. Ethiopian Journal of Science, **23(2)**:197-214
46. **Tamiru Alemayehu, Dagnachew Legesse, Tenalem Ayenew, Solomon Waltenigus, Tadesse Yirga and Mohammed Nuri, (2005).**Hydrogeology, water quality and degree of groundwater vulnerability to pollution in Addis Ababa, UNEP-UNESCO report, Kenya; pp: 115.
47. **Tenalem Ayenew , Molla Demlie , Stefan Wohnlich, (2008).**Application of Numerical Modeling for Groundwater Flow System Analysis in the Akaki

Catchment, Central Ethiopia; International Association for Mathematical Geology 2008; Math Geosciences (2008),**40**:887–906

48. **Tenalem Ayenew, Stefan Wohlinch and Molla Demlie, (2001).**Integrated Groundwater Modeling and Hydrochemical Study in Addis Ababa Area: Towards Developing Decision Support System for Wellhead Protection, Department of Earth Sciences, Addis Ababa University, Addis Ababa, Ethiopia.
49. **Tewodros Mulugeta, (2011).** Geophysical Investigation for Groundwater Potential assessment and Mapping Structures at Alidege Plain, South Afar, Ethiopia, MSc thesis.
50. **Thompson, D.T., (1982).** EULDPH, A new technique for making computer-assisted depth estimates from magnetic data, Verduzco B., Fairhead J.D., Green C. Geophysic.,**47**: 31-37.
51. **Tibebe Mengesha, (2006).** Integrated Geophysical Investigation for the Evaluation of Groundwater Resources at Ada'a plain Near Debre-Zeit, MSc thesis.
52. **UNEP-Addis Ababa report, (2003).**Groundwater vulnerability mapping of the Addis Ababa water supply aquifers.
53. **UNESCO, (1998).** UNESCO handbook for groundwater investigations. Technical report, ITC.
54. **Valeria. C.F. Barbosa, Joao B.C. Silva and Walter E.Medeiros, (1999).** Stability analysis and improvement of structural index estimation in Euler deconvolution, Geophysics. **64. No. 1.**
55. **Vander Velpen B.P.A., (1995).**RESIXIP and Win Resist software, 1st version; Interpex limited company.
56. **Varnier A., Tesfaye C, Hailesilassie Girmay, (1985).**Hydrogeology of the Addis Ababa Area, Note No. 233. Addis Ababa: Geological Survey of Ethiopia
57. **W/Gabriel Giday, Aronson, J.L., and Walter R.C., (1990).** Geology, Geochronology and Rift Basin Development in the Central Sector of the Main Ethiopian Rift ,Geological Society of America, bulletin ; **102**:439-458.
58. **WWDSE, (2008).** Geological investigation report on Raya valley basin, Northern Ethiopia. Unpublished report.

59. **WWDSE, (2009).** Acknowledgement Report of Test Wells at Groundwater Prospective Sites, Interim Report, **III**, Addis Ababa
60. **WWDSE, (2011).**Geological mapping of groundwater prospect sites, Report, **II**, Addis Ababa
61. **Zanettin, B. and Justin V. E., (1974).** The Volcanic of Western Afar and Ethiopian Rift Margins. Padova, Italy, **9**: 567–574.
62. **Zanettin, B., Justin- Visentia, E, Necolettic M, and piccirillo, E.M., (1980).** Correlation among Ethiopian Volcanic Formations with Special Reference to the Chronsgiolgical and Stratigaphical problems of the trap series atti convgni lincci, **47**: 231-252.
63. **Zohdy, A.A.R., (1973).** A computer program for automatic interpretation of Schlumberger sounding curves over horizontally stratified media. PB-232703, National Technical Information Service, Springfield, Virginia. pp.: 25.

Appendices

Annex 1: Interpreted VES curves of the each sounding points.

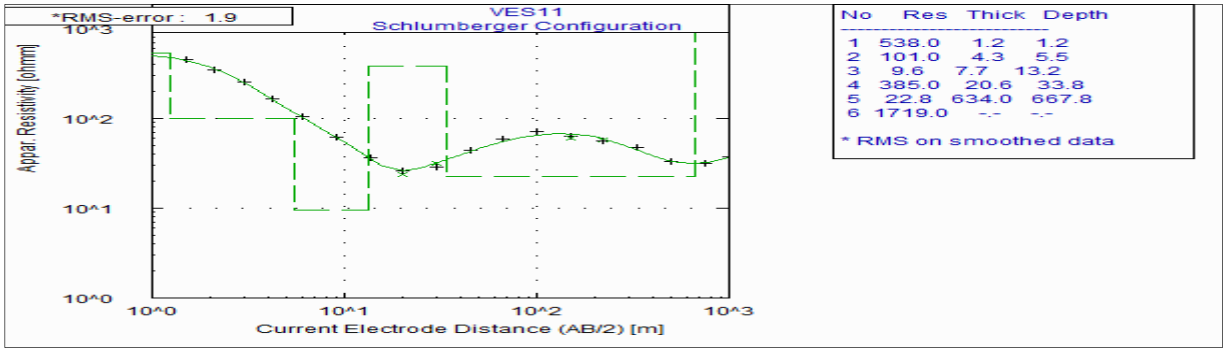

No	Res	Thick	Depth
1	538.0	1.2	1.2
2	101.0	4.3	5.5
3	9.6	7.7	13.2
4	385.0	20.6	33.8
5	22.8	634.0	667.8
6	1719.0	-.-	-.-

* RMS on smoothed data

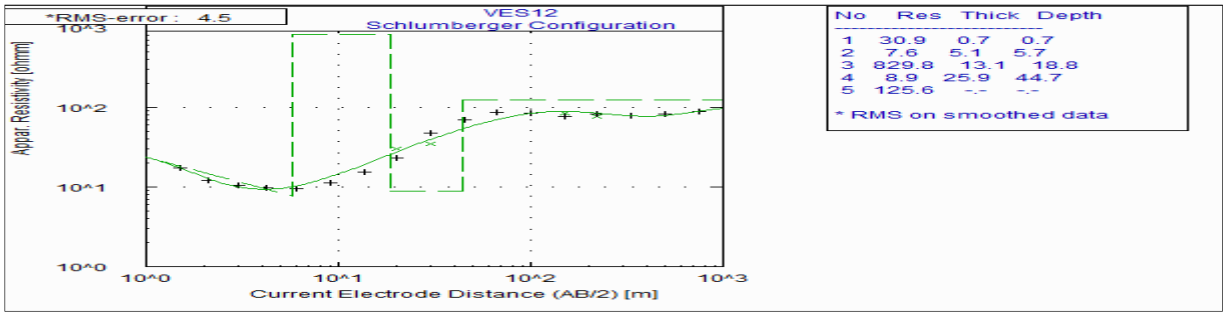

No	Res	Thick	Depth
1	30.9	0.7	0.7
2	7.6	5.1	5.7
3	829.8	13.1	18.8
4	8.9	25.9	44.7
5	125.6	-.-	-.-

* RMS on smoothed data

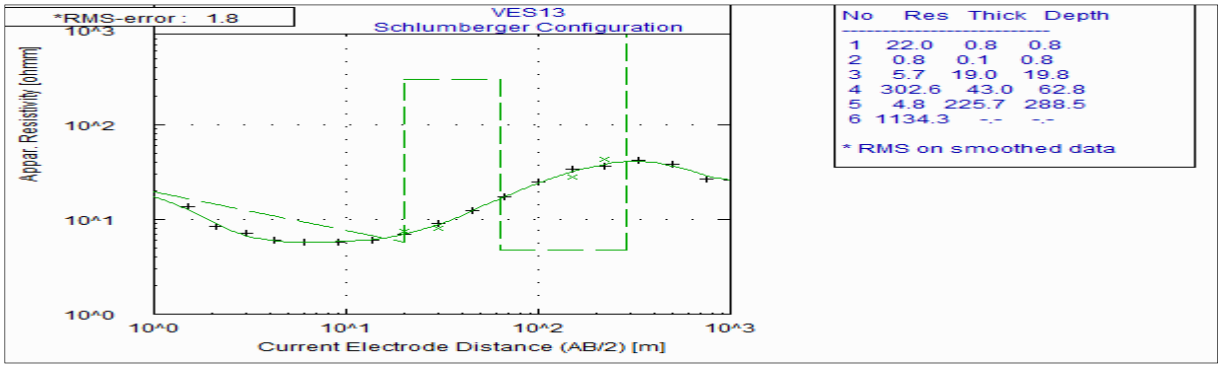

No	Res	Thick	Depth
1	22.0	0.8	0.8
2	0.8	0.1	0.8
3	5.7	19.0	19.8
4	302.6	43.0	62.8
5	4.8	225.7	288.5
6	1134.3	-.-	-.-

* RMS on smoothed data

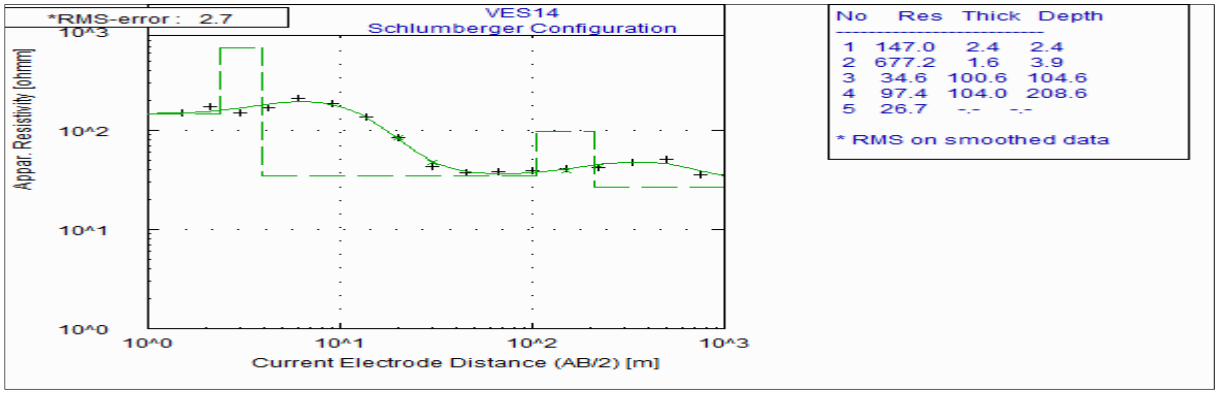

No	Res	Thick	Depth
1	147.0	2.4	2.4
2	677.2	1.6	3.9
3	34.6	100.6	104.6
4	97.4	104.0	208.6
5	26.7	-.-	-.-

* RMS on smoothed data

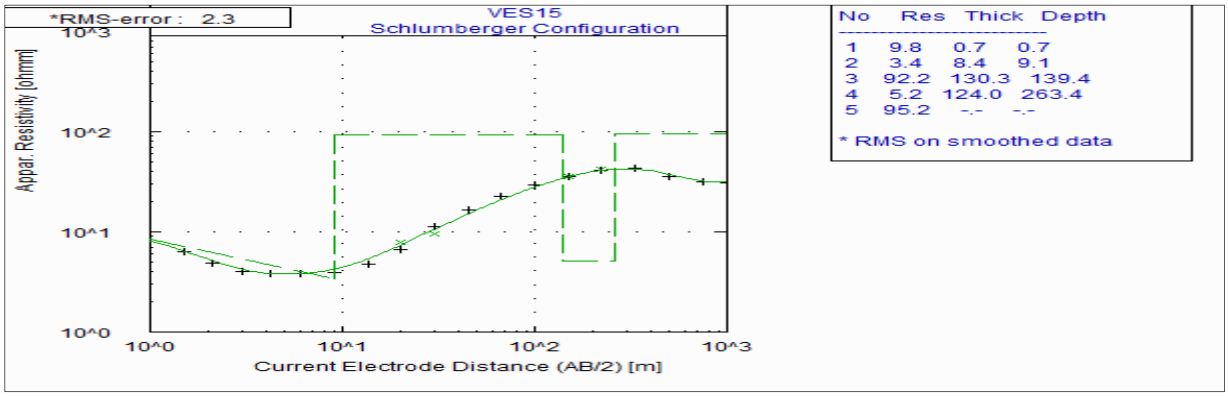
*RMS-error : 2.3
VES15
Schlumberger Configuration
Appar. Resistivity [ohmm]
10^3
10^2
10^1
10^0
10^0
10^1
10^2
10^3
Current Electrode Distance (AB/2) [m]
No Res Thick Depth
1 9.8 0.7 0.7
2 3.4 8.4 9.1
3 92.2 130.3 139.4
4 5.2 124.0 263.4
5 95.2 -.- -.-
* RMS on smoothed data

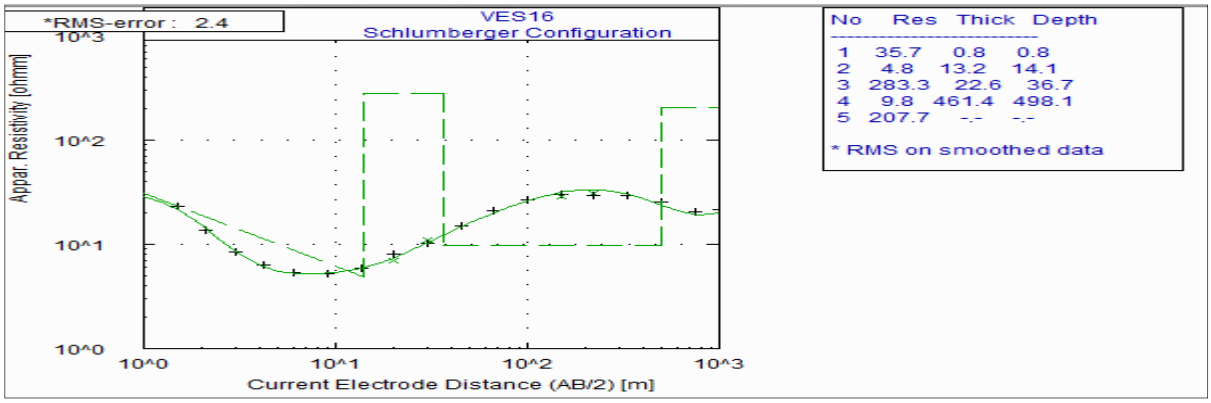
*RMS-error : 2.4
VES16
Schlumberger Configuration
Appar. Resistivity [ohmm]
10^3
10^2
10^1
10^0
10^0
10^1
10^2
10^3
Current Electrode Distance (AB/2) [m]
No Res Thick Depth
1 35.7 0.8 0.8
2 4.8 13.2 14.1
3 283.3 22.6 36.7
4 9.8 461.4 498.1
5 207.7 -.- -.-
* RMS on smoothed data

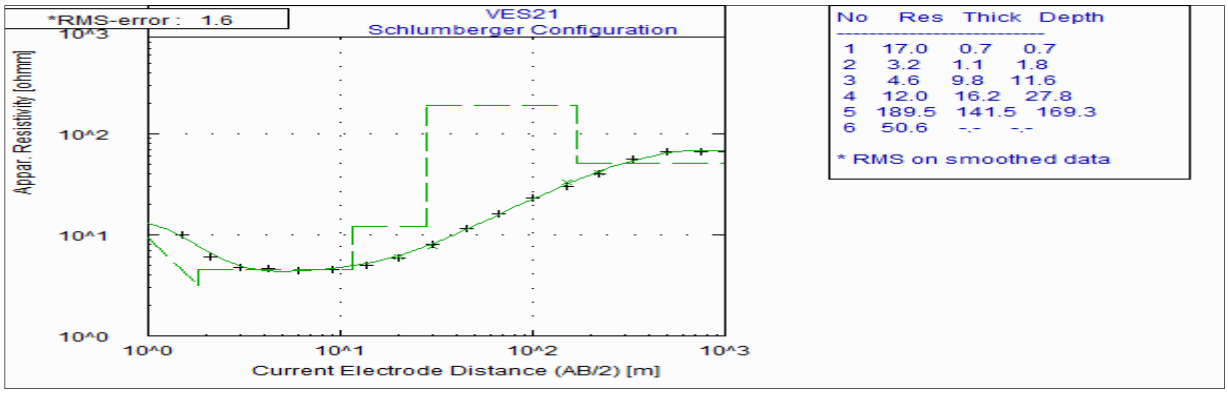
*RMS-error : 1.6
VES21
Schlumberger Configuration
Appar. Resistivity [ohmm]
10^3
10^2
10^1
10^0
10^0
10^1
10^2
10^3
Current Electrode Distance (AB/2) [m]
No Res Thick Depth
1 17.0 0.7 0.7
2 3.2 1.1 1.8
3 4.6 9.8 11.6
4 12.0 16.2 27.8
5 189.5 141.5 169.3
6 50.6 -.- -.-
* RMS on smoothed data

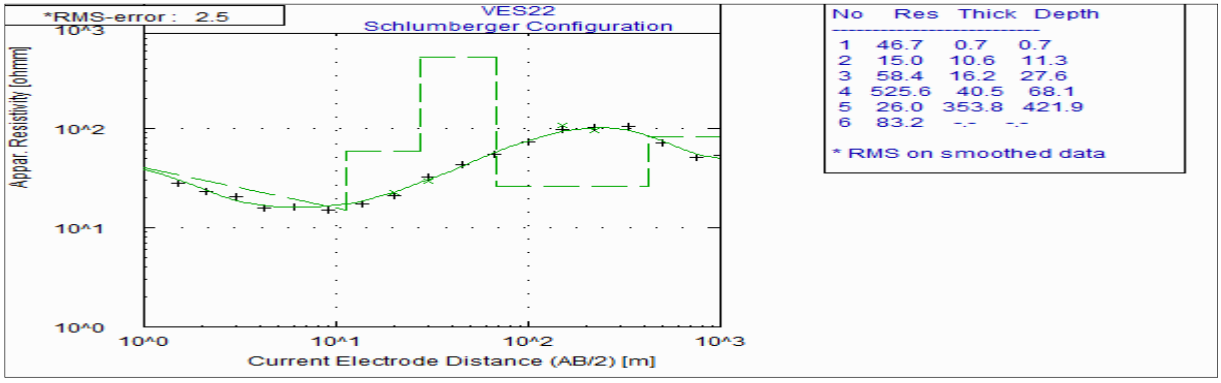
*RMS-error : 2.5
VES22
Schlumberger Configuration
Appar. Resistivity [ohmm]
10^3
10^2
10^1
10^0
10^0
10^1
10^2
10^3
Current Electrode Distance (AB/2) [m]
No Res Thick Depth
1 46.7 0.7 0.7
2 15.0 10.6 11.3
3 58.4 16.2 27.6
4 525.6 40.5 68.1
5 26.0 353.8 421.9
6 83.2 -.- -.-
* RMS on smoothed data

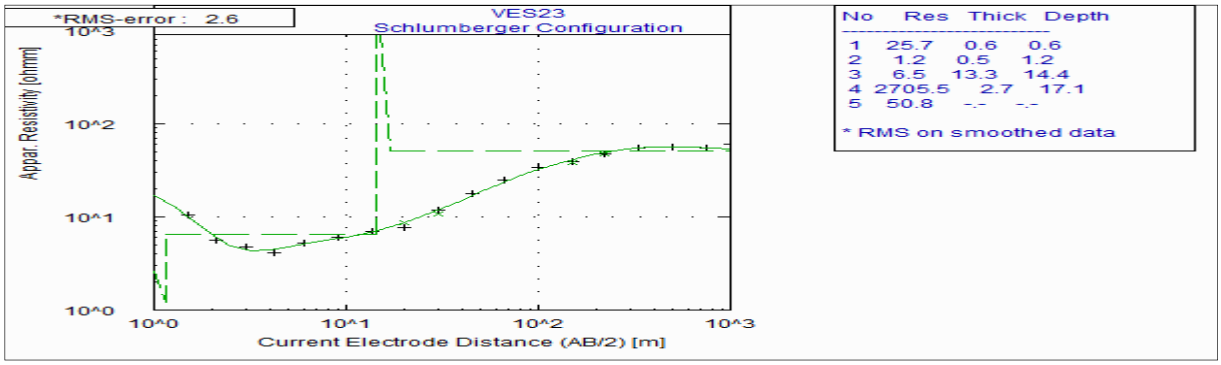
*RMS-error : 2.6
VES23
Schlumberger Configuration
Appar. Resistivity [ohmm]
10^3
10^2
10^1
10^0
10^0
10^1
10^2
10^3
Current Electrode Distance (AB/2) [m]
No Res Thick Depth
1 25.7 0.6 0.6
2 1.2 0.5 1.2
3 6.5 13.3 14.4
4 2705.5 2.7 17.1
5 50.8 -.- -.-
* RMS on smoothed data

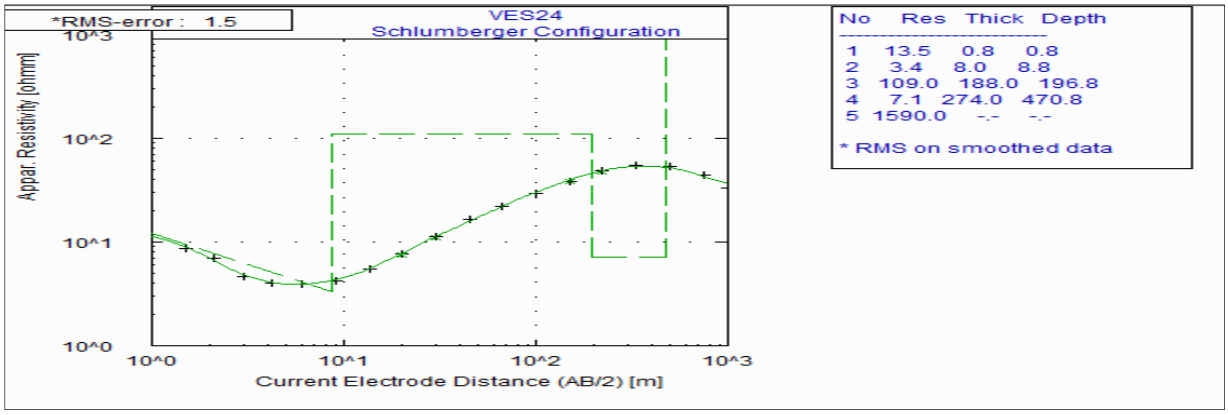
*RMS-error : 1.5
VES24
Schlumberger Configuration
Appar. Resistivity [ohmm]
10^3
10^2
10^1
10^0
10^0
10^1
10^2
10^3
Current Electrode Distance (AB/2) [m]
No Res Thick Depth
1 13.5 0.8 0.8
2 3.4 8.0 8.8
3 109.0 188.0 196.8
4 7.1 274.0 470.8
5 1590.0 -.- -.-
* RMS on smoothed data

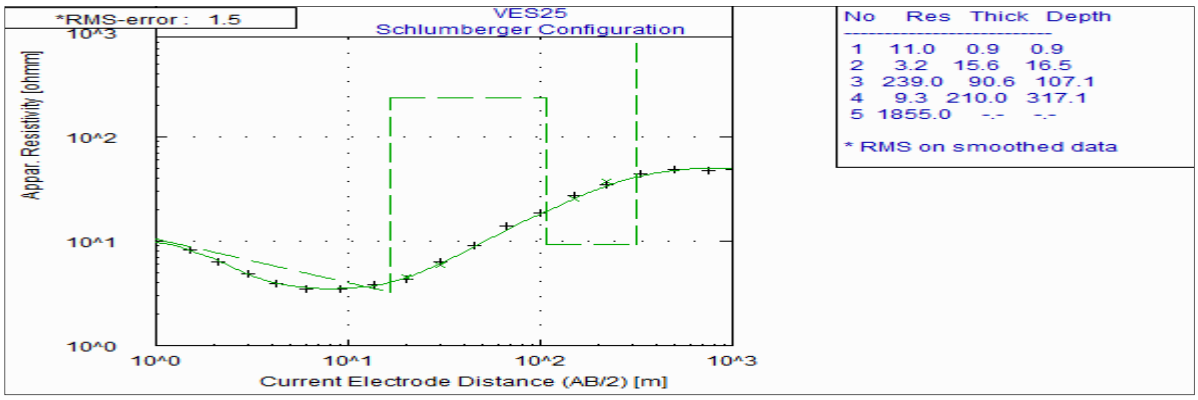
*RMS-error : 1.5
VES25
Schlumberger Configuration
Appar. Resistivity [ohmm]
10^3
10^2
10^1
10^0
10^0
10^1
10^2
10^3
Current Electrode Distance (AB/2) [m]
No Res Thick Depth
1 11.0 0.9 0.9
2 3.2 15.6 16.5
3 239.0 90.6 107.1
4 9.3 210.0 317.1
5 1855.0 -.- -.-
* RMS on smoothed data

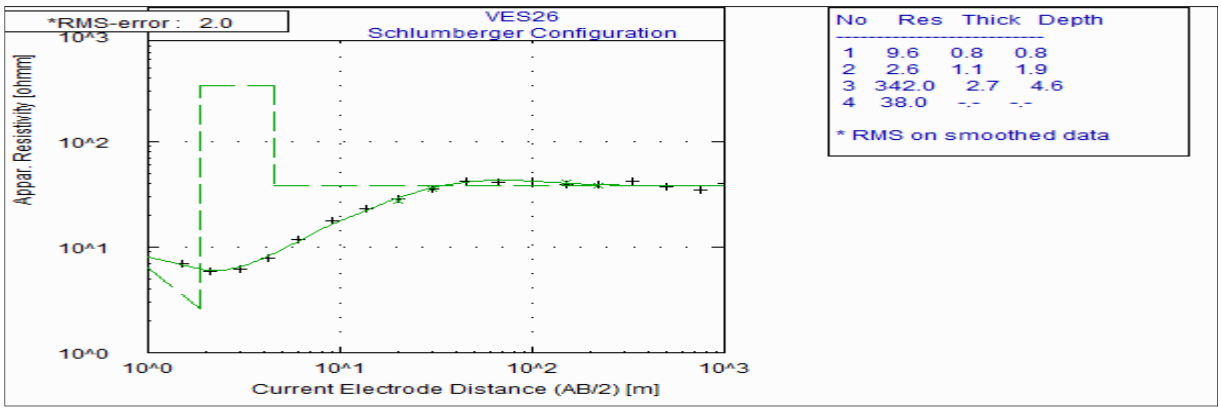
*RMS-error : 2.0
VES26
Schlumberger Configuration
Appar. Resistivity [ohmm]
10^3
10^2
10^1
10^0
10^0
10^1
10^2
10^3
Current Electrode Distance (AB/2) [m]
No Res Thick Depth
1 9.6 0.8 0.8
2 2.6 1.1 1.9
3 342.0 2.7 4.6
4 38.0 -.- -.-
* RMS on smoothed data

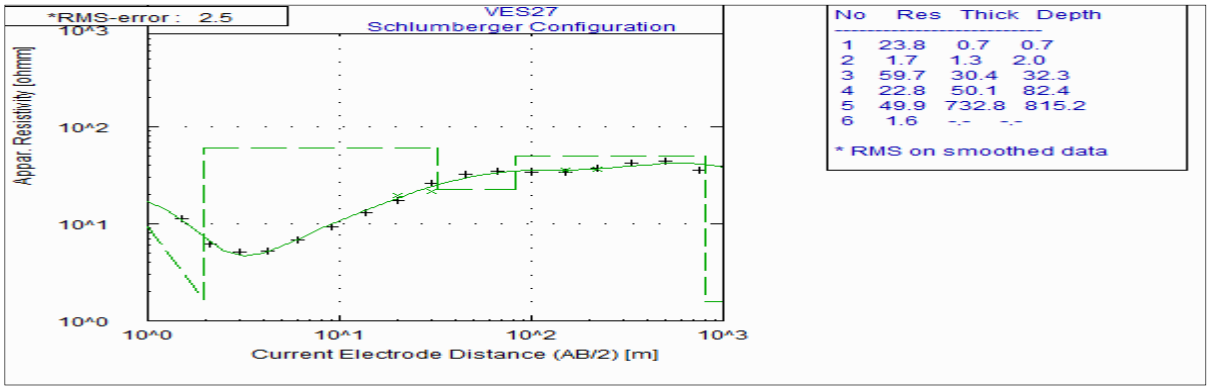

No	Res	Thick	Depth
1	23.8	0.7	0.7
2	1.7	1.3	2.0
3	59.7	30.4	32.3
4	22.8	50.1	82.4
5	49.9	732.8	815.2
6	1.6	-.-	-.-

* RMS on smoothed data

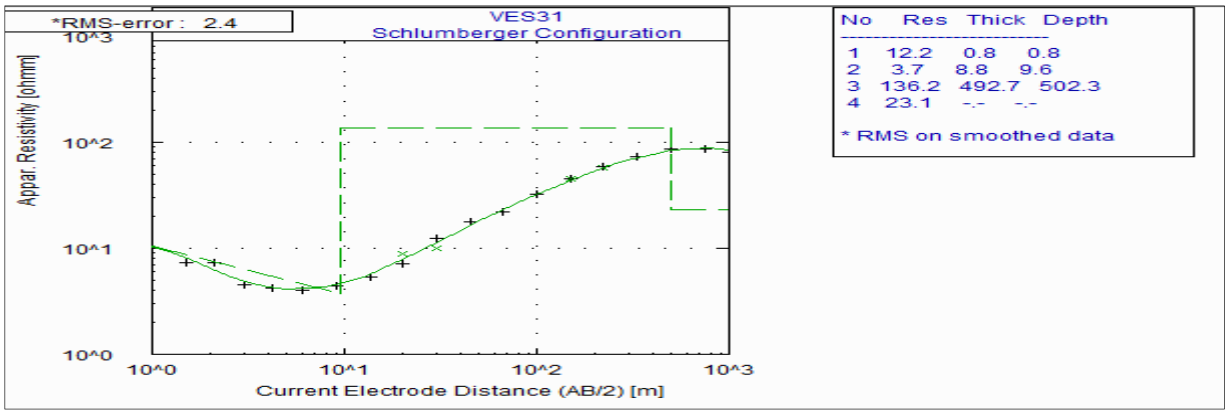

No	Res	Thick	Depth
1	12.2	0.8	0.8
2	3.7	8.8	9.6
3	136.2	492.7	502.3
4	23.1	-.-	-.-

* RMS on smoothed data

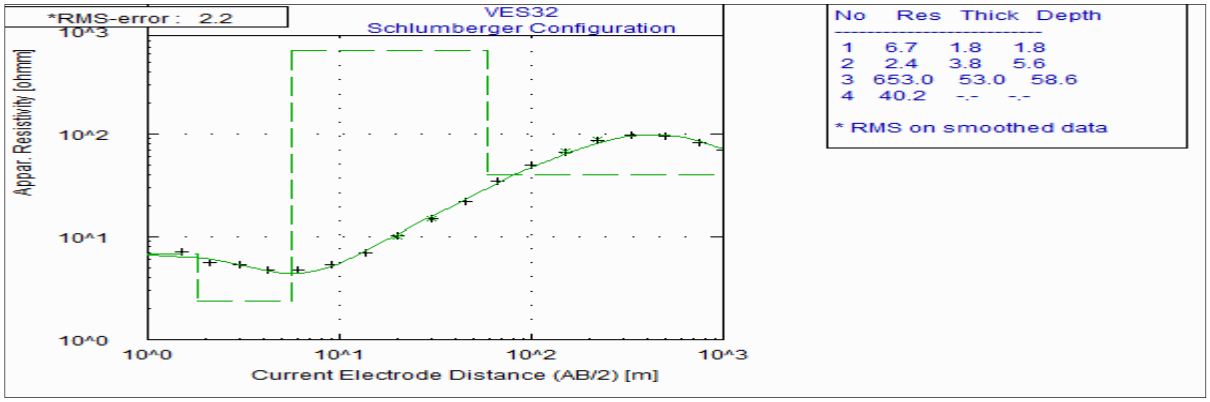

No	Res	Thick	Depth
1	6.7	1.8	1.8
2	2.4	3.8	5.6
3	653.0	53.0	58.6
4	40.2	-.-	-.-

* RMS on smoothed data

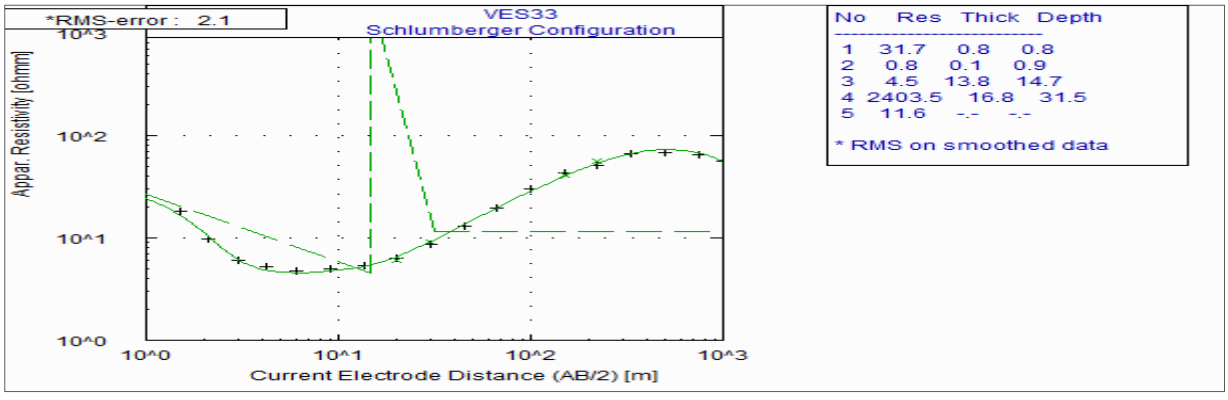

No	Res	Thick	Depth
1	31.7	0.8	0.8
2	0.8	0.1	0.9
3	4.5	13.8	14.7
4	2403.5	16.8	31.5
5	11.6	-.-	-.-

* RMS on smoothed data

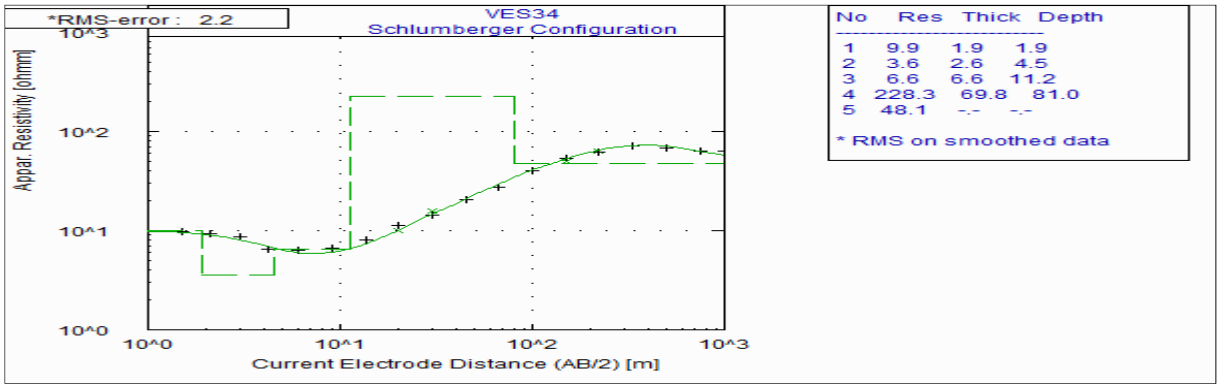

No	Res	Thick	Depth
1	9.9	1.9	1.9
2	3.6	2.6	4.5
3	6.6	6.6	11.2
4	228.3	69.8	81.0
5	48.1	-.-	-.-

* RMS on smoothed data

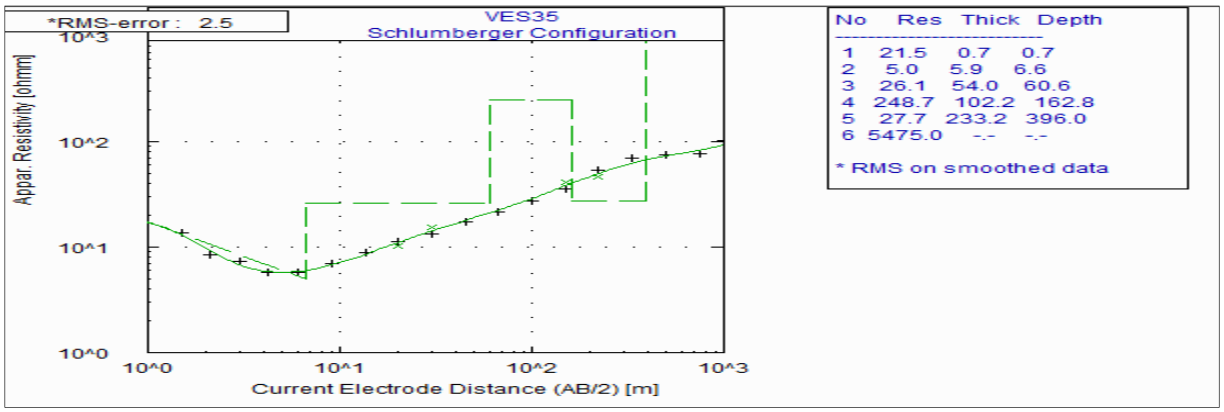

No	Res	Thick	Depth
1	21.5	0.7	0.7
2	5.0	5.9	6.6
3	26.1	54.0	60.6
4	248.7	102.2	162.8
5	27.7	233.2	396.0
6	5475.0	-.-	-.-

* RMS on smoothed data

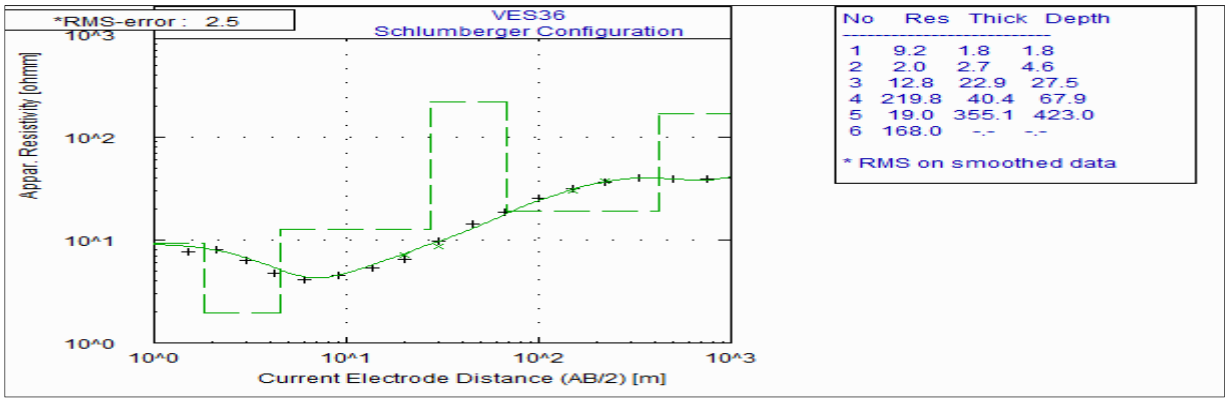

No	Res	Thick	Depth
1	9.2	1.8	1.8
2	2.0	2.7	4.6
3	12.8	22.9	27.5
4	219.8	40.4	67.9
5	19.0	355.1	423.0
6	168.0	-.-	-.-

* RMS on smoothed data

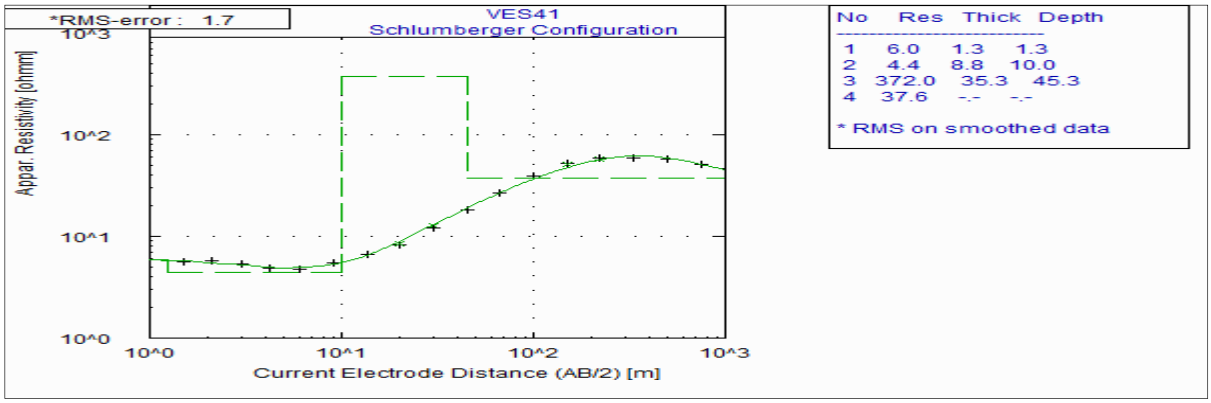

No	Res	Thick	Depth
1	6.0	1.3	1.3
2	4.4	8.8	10.0
3	372.0	35.3	45.3
4	37.6	-.-	-.-

* RMS on smoothed data

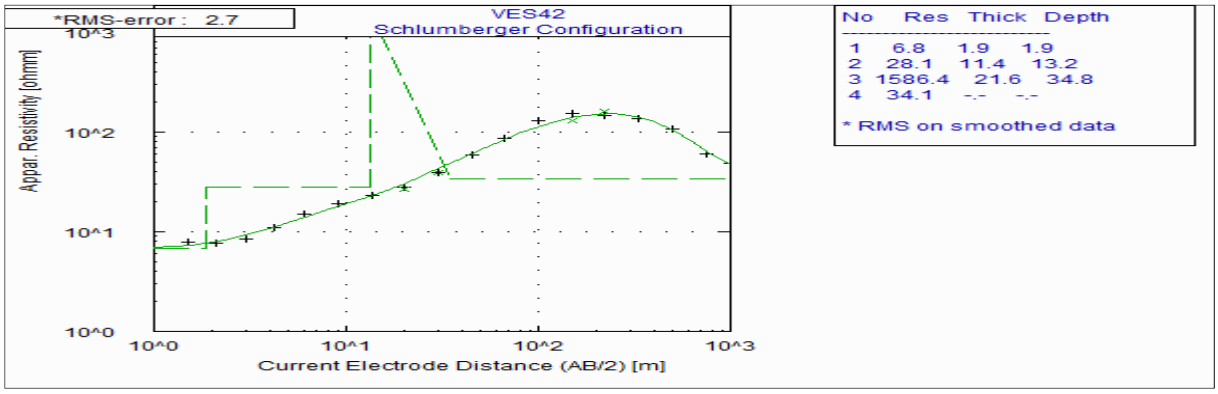
*RMS-error : 2.7
VES42
Schlumberger Configuration
Appar. Resistivity [ohmm]
10^3
10^2
10^1
10^0
10^0
10^1
10^2
10^3
Current Electrode Distance (AB/2) [m]
No Res Thick Depth
1 6.8 1.9 1.9
2 28.1 11.4 13.2
3 1586.4 21.6 34.8
4 34.1 -.- -.-
* RMS on smoothed data

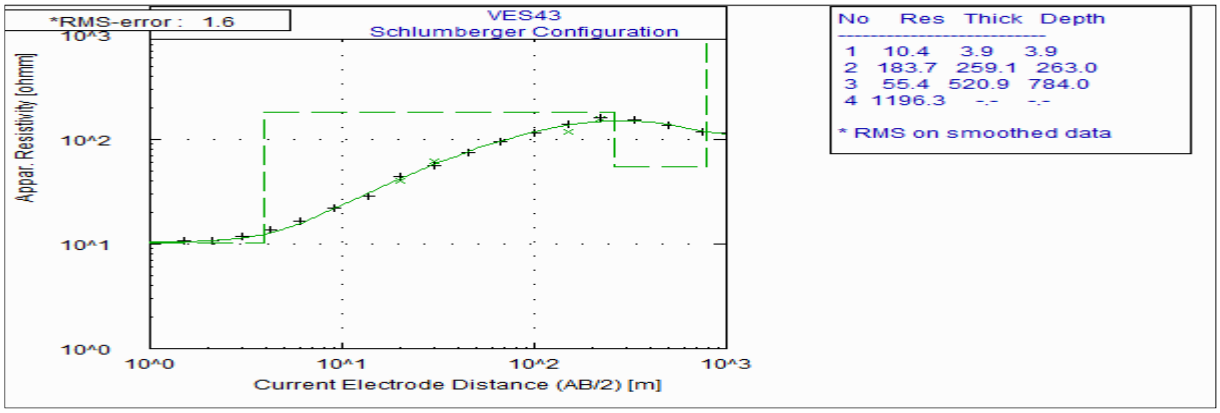
*RMS-error : 1.6
VES43
Schlumberger Configuration
Appar. Resistivity [ohmm]
10^3
10^2
10^1
10^0
10^0
10^1
10^2
10^3
Current Electrode Distance (AB/2) [m]
No Res Thick Depth
1 10.4 3.9 3.9
2 183.7 259.1 263.0
3 55.4 520.9 784.0
4 1196.3 -.- -.-
* RMS on smoothed data

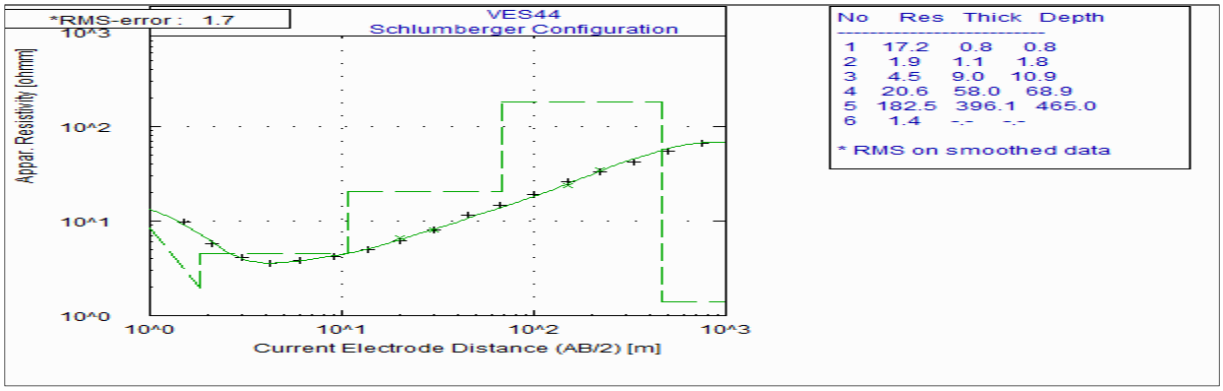
*RMS-error : 1.7
VES44
Schlumberger Configuration
Appar. Resistivity [ohmm]
10^3
10^2
10^1
10^0
10^0
10^1
10^2
10^3
Current Electrode Distance (AB/2) [m]
No Res Thick Depth
1 17.2 0.8 0.8
2 1.9 1.1 1.8
3 4.5 9.0 10.9
4 20.6 58.0 68.9
5 182.5 396.1 465.0
6 1.4 -.- -.-
* RMS on smoothed data

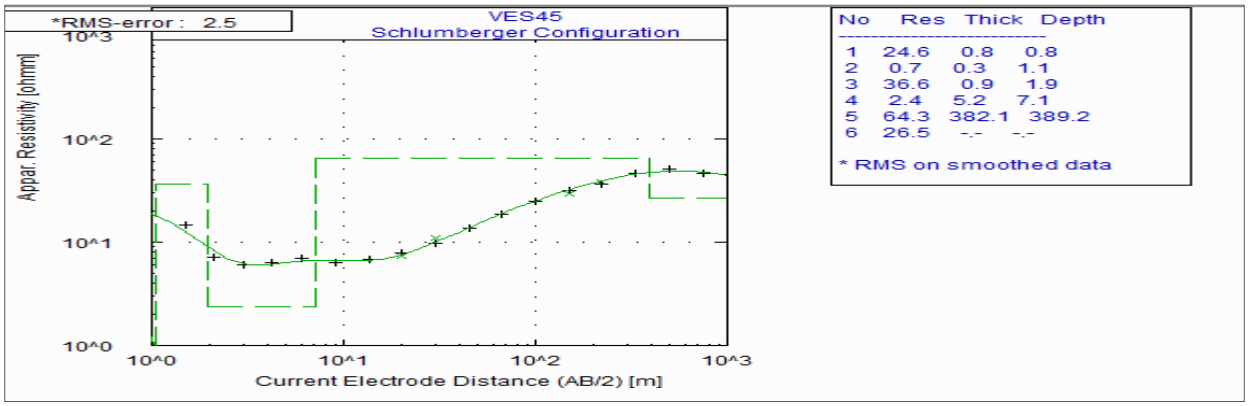
*RMS-error : 2.5
VES45
Schlumberger Configuration
Appar. Resistivity [ohmm]
10^3
10^2
10^1
10^0
10^0
10^1
10^2
10^3
Current Electrode Distance (AB/2) [m]
No Res Thick Depth
1 24.6 0.8 0.8
2 0.7 0.3 1.1
3 36.6 0.9 1.9
4 2.4 5.2 7.1
5 64.3 382.1 389.2
6 26.5 -.- -.-
* RMS on smoothed data

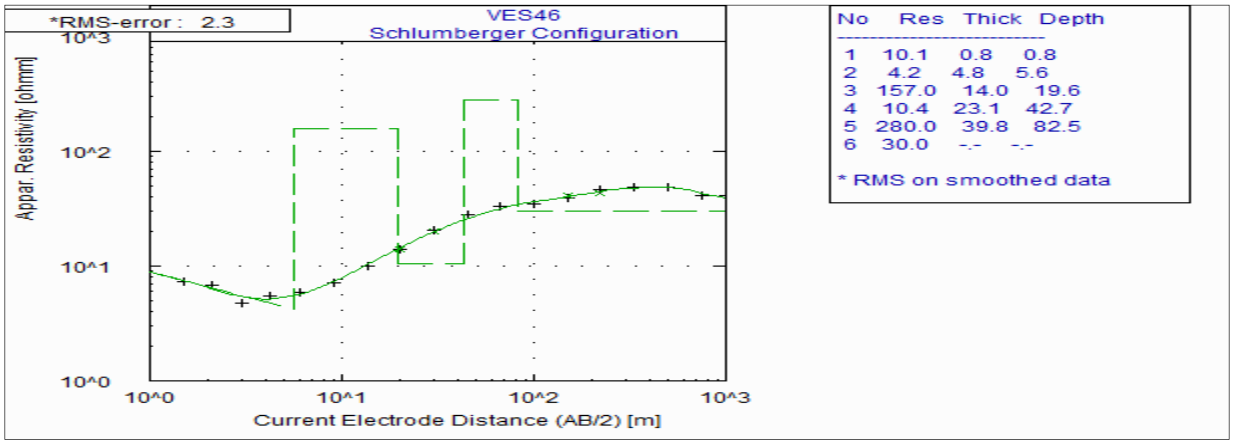

Annex 2: Boreholes

A) SWAWF3 (471027 E, 973709 N)

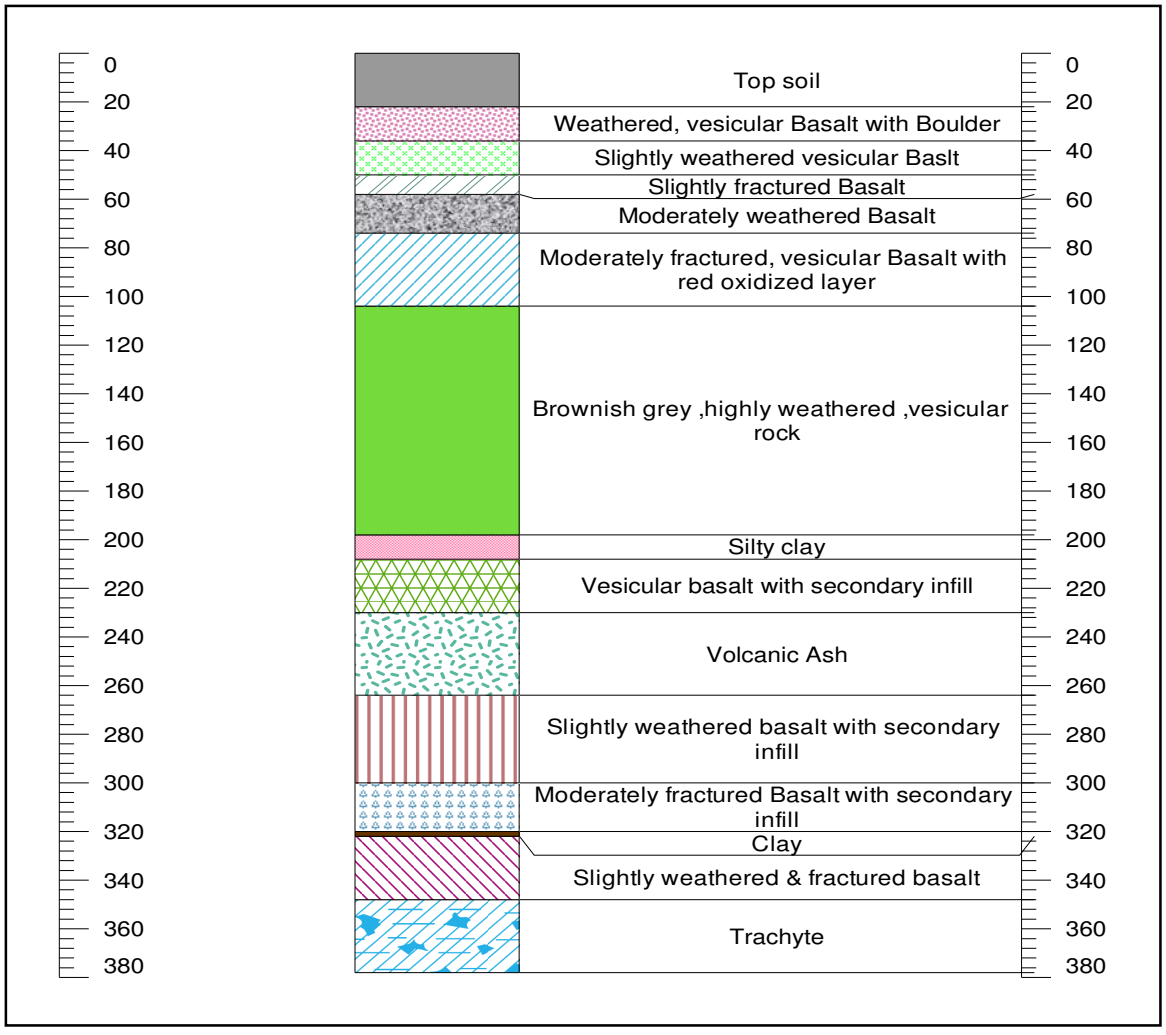

B) Dewara Guda (473576E, 972821N)

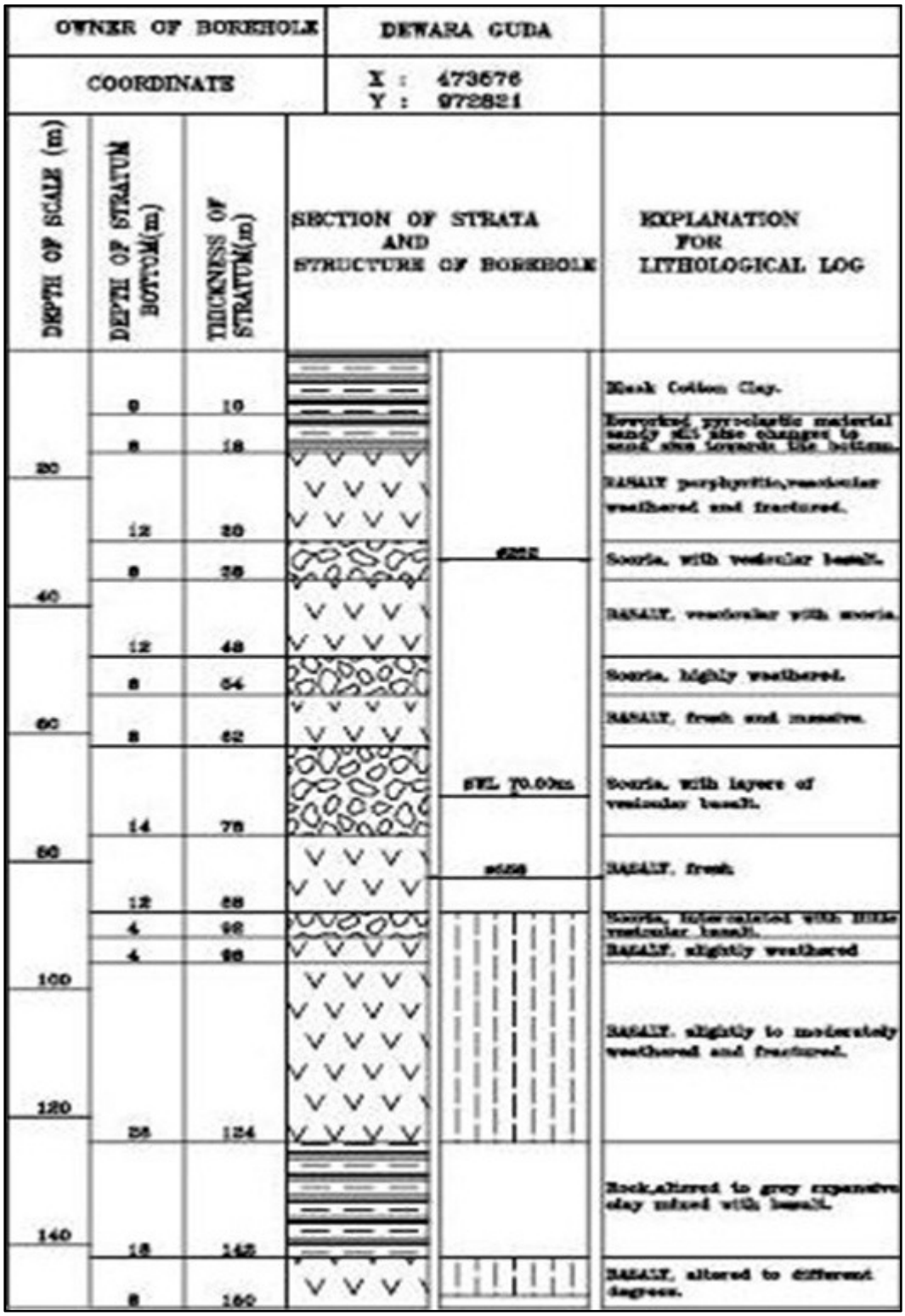

C) BH24 (477330E, 976793N)

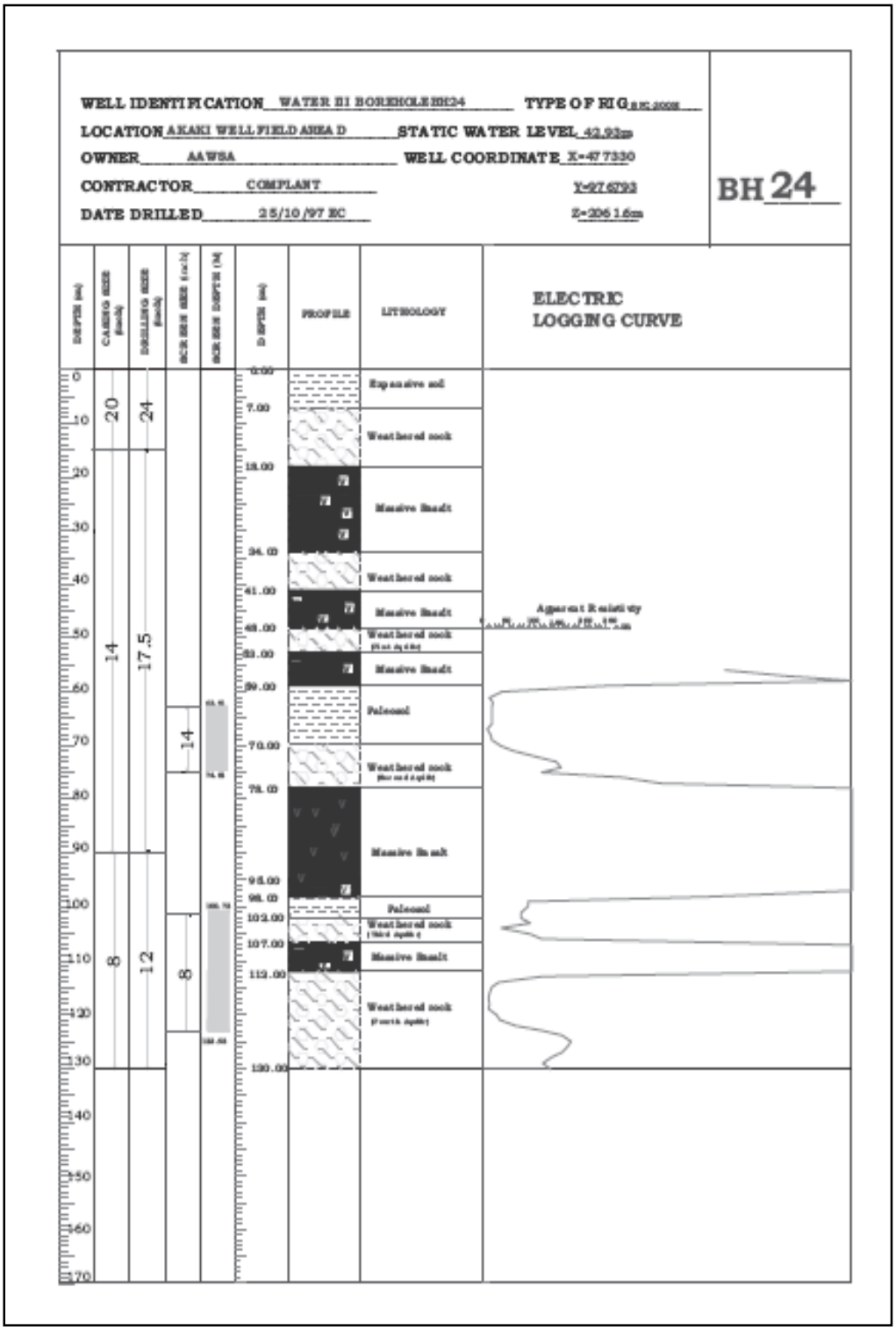

D) BH 23 (477477E, 977216N)

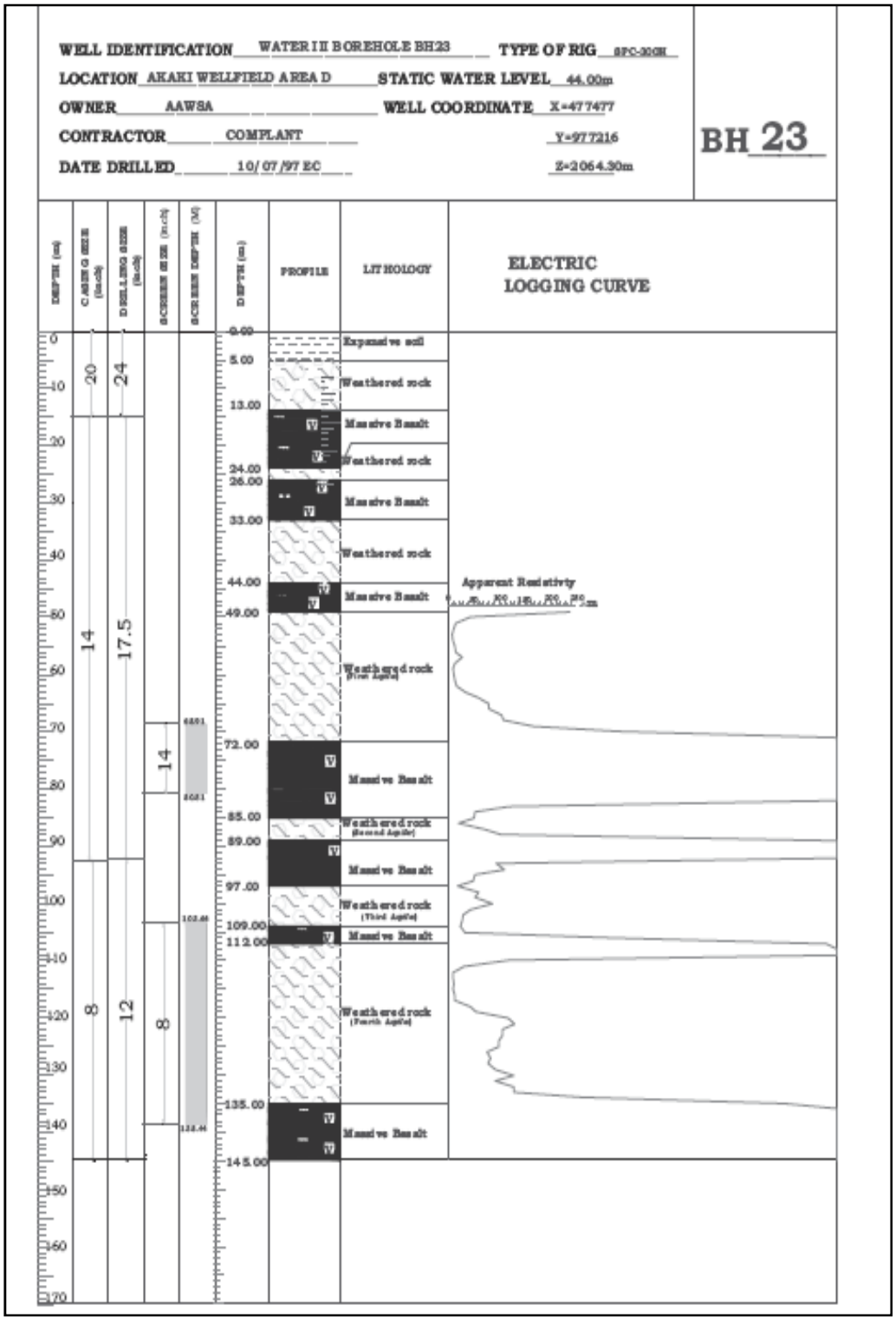

E) BH 17 (478204E, 976364N)

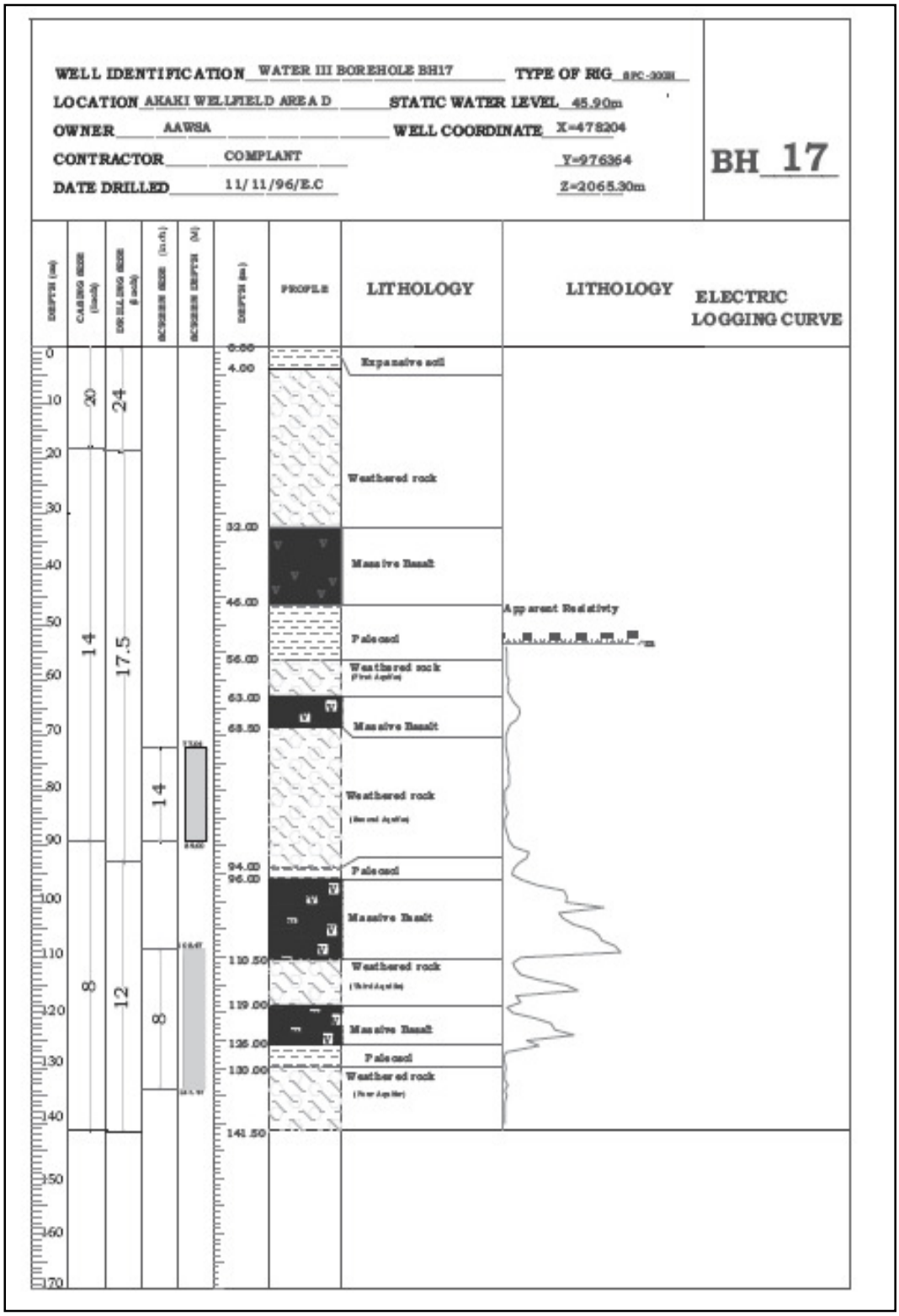

Declaration

I, the undersigned, declare that this thesis is my original Work, has not been presented for degrees in any other University and all sources of material used for thesis have been properly duly acknowledged.

Name: **EYASU LETA ALEMU**

Signature_____

Date_____

This thesis has been submitted for examination with approval as University advisor:

_____

Dr. Tigistu Haile

_____

Dr. Tilahun Mammo